PHYSICAL REVIEW D **95,** 075006 (2017)

Nonperturbative analysis of the spectrum of meson resonances in an ultraviolet-complete composite-Higgs model

Nicolas Bizot,[1] Michele Frigerio,[1] Marc Knecht,[2] and Jean-Loïc Kneur[1]
[1]*Laboratoire Charles Coulomb (L2C), UMR 5221 CNRS-Université de Montpellier, F-34095 Montpellier Cedex 5, France*
[2]*Centre de Physique Théorique (CPT), UMR 7332 CNRS/Aix-Marseille Univ./Univ. du Sud Toulon-Var, F-13288 Marseille cedex 9, France*
(Received 21 December 2016; published 5 April 2017)

We consider a vectorlike gauge theory of fermions that confines at the multi-TeV scale, and that realizes the Higgs particle as a composite Goldstone boson. The weak interactions are embedded in the unbroken subgroup $Sp(4)$ of a spontaneously broken $SU(4)$ flavor group. The meson resonances appear as poles in the two-point correlators of fermion bilinears, and include the Goldstone bosons plus a massive pseudoscalar η', as well as scalars, vectors and axial vectors. We compute the mass spectrum of these mesons, as well as their decay constants, in the chiral limit, in the approximation where the hypercolor $Sp(2N)$ dynamics is described by four-fermion operators, à la Nambu-Jona Lasinio. By resumming the leading diagrams in the $1/N$ expansion, we find that the spin-one states lie beyond the LHC reach, while spin-zero electroweak-singlet states may be as light as the Goldstone-boson decay constant, $f \sim 1$ TeV. We also confront our results with a set of available spectral sum rules. In order to supply composite top-quark partners, the theory contains additional fermions carrying both hypercolor and ordinary color, with an associated flavor symmetry-breaking pattern $SU(6)/SO(6)$. We identify and analyze several nontrivial features of the complete two-sector gauge theory: the 't Hooft anomaly matching conditions; the higher-dimension operator which incorporates the effects of the hypercolor axial-singlet anomaly; the coupled mass-gap equations; the mixing between the singlet mesons of the two sectors, resulting in an extra Goldstone boson η_0, and novel spectral sum rules. Assuming that the strength of the four-fermion interaction is the same in the two sectors, we find that the colored vector and scalar mesons have masses $\gtrsim 4f$, while the masses of colored pseudo-Goldstone bosons, induced by gluon loops, are $\gtrsim 1.5f$. We discuss the scaling of the meson masses with the values of N, of the four-fermion couplings, and of a possible fermion mass.

DOI: 10.1103/PhysRevD.95.075006

I. INTRODUCTION

After the first LHC 13 TeV data have been analyzed, we are left with a 125 GeV Higgs boson and no evidence for other new states. Yet, it is too early to remove from consideration sufficiently weakly-coupled new particles in the sub-TeV range, or even new colored particles in the multi-TeV range. Even though the little hierarchy between the Higgs mass and the new states seem to require an adjustment of parameters, the theories addressing the quantum stability of the electroweak scale may still solve larger hierarchy problems. A classical possibility is a strongly coupled sector that dynamically generates the electroweak scale. The observation of a scalar state, significantly lighter than the strong-coupling scale, suggests that the Higgs particle may be composite and, in good approximation, a Nambu-Goldstone boson (NGB) associated to the global symmetries of the new sector [1–4]. While an effective description of the composite Higgs couplings is possible without specifying the strong dynamics, the spectrum of additional composite states essentially depends on the underlying ultraviolet theory. Barring extra space-time dimensions, the simplest, well-understood, explicit realization is provided by a gauge theory of fermions that confines at the multi-TeV scale, with quantum chromodynamics (QCD) as a prototype. The historical incarnation being technicolor [5,6], in recent years models of this sort featuring the Higgs as a composite NGB have been built [7–12] and classified in some generality [11,13]. Alternative ultraviolet completions of composite Higgs models are discussed in Refs. [14–17].

Our motivations to analyze in detail such a scenario are manifold. A characterization of the spectrum of composite states is critical to confront with the LHC program: does one foresee Standard Model (SM) singlet resonances close to one TeV? what are the expectations for the masses of the lightest charged and color states? These intrinsically nonperturbative questions are especially pressing, in order to compare with the well-defined predictions of weakly-coupled theories. In addition, a quantitative description of the composite masses and couplings would allow for an explicit computation of the Higgs low energy properties, improving on the predictivity of the composite Higgs effective theory. Furthermore, decades of QCD studies have provided us with a notable collection of nonperturbative, analytic techniques to study strongly-coupled gauge theories, that have been hardly exploited in the context of models for the electroweak scale. A partial list includes anomaly matching [18], spectral sum rules [19],

large-N expansions [20,21], and the Nambu-Jona Lasinio (NJL) effective model [22,23] (see also Refs. [24,25]). With this approach one can reach several nontrivial results, holding within well-defined approximations, with a relatively small computational effort, and thus one may broadly characterize several, different, possible models. This is complementary to lattice simulations, which are suitable for potentially more precise computations, in specific and/or simplified scenarios. Interestingly, we will also find that the peculiar structure of composite Higgs models requires a gauge theory that is qualitatively different from QCD, in a handful of significant features.

We engage into this program by choosing, as a case study, an electroweak sector with global symmetry $SU(4)$ spontaneously broken to $Sp(4)$. This is the most economical possibility to obtain a Nambu-Goldstone Higgs doublet with custodial symmetry, starting from a set of constituent fermions. This model, with a hypercolor gauge group $Sp(2N)$, emerges as the minimal benchmark for an ultraviolet-complete composite Higgs sector. The most significant challenge facing this class of theories is to generate the large top quark Yukawa coupling, as it requires nonrenormalizable operators to couple the top to the electroweak symmetry breaking (EWSB) order parameter. A promising way to circumvent the potential suppression of the top Yukawa is partial compositeness [26], which calls for composite fermion resonances with the quantum number of the top quark. A minimal realization of top partial compositeness is provided by an additional sector of hypercolor fermions, which are charged under QCD, with global symmetry $SU(6)$ spontaneously broken to $SO(6)$. While this particular choice for the color sector appears less compelling than the one for the electroweak sector, we will show that it is instructive to study it explicitly in detail. Indeed, one needs to surmount a number of model-building difficulties, which require quite technical complications: on the one hand this assesses the price to pay for top partners, on the other hand the interplay of the two sectors reveals a few novel physical phenomena, whose interest transcends the specific model under consideration.

Our analysis builds on an early, enlightening study [8], which employed four-fermion operators to understand the dynamics of this $SU(4) \times SU(6)$ model with hypercolor group $Sp(2N)$, in close analogy with the NJL description of QCD (NJL techniques have been applied to different ultraviolet-complete composite-Higgs models as well [15]). We will provide the first, thorough computation of the spectrum of the meson resonances in this scenario. To this end, we will perform a detailed scrutiny of the symmetry structure of the model, which allows for several nontrivial consistency checks, as well as for an accurate determination of the allowed range of parameters. In most of our analysis, we will stick to the chiral limit, where the constituent fermions have no bare masses, and the SM gauge and Yukawa couplings are neglected. In this limit the Higgs and the other NGBs are massless. When relevant, we will discuss in some detail the effect of fermion masses and of switching on the SM gauge fields, however we will not study the generation of Yukawa couplings and of the NGB effective potential: the usual effective theory techniques to address these issues [27,28] hold in the present scenario as well, but we leave for future work a more specific treatment of this subject.

The paper is organized as follows. In Sec. II, we review exact results on vectorlike gauge theories, especially concerning the spontaneous breaking of the flavor symmetries, the associated spectral sum rules, the NGB couplings to external gauge fields. The reader more interested in the phenomenology of a specific model may just consult this part to inspect general formulas and conventions. In Sec. III, we study the electroweak sector with coset $SU(4)/Sp(4)$, in terms of four-fermion operators, à la NJL. The symmetry breaking is examined through the gap equation for the dynamical fermion mass, while the spin-zero and spin-one meson masses are extracted from the poles of resummed two-point correlators. The spectrum of resonances is analyzed in units of the NGB decay constant, and compared with available lattice results, as well as with spectral sum rules. This analysis of the electroweak sector in isolation is self-sufficient and it already illustrates the main potentialities of our approach. The following sections require some extra model-building and rather technical computations, that however may be skipped to move directly to the phenomenological results. In Sec. IV, we introduce additional, colored constituent fermions, in a different representation of $Sp(2N)$, to provide partners for the top quark. The consequences include nontrivial anomaly matching conditions, mixed sum rules across the two sectors, and mixed operators induced by the hypercolor gauge anomaly. In Sec. V, we study the system of coupled mass-gap equations for the two sectors and derive the masses of colored mesons. In addition, the mixing between the two flavor singlet (pseudo) scalars leads to a peculiar mass spectrum and phenomenology. Finally, in Sec. VI, we summarize the main results of the analysis and delineate future directions. Technical material is collected in the appendixes: the generators of the flavor symmetry group in Appendix A, the relevant loop functions in Appendix B, some details on the computation of two-point correlators in Appendix C, and the Fierz identities relating different four-fermion operators in Appendix D.

II. GENERAL PROPERTIES OF FLAVOR SYMMETRIES IN VECTORLIKE GAUGE THEORIES

The composite-Higgs model that we will study belongs to the class of vectorlike gauge theories, namely an asymptotically free and confining gauge theory, with a set of N_f Dirac fermions transforming under a (possibly reducible) self-contragredient (i.e. unitarily equivalent to its complex conjugate) representation of the gauge group, in such a way that it is possible to make all fermions massive

in a gauge invariant way.[1] Exact results concerning nonperturbative dynamical aspects in these theories are scarce, and in this section, we briefly review some of those that are actually available. They concern issues related to the spontaneous breaking of the global flavor symmetries and the spectrum of low-lying bound states.

A. Restrictions on the pattern of spontaneous symmetry breaking

An important result for the spontaneous breaking of the global flavor symmetry group G for fermions with vectorlike couplings to gauge fields has been obtained by Vafa and Witten [29]. The theorem they have proven makes the following statement: in any vectorlike gauge theory with massless fermions and vanishing vacuum angles, the subgroup H_m of the flavor group G that corresponds to the remaining global symmetry when all fermion flavors are given identical gauge invariant masses, cannot be spontaneously broken. In other words, if G undergoes spontaneous breaking towards some subgroup H, then $H_m \subseteq H$ (in the absence of any vacuum angle). This theorem is particularly powerful when H_m corresponds to a maximal subgroup of G, since it then allows only two alternatives: either G is not spontaneously broken at all, or G is spontaneously broken towards H_m. This is actually what happens in the three cases that we can encounter in vectorlike theories [31,32]: $G = SU(N_f)_L \times SU(N_f)_R$ and $H_m = SU(N_f)_V$[2]; $G = SU(2N_f)$ and $H_m = SO(2N_f)$; $G = SU(2N_f)$ and $H_m = Sp(2N_f)$.

Of particular interest for the discussion that follows are the Noether currents $\mathcal{J}^A_\mu$, corresponding to the generators T^A of the unbroken subgroup H_m, and $\mathcal{J}^{\hat{A}}_\mu$, corresponding to the generators $T^{\hat{A}}$ in the coset G/H_m. Since the latter is a symmetric space for the three cases that have just been listed, we will usually refer to the currents $\mathcal{J}^A_\mu$ ($\mathcal{J}^{\hat{A}}_\mu$) as vector (axial) currents. When the fermions transform under an irreducible but real ($\epsilon = +1$ below) or pseudoreal ($\epsilon = -1$) representation of the gauge group, $G = SU(2N_f)$, and $H_m = SO(2N_f)$ or $H_m = Sp(2N_f)$, respectively. In these two cases, it is convenient to write the fermion fields in terms of left-handed Weyl spinors ψ_α. The currents are then defined as follow [$\bar{\psi}_i \equiv \psi^\dagger_j (\Omega_\varepsilon)_{ji}$, where i and j denote gauge indices, while spinor and flavor indices are omitted]:

$$\mathcal{J}^A_\mu = \frac{1}{2}(\Omega_\varepsilon)_{ij}[\varepsilon\bar{\psi}_i\bar{\sigma}_\mu T^A\psi_j - \psi_i\sigma_\mu(T^A)^T\bar{\psi}_j],$$
$$\mathcal{J}^{\hat{A}}_\mu = \frac{1}{2}(\Omega_\varepsilon)_{ij}[\varepsilon\bar{\psi}_i\bar{\sigma}_\mu T^{\hat{A}}\psi_j - \psi_i\sigma_\mu(T^{\hat{A}})^T\bar{\psi}_j]. \quad (2.1)$$

The gauge contraction Ω_ε is an invariant tensor under the action of the gauge group, which is symmetric for $\varepsilon = +1$ and antisymmetric for $\varepsilon = -1$, with $(\Omega^2_\varepsilon)_{ij} = \varepsilon\delta_{ij}$. The generators T^A and $T^{\hat{A}}$ are characterized by the properties

$$T^A\Sigma_\varepsilon + \Sigma_\varepsilon(T^A)^T = 0, \qquad T^{\hat{A}}\Sigma_\varepsilon - \Sigma_\varepsilon(T^{\hat{A}})^T = 0, \quad (2.2)$$

and are normalized as

$$\mathrm{Tr}(T^AT^B) = \frac{1}{2}\delta^{AB},$$
$$\mathrm{Tr}(T^{\hat{A}}T^{\hat{B}}) = \frac{1}{2}\delta^{\hat{A}\hat{B}},$$
$$\mathrm{Tr}(T^AT^{\hat{B}}) = 0. \quad (2.3)$$

The $2N_f \times 2N_f$ matrix Σ_ε is an invariant tensor of the subgroup H_m of the flavor group. It plays for this subgroup a role analogous to the role played by Ω_ε for the gauge group. In particular, it can be chosen real, it is symmetric for $\varepsilon = +1$ and antisymmetric for $\varepsilon = -1$, and satisfies $\Sigma^2_\varepsilon = \varepsilon\mathbb{1}$, where $\mathbb{1}$ denotes the $2N_f \times 2N_f$ unit matrix in flavor space.

B. 't Hooft's anomaly matching condition

Whereas the theorem of Vafa and Witten restricts the pattern of spontaneous breaking of the global flavor symmetry group G, it does not by itself provide information on which alternative will eventually be realized. Additional information is required to that effect. The anomaly matching condition proposed by 't Hooft [18] can prove helpful in this respect. This condition uses the fact that the Ward identities satisfied by the three-point functions of the Noether currents corresponding to the symmetry group G receive anomalous contributions from the massless elementary fermions [33–35]

$$i(q_1+q_2)^\rho \int d^4x_1 \int d^4x_2 e^{iq_1\cdot x_1 + iq_2\cdot x_2} \times \langle \mathrm{vac}|T\{\mathcal{J}^A_\mu(x_1)\mathcal{J}^B_\nu(x_2)\mathcal{J}^{\hat{C}}_\rho(0)\}|\mathrm{vac}\rangle = -\frac{d_{HC}}{8\pi^2}\epsilon_{\mu\nu\alpha\beta}q_1^\alpha q_2^\beta d^{AB\hat{C}}, \quad (2.4)$$

with $d^{AB\hat{C}} = 2\mathrm{tr}(\{T^A, T^B\}T^{\hat{C}})$, where the trace is over the flavor group only, and d_{HC} denotes the dimension of the representation of the gauge group under which the fermions transform. These anomalous contributions imply that the corresponding three-point functions have very specific physical singularities at vanishing momentum transfer [18,36,37]. Moreover, this type of singularities can only

[1] It is also possible to give all fermions gauge invariant masses in the case of an odd number of Weyl fermions in the same *real* representation of the gauge group. Such theories do not have a conserved fermion number, and are not vectorlike [29,30]. Although it can provide interesting composite-Higgs models, as discussed, for instance, in Ref. [10], this class of theories will not be addressed here.

[2] The issue of the $U(1)_V$ symmetry is somewhat subtle, but we will not need to discuss it here.

be produced by physical intermediate states consisting either of a single massless spin zero particle, or of a pair of massless spin one-half particles. If the symmetries of G are not spontaneously broken, the first option is excluded. If the theory confines, this then implies that it has to produce massless spin one-half bound states (that we will call baryons). These fermionic bound states will occur in multiplets of G, and their multiplicities must be chosen such as to exactly reproduce the coefficient of the singularities in the current three-point functions. If it is not possible to saturate this anomaly coefficient with the exchange of massless fermionic bound states only, then massless spin-zero bound states coupled to the currents of G are required, and hence G is spontaneously broken. If this anomaly matching condition can be satisfied with massless spin one-half bound states only, the spontaneous breaking of G towards H_m is not a necessity, but it cannot be excluded either.

In particular, the global symmetry is necessarily spontaneously broken if, after confinement, the theory cannot produce fermionic bound states at all. If we restrict ourselves to constituent fermions in the fundamental representation of the gauge group, this happens when the gauge group is $SU(2N)$, $SO(2N)$, or $Sp(2N)$. In these cases, the flavor group G, therefore, necessarily suffers spontaneous breaking towards H_m. On the contrary, fermionic bound states can be formed in the case of $SU(N)$ or $SO(N)$ gauge groups with N odd. Novel fermionic bound states may be possible if one admits elementary fermions transforming in other representations than the fundamental under the gauge group. We will discuss one such scenario below in Sec. IV.

C. Mass inequalities

Various inequalities [38–42] involving the masses of the gauge-singlet bound states in confining vectorlike gauge theories provide additional insight into the fate of flavor symmetries in these theories, complementary to the constraints arising from the Vafa-Witten theorem and from 't Hooft's anomaly matching condition. The most rigorous versions of these inequalities hold under the same positivity constraint on the path-integral measure in euclidian space as required for the proof of the Vafa-Witten theorem, namely the absence of any vacuum angle. A review on these inequalities is provided by Ref. [43]. Of particular interest in the present context is the inequality of the type [38,40–42]

$$M_{1/2} \geq C(N, N_f) M_0, \tag{2.5}$$

involving, on the one hand, the mass $M_{1/2}$ of any baryon state and, on the other hand, the mass M_0 of the lightest quark-antiquark spin-zero state having the flavor quantum numbers of the G/H_m currents. The precise value of the (positive) constant $C(N, N_f)$ and its dependence on the number of hypercolors N and/or number of flavors N_f is not so important here, the main point being that such an inequality again provides a strong indication that the flavor symmetry G is necessarily spontaneously broken towards G/H_m.

D. Superconvergent spectral sum rules

Assuming that G is spontaneously broken towards H_m, correlation functions that are at the same time order parameters become of particular interest, since they enjoy a smooth behavior at short distances. These improved high-energy properties allow in turn to write superconvergent sum rules for the corresponding spectral densities. The paradigmatic example is provided by the Weinberg sum rules [19], once interpreted [44] and justified in the framework of QCD and of the operator-product expansion [45], including nonperturbative power corrections [46].

Here we will consider two-point functions of certain fermion-bilinear operators, when the fermions transform under an irreducible but real or pseudoreal representation of the gauge group. Specifically, these operators comprise the Noether currents defined in Eq. (2.1), to which we add the scalar and pseudoscalar densities defined as

$$\begin{aligned}
\mathcal{S}^{\hat{A}} &= \frac{1}{2}(\Omega_\varepsilon)_{ij}[\bar{\psi}_i T^{\hat{A}} \Sigma_\varepsilon \bar{\psi}_j + \psi_i \Sigma_\varepsilon T^{\hat{A}} \psi_j], \\
\mathcal{S}^{0} &= \frac{1}{2}(\Omega_\varepsilon)_{ij}[\bar{\psi}_i T^{0} \Sigma_\varepsilon \bar{\psi}_j + \psi_i \Sigma_\varepsilon T^{0} \psi_j], \\
\mathcal{P}^{\hat{A}} &= \frac{1}{2i}(\Omega_\varepsilon)_{ij}[\bar{\psi}_i T^{\hat{A}} \Sigma_\varepsilon \bar{\psi}_j - \psi_i \Sigma_\varepsilon T^{\hat{A}} \psi_j], \\
\mathcal{P}^{0} &= \frac{1}{2i}(\Omega_\varepsilon)_{ij}[\bar{\psi}_i T^{0} \Sigma_\varepsilon \bar{\psi}_j - \psi_i \Sigma_\varepsilon T^{0} \psi_j].
\end{aligned} \tag{2.6}$$

The singlet densities are normalized consistently with the other densities by taking $T^0 = \mathbb{1}/(2\sqrt{N_f})$. The two-point correlation functions of interest are then defined as

$$\begin{aligned}
&\Pi_V(q^2)\delta^{AB}(q_\mu q_\nu - \eta_{\mu\nu} q^2) \\
&\quad = i \int d^4x e^{iq\cdot x} \langle \mathrm{vac}|T\{\mathcal{J}^A_\mu(x)\mathcal{J}^B_\nu(0)\}|\mathrm{vac}\rangle, \\
&\Pi_A(q^2)\delta^{\hat{A}\hat{B}}(q_\mu q_\nu - \eta_{\mu\nu} q^2) \\
&\quad = i \int d^4x e^{iq\cdot x} \langle \mathrm{vac}|T\{\mathcal{J}^{\hat{A}}_\mu(x)\mathcal{J}^{\hat{B}}_\nu(0)\}|\mathrm{vac}\rangle,
\end{aligned} \tag{2.7}$$

$$\begin{aligned}
\Pi_S(q^2)\delta^{\hat{A}\hat{B}} &= i \int d^4x e^{iq\cdot x} \langle \mathrm{vac}|T\{\mathcal{S}^{\hat{A}}(x)\mathcal{S}^{\hat{B}}(0)\}|\mathrm{vac}\rangle, \\
\Pi_P(q^2)\delta^{\hat{A}\hat{B}} &= i \int d^4x e^{iq\cdot x} \langle \mathrm{vac}|T\{\mathcal{P}^{\hat{A}}(x)\mathcal{P}^{\hat{B}}(0)\}|\mathrm{vac}\rangle,
\end{aligned} \tag{2.8}$$

where $\hat{A} \neq 0$, $\hat{B} \neq 0$, and

$$\Pi_{S^0}(q^2) = i\int d^4x e^{iq\cdot x}\langle \mathrm{vac}|T\{\mathcal{S}^0(x)\mathcal{S}^0(0)\}|\mathrm{vac}\rangle,$$
$$\Pi_{P^0}(q^2) = i\int d^4x e^{iq\cdot x}\langle \mathrm{vac}|T\{\mathcal{P}^0(x)\mathcal{P}^0(0)\}|\mathrm{vac}\rangle. \quad (2.9)$$

The combinations

$$\Pi_{V-A}(q^2) \equiv \Pi_V(q^2) - \Pi_A(q^2), \quad (2.10)$$

$$\Pi_{S-P}(q^2) \equiv \Pi_S(q^2) - \Pi_P(q^2),$$
$$\Pi_{S-P^0}(q^2) \equiv \Pi_S(q^2) - \Pi_{P^0}(q^2),$$
$$\Pi_{S^0-P}(q^2) \equiv \Pi_{S^0}(q^2) - \Pi_P(q^2), \quad (2.11)$$

are order parameters[3] for the spontaneous breaking of $SU(2N_f)$ towards H_m for all values of q^2. As a consequence, these two-point functions behave smoothly at short distances ($Q^2 \equiv -q^2 > 0$):

$$\lim_{Q^2\to+\infty}(Q^2)^2 \times \Pi_{V-A}(-Q^2) = 0,$$
$$\lim_{Q^2\to+\infty} Q^2 \times \{\Pi_{S-P}(-Q^2); \Pi_{S^0-P}(-Q^2); \Pi_{S-P^0}(-Q^2)\} = \{0;0;0\}. \quad (2.12)$$

From these short-distance properties, one then derives the following superconvergent spectral sum rules

$$\int_0^\infty dt\, \mathrm{Im}\Pi_{V-A}(t) = 0,$$
$$\int_0^\infty dt\, t\, \mathrm{Im}\Pi_{V-A}(t) = 0, \quad (2.13)$$

$$\int_0^\infty dt\, \mathrm{Im}\Pi_{S-P}(t) = 0,$$
$$\int_0^\infty dt\, \mathrm{Im}\Pi_{S^0-P}(t) = 0,$$
$$\int_0^\infty dt\, \mathrm{Im}\Pi_{S-P^0}(t) = 0. \quad (2.14)$$

We will examine in the following to which extent these Weinberg-type sum rules, whose validity is quite general in view of the short-distance properties of asymptotically-free vectorlike gauge theories, are actually satisfied in the specific NJL four-fermion interaction approximation. For the sake of completeness, let us mention that the two-point function

$$\Pi_{AP}(q^2)\delta^{\hat{A}\hat{B}} q_\mu = \int d^4x e^{iq\cdot x}\langle \mathrm{vac}|T\{\mathcal{J}^{\hat{A}}_\mu(x)\mathcal{P}^{\hat{B}}(0)\}|\mathrm{vac}\rangle, \quad (2.15)$$

also defines an order-parameter. However, there is no associated sum rule, since, as a consequence of the Ward identities, this correlator is entirely saturated by the Goldstone-boson pole ($\langle\mathcal{S}^0\rangle$ denotes the vacuum expectation value of $\mathcal{S}^0$)

$$\Pi_{AP}(q^2) = \frac{1}{q^2}\frac{\langle\mathcal{S}^0\rangle}{\sqrt{N_f}}. \quad (2.16)$$

It may be useful to stress, at this stage, that the sum rules displayed above are only valid in the absence of any explicit symmetry breaking effects. Introducing, for instance, masses for the fermions would modify the short-distance properties of these correlators, and thus spoil the convergence of the integrals of the corresponding spectral functions. Let us briefly illustrate the changes that occur by giving the fermions a common mass m, so that the currents belonging to the subgroup H_m remain conserved. For the remaining currents, one now has

$$\partial^\mu \mathcal{J}^{\hat{A}}_\mu = 2m\mathcal{P}^{\hat{A}}. \quad (2.17)$$

As far as the current-current correlators are concerned, while the two-point function of the vector currents remains transverse, the correlator of two axial currents receives a longitudinal part,

$$i\int d^4x e^{iq\cdot x}\langle \mathrm{vac}|T\{\mathcal{J}^{\hat{A}}_\mu(x)\mathcal{J}^{\hat{B}}_\nu(0)\}|\mathrm{vac}\rangle$$
$$= \delta^{\hat{A}\hat{B}}[\Pi_A(q^2)(q_\mu q_\nu - \eta_{\mu\nu}q^2) + \Pi^L_A(q^2)q_\mu q_\nu]. \quad (2.18)$$

If one considers only corrections that are at most linear in m, then one can still write a convergent sum rule [47],

$$\int_0^\infty dt[\mathrm{Im}\Pi_V(t) - \mathrm{Im}\Pi_A(t) - \mathrm{Im}\Pi^L_A(t)] = \mathcal{O}(m^2). \quad (2.19)$$

[3]Concerning $\Pi_{S-P}(q^2)$, this statement and the ensuing sum rule hold only to the extent that the tensor $d^{\hat{A}\hat{B}\hat{C}} \equiv 2\mathrm{tr}(\{T^{\hat{A}}, T^{\hat{B}}\}T^{\hat{C}})$ does not vanish identically, which is not the case, for instance, when $G = SU(2)_L \times SU(2)_R$ and $H_m = SU(2)_V$, but also, more interestingly for our purposes, when $G = SU(4)$ and $H_m = Sp(4)$.

Notice that the Ward identities relate this longitudinal piece to the two-point function of the pseudoscalar densities and to the scalar condensate,

$$(q^2)^2\Pi_A^L(q^2) = 4m^2\Pi_P(q^2) + 2m\frac{\langle\mathcal{S}^0\rangle}{\sqrt{N_f}}. \tag{2.20}$$

The presence of a fermion mass m also shifts the masses of the Goldstone bosons away from zero, by an amount $\Delta_m M_G^2$ whose expression, at first order in m, actually follows from this identity and reads

$$F_G^2\Delta_m M_G^2 = -2m\frac{\langle\mathcal{S}^0\rangle}{\sqrt{N_f}} + \mathcal{O}(m^2\ln m). \tag{2.21}$$

This formula involves the Goldstone-boson decay constant F_G in the limit where m vanishes, defined as

$$\langle\mathrm{vac}|\mathcal{J}_\mu^{\hat{A}}(0)|G^{\hat{B}}(p)\rangle = ip_\mu F_G\delta^{\hat{A}\hat{B}}, \qquad p^2 = 0. \tag{2.22}$$

Defining the coupling of the Goldstone bosons to the pseudoscalar densities,

$$\langle\mathrm{vac}|\mathcal{P}^{\hat{A}}(0)|G^{\hat{B}}(p)\rangle = G_G\delta^{\hat{A}\hat{B}}, \qquad p^2 = 0, \tag{2.23}$$

the identity obtained in Eq. (2.16) implies

$$F_G G_G = -\frac{\langle\mathcal{S}^0\rangle}{\sqrt{N_f}}, \tag{2.24}$$

in the massless limit.

In contrast to the symmetry currents and to quantities derived from them, like F_G or $\Pi_{V/A}(q^2)$ for instance, the (pseudo)scalar densities and their matrix elements, whether $\Pi_{S/P}(q^2)$ or G_G, need to be multiplicatively renormalized, and are, therefore, not invariant under the action of the renormalization group. This dependence on the short-distance renormalization scale does not impinge on the validity or usefulness of the sum rules in Eqs. (2.14) or (2.19), which hold at every scale. Likewise, this scale dependence is exactly balanced out between the right- and left-hand sides of relations like (2.16) or (2.24).

E. Coupling to external gauge fields

Eventually, some currents of the global symmetry group G become weakly coupled to the standard model gauge fields. If, in the absence of these weakly coupled gauge fields, the global symmetry group G is spontaneously broken towards H_m, turning on the gauge interactions will produce two effects. First, the Goldstone bosons will acquire radiatively generated masses. Second, transitions of a single Goldstone boson into a pair of gauge bosons are induced and, at lowest order in the couplings to the external gauge fields, the amplitude describing the transition towards a pair of zero-virtuality gauge bosons is fixed by the anomalous Ward identities in Eq. (2.4). Let us briefly discuss these two aspects in general terms.

Let $|G^{\hat{A}}(p)\rangle$ denote the massless Goldstone-boson states corresponding to the generators $T^{\hat{A}}$ spanning the (symmetric) coset space G/H_m. In the presence of a perturbation that explicitly breaks the global symmetry, these Goldstone bosons become pseudo-Goldstone bosons, and their masses are shifted away from zero. At lowest order in the external perturbation, these mass shifts are given by

$$\Delta M_{G_{\hat{A}}}^2 = -\langle G^{\hat{A}}(p)|\Delta\mathcal{L}(0)|G^{\hat{A}}(p)\rangle, \qquad p^2 = 0, \tag{2.25}$$

with $\Delta\mathcal{L}(x)$ the symmetry-breaking interaction term in the Lagrangian. We are interested in particular in an interaction due to the presence of massless gauge fields that is considered weak (in particular nonconfining) at the scale under consideration, so that its effect can be considered as a perturbation. These external gauge fields couple to some linear combinations of the currents of the global symmetry group G. For a single gauge field $\mathcal{W}^\mu$, this interaction reads

$$\begin{aligned}\mathcal{L}_{\mathrm{int}} &= -ig_{\mathcal{W}}\mathcal{W}^\mu\mathcal{J}_\mu^{\mathcal{W}},\\ \mathcal{J}_\mu^{\mathcal{W}} &= \frac{1}{2}(\Omega_\varepsilon)_{ij}[\varepsilon\bar{\psi}_i\bar{\sigma}_\mu T^{\mathcal{W}}\psi_j - \psi_i\sigma_\mu(T^{\mathcal{W}})^T\bar{\psi}_j],\end{aligned} \tag{2.26}$$

where $T^{\mathcal{W}}$ is an element of the algebra of G. At first nontrivial order in the corresponding coupling $g_{\mathcal{W}}$, one has

$$\Delta\mathcal{L}(x) = \frac{g_{\mathcal{W}}^2}{2}\int\frac{d^4q}{(2\pi)^4}\frac{\eta^{\mu\nu}}{q^2}\int d^4y e^{iq\cdot y}T\{\mathcal{J}_\mu^{\mathcal{W}}(x+y)\mathcal{J}_\nu^{\mathcal{W}}(x)\}. \tag{2.27}$$

Decomposing $T^{\mathcal{W}}$ as $T^{\mathcal{W}} = T^W + T^{\hat{W}}$, where T^W ($T^{\hat{W}}$) is a linear combination of the generators T^A ($T^{\hat{A}}$) of H_m (of G/H_m), and taking further the soft-Goldstone-boson limit in Eq. (2.25), then results in the following expressions for the mass shifts [31,48]

$$\begin{aligned}\Delta M_{G_{\hat{A}}}^2 = &-\frac{3}{4\pi}\times\frac{1}{F_G^2}\times\frac{g_{\mathcal{W}}^2}{4\pi}\times\int_0^\infty dQ^2Q^2\Pi_{V-A}(-Q^2)\\ &\times\left[\sum_{\hat{B}}(f^{\hat{A}W\hat{B}})^2 - \sum_B(f^{\hat{A}\hat{W}B})^2\right].\end{aligned} \tag{2.28}$$

Again, F_G refers to the Goldstone-boson decay constant in the limit where any explicit symmetry-breaking effects vanish, see Eq. (2.22), and we have used the short-hand notation

$$\mathrm{Tr}(T^W[T^{\hat{A}}, T^{\hat{B}}]) \equiv \frac{1}{2i} f^{\hat{A}W\hat{B}},$$
$$\mathrm{Tr}(T^{\hat{W}}[T^{\hat{A}}, T^B]) \equiv \frac{1}{2i} f^{\hat{A}\,\hat{W}\,B}, \tag{2.29}$$

with the generators normalized as in Eq. (2.3). Since, according to the Witten inequality [39], $-Q^2\Pi_{V-A}(-Q^2)$ is positive, the sign of $\Delta M^2_{G_{\hat{A}}}$, and hence the misalignment of the vacuum, hinges on the sign of the last factor on the right-hand side of Eq. (2.28). If it is positive, $\Delta M^2_{G_{\hat{A}}}$ is positive, and the vacuum is stable under this perturbation by a weak gauge field. If it is negative, then $\Delta M^2_{G_{\hat{A}}}$ is negative, which signals the instability of the unperturbed vacuum under this perturbation. In particular, if the gauge field couples only to the currents $\mathcal{J}^A_\mu$ corresponding to the unbroken generators (i.e. $T^{\hat{W}} = 0$), then $\Delta M^2_{G_{\hat{A}}} \geq 0$. This is the case, for instance, of the electromagnetic field in QCD, which gives the charged pions a positive mass [49] (see also the discussion in Ref. [50]),

$$\Delta M^2_{\pi^\pm} = -\frac{3}{4} \times \frac{1}{F_\pi^2} \frac{\alpha}{\pi} \times \int_0^\infty dQ^2 Q^2 \Pi^{\mathrm{QCD}}_{V-A}(-Q^2), \tag{2.30}$$

while the neutral pion remains massless. If several gauge fields are present, the total mass shift is given by a sum of contributions of the type (2.28), one for each gauge field, and the stability of the vacuum may then also depend on the relative strengths of the various gauge couplings. For instance, if a subgroup H_W of H_m is gauged, and if the Goldstone bosons transform as an irreducible representation R_W under H_W, the (positive) induced mass shift can be expressed [48] in terms of the quadratic Casimir invariant of H_W for the representation R_W,

$$\Delta M^2_{G_{\hat{A}}} = -\frac{3}{4\pi} \times \frac{1}{F_G^2} \times \frac{g^2_{\mathcal{W}}}{4\pi} \times \int_0^\infty dQ^2 Q^2 \Pi_{V-A}(-Q^2) \times C_2^{(H_W)}(R_W). \tag{2.31}$$

The expression (2.28) can also be rewritten as a contribution to the effective potential induced by a gauge-field loop. In terms of the Goldstone field

$$U(x) = e^{iG(x)/F_G}\Sigma_\varepsilon, \qquad G(x) = 2\sum_{\hat{A}} G^{\hat{A}}(x) T^{\hat{A}}, \tag{2.32}$$

the relevant terms of the effective low-energy Lagrangian read [51]

$$\mathcal{L}_{\mathrm{eff}} = \frac{F_G^2}{4}\langle \partial_\mu U^\dagger \partial^\mu U\rangle - C_{\mathcal{W}}\langle T^{\mathcal{W}} U (T^{\mathcal{W}})^T U^\dagger\rangle + \cdots, \tag{2.33}$$

with $\langle\cdots\rangle$ denoting the flavor trace, and

$$C_{\mathcal{W}} = -\frac{3}{8\pi} \times \frac{g^2_{\mathcal{W}}}{4\pi} \times \int_0^\infty dQ^2 Q^2 \Pi_{V-A}(-Q^2). \tag{2.34}$$

As a side remark, let us notice that the procedure used here in order to determine the induced mass shifts of the Goldstone bosons can also be applied in the case where $\Delta\mathcal{L}$ in Eq. (2.25) stands for a mass term for the fermions, e.g.

$$\Delta_m \mathcal{L} = -2\sqrt{N_f} m \mathcal{S}^0. \tag{2.35}$$

Going successively through the same steps, one then reproduces the expression given in Eq. (2.21).

We now turn to the second issue, namely the matrix element for the transition of a Goldstone bosons into a pair of external gauge bosons with zero virtualities. At lowest order in the gauge couplings, and for $q^2 = (p-q)^2 = 0$, this matrix element reads

$$g^2_{\mathcal{W}} \times i \int d^4x e^{iq\cdot x}\langle \mathrm{vac}|T\{\mathcal{J}^{\mathcal{W}}_\mu(x)\mathcal{J}^{\mathcal{W}}_\nu(0)\}|G^{\hat{A}}(p)\rangle = -\frac{g^2_{\mathcal{W}} d_{HC}}{8\pi^2 F_G}\epsilon_{\mu\nu\rho\sigma} q^\rho p^\sigma d^{WW\hat{A}}[1 + \mathcal{O}(m)], \tag{2.36}$$

with $d^{WW\hat{A}} \equiv 2\mathrm{Tr}(\{T^W, T^W\}T^{\hat{A}})$, and d_{HC} denotes the dimension of the representation of the hypercolor gauge group to which the fermions making up the current $\mathcal{J}^{\mathcal{W}}_\mu(x)$ belong. Here we are assuming (this will be the case of interest in the context of the composite Higgs models discussed below) that only generators of H_m are weakly coupled to the external gauge fields (i.e. $T^{\hat{W}} = 0$). The expression on the right-hand side is then obtained by saturating the Ward identity in Eq. (2.4) with the Goldstone poles. Again, if the fermions are given masses, there are corrections, indicated as $\mathcal{O}(m)$. At the level of the low-energy theory, this coupling is reproduced by the Wess-Zumino-Witten effective action [52–54]. Writing only the relevant term, one has

$$\mathcal{L}^{\mathrm{WZW}}_{\mathrm{eff}} = -\frac{g^2_{\mathcal{W}} d_{HC}}{64\pi^2 F_G}\epsilon_{\mu\nu\rho\sigma}\mathcal{W}^{\mu\nu}(x)\mathcal{W}^{\rho\sigma}(x) \times \sum_{\hat{A}} d^{WW\hat{A}} G^{\hat{A}}(x) + \cdots. \tag{2.37}$$

III. THE ELECTROWEAK SECTOR

In this section, we analyze a composite model for the Higgs sector of the SM. We consider a flavor symmetry group $G = SU(4) \simeq SO(6)$, spontaneously broken towards a subgroup $Sp(4) \simeq SO(5)$. The five Goldstone bosons transform as $(1_L, 1_R) + (2_L, 2_R)$ under the custodial symmetry $SU(2)_L \times SU(2)_R \subset Sp(4)$, corresponding to a real scalar singlet plus the complex Higgs doublet. Composite Higgs models based on this coset have been studied in Refs. [55–57], as effective theories with a

nonspecified strongly-coupled dynamics. A simple UV completion is provided by a gauge theory with four Weyl fermions ψ^a in a pseudoreal representation of the gauge group, and which form a condensate $\langle\psi^a\psi^b\rangle \neq 0$. Such a theory was considered in Refs. [7,9,13,58], as a minimal hypercolor model. The first analysis of the low energy dynamics of this theory in terms of four-fermion interactions (à la NJL) was provided in Ref. [8]. We extend this former study by deriving additional phenomenological predictions. We will particularize the general results of Sec. II to this specific case, and in addition we will compute the masses of the spin-zero and spin-one bound states, as well as their decay constants, by using NJL techniques.

A. Scalar interactions of fermion bilinears and the mass gap

Let us consider a $Sp(2N)$ hypercolor gauge theory and introduce four Weyl spinors ψ^a, in the fundamental representation of $Sp(2N)$, which is pseudoreal. The transformation properties of these elementary fermions are summarized in Table I. The dynamics of the $SU(4)/Sp(4)$ spontaneous symmetry breaking can be studied in terms of four-fermion interactions, constructed out of hypercolor-invariant, spin-zero fermion bilinears, in a NJL-like manner [22–25]. The Lagrangian reads [8]

$$\mathcal{L}^{\psi}_{\rm scal} = \frac{\kappa_A}{2N}(\psi^a\psi^b)(\bar\psi_a\bar\psi_b) - \frac{\kappa_B}{8N}[\epsilon_{abcd}(\psi^a\psi^b)(\psi^c\psi^d) + \text{H.c.}], \quad (3.1)$$

where $a, b, \cdots = 1, 2, 3, 4$ are $SU(4)$ indices, ϵ_{abcd} is the Levi-Civita symbol and $\kappa_{A,B}$ are real, dimensionful couplings. The phase of κ_B can be absorbed by the phase of ψ, so that we may take κ_B real and positive without loss of generality.[4] Each fermion bilinear between brackets is contracted into a Lorentz and $Sp(2N)$ invariant quantity. The hypercolor-invariant contraction is defined as

$$(\psi^a\psi^b) \equiv \psi^a_i\Omega_{ij}\psi^b_j = -(\psi^b\psi^a), \quad (3.2)$$

where Ω is the antisymmetric $2N \times 2N$ matrix

$$\Omega = \begin{pmatrix} 0 & \mathbb{1}_N \\ -\mathbb{1}_N & 0 \end{pmatrix}. \quad (3.3)$$

The antisymmetry of the hypercolor contraction implies antisymmetry in the flavor $SU(4)$ indices. Other four-fermion interactions, involving spin-one fermion bilinears, are irrelevant for the discussion of spontaneous symmetry breaking. We will introduce them later, in Sec. III C, when we discuss spin-one resonances.

TABLE I. The transformation properties of the elementary fermions, and of the spin-0 and spin-1 fermion bilinears, in the electroweak sector of the model. Spinor indexes are understood, and brackets stand for a hypercolor-invariant contraction of the $Sp(2N)$ indexes.

	Lorentz	$Sp(2N)$	$SU(4)$	$Sp(4)$
ψ^a_i	$(1/2,0)$	$\square_i$	4^a	4
$\bar\psi_{ai} \equiv \psi^\dagger_{aj}\Omega_{ji}$	$(0,1/2)$	$\square_i$	$\bar 4_a$	4^*
$M^{ab} \sim (\psi^a\psi^b)$	(0,0)	1	6^{ab}	$5+1$
$\bar M_{ab} \sim (\bar\psi_a\bar\psi_b)$	(0,0)	1	$\bar 6_{ab}$	$5+1$
$a^\mu \sim (\bar\psi_a\bar\sigma^\mu\psi^a)$	$(1/2,1/2)$	1	1	1
$(V^\mu, A^\mu)^b_a \sim (\bar\psi_a\bar\sigma^\mu\psi^b)$	$(1/2,1/2)$	1	15^a_b	$10+5$

Note that for $\kappa_B = 0$ there is an additional global $U(1)_\psi$ symmetry, which reflects a classical invariance of the $Sp(2N)$ gauge theory, the associated Noether current being

$$\mathcal{J}^0_{\psi\mu} = -\frac{1}{2}\Omega_{ij}[\bar\psi_i\bar\sigma_\mu\psi_j + \psi_i\sigma_\mu\bar\psi_j], \quad (3.4)$$

as follows from Eq. (2.1) upon taking $\varepsilon = -1$ and a singlet generator normalized to $\mathbb{1}_4$. At the quantum level, this current has a hypercolor gauge anomaly,

$$\partial^\mu\mathcal{J}^0_{\psi\mu} = \frac{N^\psi_f g^2_{HC}}{32\pi^2}\sum_{I=1}^{N(2N+1)}\epsilon_{\mu\nu\rho\sigma}G^{I,\mu\nu}_{HC}G^{I,\rho\sigma}_{HC}, \quad (3.5)$$

and the corresponding symmetry is explicitly broken by instantons [59,60]. Here $N^\psi_f = 2$ denotes the number of Dirac flavors. The effect of the instantons can be represented by an effective vertex [59–61] that breaks the $U(1)_\psi$ invariance. The important observation here is that for $2N^\psi_f = 4$ Weyl fermions in the fundamental representation of the $Sp(2N)$ gauge group, this effective vertex is precisely given by the term proportional to κ_B. It is both quartic in the fermion fields, which provides the amount of $U(1)_\psi$ breaking required, for $N^\psi_f = 2$, by the index theorem and the instanton solution with unit winding number, and invariant under the $SU(4)$ global symmetry [62]. It plays the same role as the analogous six-fermion 't Hooft determinant effective Lagrangian [59–61] for QCD with three flavors, which parametrizes the instanton-induced anomaly interactions, explaining an η' mass much larger than the masses of the other Goldstone boson states. Such a term was originally constructed in the quark model [63], and later also introduced in the NJL model [64,65], see also [66]. Similarly, in the present case, $\kappa_B \neq 0$ is, therefore, crucial in order to evade the additional $U(1)_\psi$ Goldstone boson.

[4] In comparison to Ref. [8], we choose an opposite sign for κ_B, and a different but equivalent vacuum alignment defined by Eq. (3.6). Combining these two different conventions, the mass gap defined by Eq. (3.17) has the same expression as in Ref. [8]. This is because the two vacua are related by a $U(4)$ transformation with determinant minus one, that changes the sign of ϵ_{abcd}.

While this picture is essentially correct when considering the electroweak $SU(4)$ sector in isolation, we stress that it will be significantly modified when a colored sector is introduced, in order to provide composite partners for the top quark, as we will discuss in Sec. IV. This sector also has an anomalous extra $U(1)_X$ symmetry, but one linear combination of the two $U(1)$ currents remains anomaly free, which implies that the effective 't Hooft determinant term is no longer given by the κ_B operator. This will have some important consequences on the spectrum of resonances, but at a first stage we prefer to neglect the mixing with the colored sector, as the results are much more transparent and it will be easy to generalize them.

We assume that the $SU(4)$ global symmetry is exact, that is, we work in the chiral limit where ψ^a has no elementary mass term. The $SU(4)$ Noether currents are given by Eq. (2.1), with $\Omega_\epsilon = \Omega$ defined in Eq. (3.3). The $SU(4)$ generators decompose into five broken ones, $T^{\hat{A}}$, living in the $SU(4)/Sp(4)$ coset, and ten unbroken ones, T^A, whose explicit expressions are given in Appendix A. They satisfy the conditions spelled out in Eq. (2.2), where Σ_ϵ stands for

$$\Sigma_0 \equiv \begin{pmatrix} 0 & 0 & 1 & 0 \\ 0 & 0 & 0 & 1 \\ -1 & 0 & 0 & 0 \\ 0 & -1 & 0 & 0 \end{pmatrix}. \tag{3.6}$$

By introducing in a standard manner [8,24,25] an auxiliary (antisymmetric) scalar field M, transforming as a gauge singlet and a flavor $SU(4)$ sextet, the Lagrangian (3.1) can be rewritten equivalently as

$$\begin{aligned}\mathcal{L}^{\psi}_{scal} = &-\frac{1}{\kappa_A+\kappa_B}\left[\left(\kappa_A M^*_{ab} - \frac{\kappa_B}{2}\epsilon_{abcd}M^{cd}\right)(\psi^a\psi^b) + \text{H.c.}\right] \\ &- \frac{2N\kappa_A}{(\kappa_A+\kappa_B)^2}M^{ab}M^*_{ab} \\ &+ \frac{1}{2}\frac{N\kappa_B}{(\kappa_A+\kappa_B)^2}(\epsilon_{abcd}M^{ab}M^{cd} + \text{H.c.}),\end{aligned} \tag{3.7}$$

where the equation of motion for M gives

$$M^{ab} = -\frac{\kappa_A+\kappa_B}{2N}(\psi^a\psi^b). \tag{3.8}$$

The matrix field M, being complex and antisymmetric, can always be rotated by an $SU(4)$ transformation into the form

$$M = \begin{pmatrix} 0 & 0 & m_1 & 0 \\ 0 & 0 & 0 & m_2 \\ -m_1 & 0 & 0 & 0 \\ 0 & -m_2 & 0 & 0 \end{pmatrix}. \tag{3.9}$$

Once a $(\psi^a\psi^b)$ condensate forms, M acquires a vacuum expectation value (vev) and the Yukawa couplings induce dynamical fermion masses. One can derive from Eq. (3.7) the one-loop Coleman-Weinberg effective potential [67], by integrating over fermions, and study the occurrence of spontaneous symmetry breaking by looking for a nontrivial minimum with $\langle m_{1,2}\rangle \neq 0$ [8]. One finds that spontaneous symmetry breaking is only possible for $2\langle m_1\rangle = 2\langle m_2\rangle \equiv M_\psi$, in agreement with the Vafa-Witten theorem. Below we provide an alternative derivation of the same result, which will also be useful for studying the spectrum of scalar resonances.

It is convenient to introduce the combination

$$\overline{M}_{ab} = \frac{1}{\kappa_A+\kappa_B}\left(\kappa_A M^*_{ab} - \frac{\kappa_B}{2}\epsilon_{abcd}M^{cd}\right), \tag{3.10}$$

which can be expanded around the vacuum as

$$\overline{M} = \frac{1}{2}M_\psi\Sigma_0 + (\sigma + i\eta')\Sigma_0 T^0_\psi + (S^{\hat{A}} + iG^{\hat{A}})\Sigma_0 T^{\hat{A}}. \tag{3.11}$$

The matrix $\overline{M}$ decomposes, according to $6_{SU(4)} = (1+5)_{Sp(4)}$, into a scalar singlet σ, a pseudoscalar singlet η', a scalar quintuplet $S^{\hat{A}}$, and a pseudoscalar quintuplet $G^{\hat{A}}$, which will be identified with the physical meson resonances. Using the identity $\epsilon_{abcd} = -(\Sigma_0)_{ab}(\Sigma_0)_{cd} + (\Sigma_0)_{ac}(\Sigma_0)_{bd} - (\Sigma_0)_{ad}(\Sigma_0)_{bc}$, and since, as already noted, κ_B can be taken real and positive without loss of generality, the Lagrangian (3.7) can be rewritten as

$$\mathcal{L}^{\psi}_{scal} = -(\psi\overline{M}\psi + \text{H.c.}) - N[P_-(\sigma^2 + G^2_{\hat{A}}) + P_+(\eta'^2 + S^2_{\hat{A}})], \tag{3.12}$$

where

$$P_\pm = \frac{\kappa_A}{\kappa_A^2-\kappa_B^2} \pm \frac{\kappa_B}{|\kappa_A^2-\kappa_B^2|} = \frac{1}{\kappa_A \mp \kappa_B}. \tag{3.13}$$

The sign in the last equality corresponds to the case $\kappa_A^2 > \kappa_B^2$, which will turn out to be the relevant region of parameter space. Eqs. (3.11) and (3.12) define the Feynman rules for the fermion Yukawa couplings to the mesons: the four-fermion interactions mediated by σ and $G^{\hat{A}}$ are proportional to P_-^{-1}, while the interactions mediated by η' and $S^{\hat{A}}$ are proportional to P_+^{-1}.

Indeed, the Lagrangian in Eq. (3.1) can be directly written in terms of the fermion bilinears coupled to the mesons, upon using Fierz identities for $SU(4)$ and $Sp(4)$, derived in Appendix D. The replacements $\delta^c_a\delta^d_b - \delta^d_a\delta^c_b = 4(\Sigma_0 T^0_\psi)_{ab}(T^0_\psi\Sigma_0)^{cd} + 4(\Sigma_0 T^{\hat{A}})_{ab}(T^{\hat{A}}\Sigma_0)^{cd}$ and $\epsilon_{abcd} = -4(\Sigma_0 T^0_\psi)_{ab}(\Sigma_0 T^0_\psi)_{cd} + 4(\Sigma_0 T^{\hat{A}})_{ab}(\Sigma_0 T^{\hat{A}})_{cd}$ in Eq. (3.1), lead to

$$\mathcal{L}^{\psi}_{scal} = 2\frac{\kappa_A}{(2N)}[(\psi\Sigma_0 T^0_\psi\psi)(\bar\psi T^0_\psi\Sigma_0\bar\psi) + (\psi\Sigma_0 T^{\hat A}\psi)(\bar\psi T^{\hat A}\Sigma_0\bar\psi)] + \frac{\kappa_B}{(2N)}[(\psi\Sigma_0 T^0_\psi\psi)(\psi\Sigma_0 T^0_\psi\psi) - (\psi\Sigma_0 T^{\hat A}\psi)(\psi\Sigma_0 T^{\hat A}\psi) + \text{H.c.}]. \quad (3.14)$$

Most of the resonance spectrum calculations could be performed directly from the four-fermion interactions in Eq. (3.14). Nonetheless, the introduction of auxiliary fields is convenient, because Eq. (3.11) identifies the relevant scalar degrees of freedom, which will become dynamical resonances upon $1/N$ resummation of the interactions in their respective channels, as we will examine below.

The first important step for the dynamical calculations of the resonance spectrum is to determine the mass gap, namely whether a nontrivial dynamical fermion mass, signalling the spontaneous breaking of $SU(4)$ to $Sp(4)$, develops within the NJL approximation. Let us consider the self-consistent mass gap equation [22,24,25], obtained from the one-loop tadpole graph, as illustrated in Fig. 1. It is well known that this is equivalent to computing the minimum of the one-loop effective potential. Note that, just like for the standard NJL model, only the σ exchange does contribute, namely only the spin-zero, parity-even, $Sp(4)$-singlet fermion bilinear can take a vev. Therefore, the mass-gap equation involves solely the inverse coupling P_-. The computation of the diagrams in Fig. 1 leads to a self-consistent condition on the dynamical fermion mass M_ψ,

$$-iM_\psi = 2\left(i\frac{2P_-^{-1}}{8(2N)}\right)(-2)\mathrm{Tr}[\Omega^2]\mathrm{Tr}[\Sigma_0^2] \times \int^\Lambda \frac{d^4k}{(2\pi)^4}\frac{iM_\psi}{k^2 - M_\psi^2 + i\varepsilon}, \quad (3.15)$$

where the first factor 2 accounts for the normalization $M_\psi \equiv 2\langle m_{1,2}\rangle$, (-2) is the trace over Weyl spinor indices in the loop, $\mathrm{Tr}[\Omega^2] = -2N$ is the trace over hypercolor, and $\mathrm{Tr}[\Sigma_0^2] = -4$ the one over flavor. Note that the factors $2N$ cancel, thanks to the appropriate large-N normalization of the original couplings $\kappa_{A,B}$ in Eq. (3.14). Thus, one obtains

$$1 - 4P_-^{-1}\tilde A_0(M_\psi^2) = 0, \quad (3.16)$$

where the basic one-loop scalar integral $\tilde A_0$ is defined in Appendix B. In order to regularize the otherwise divergent integral, we introduce a (covariant four-dimensional) cutoff Λ, which parametrizes the scale at which the effective four-fermion interaction ceases to be valid and all degrees of freedom of the underlying gauge theory become relevant. Computing the integral, the gap equation takes the explicit form

$$1 - \frac{M_\psi^2}{\Lambda^2}\ln\left(\frac{\Lambda^2 + M_\psi^2}{M_\psi^2}\right) = \frac{4\pi^2}{\Lambda^2}P_- \equiv \frac{1}{\xi}, \quad (3.17)$$

in full agreement with the minimization of the one-loop effective potential in Ref. [8].

Equation (3.17) has a nontrivial solution, $M_\psi \neq 0$, as long as $\xi > 1$, which implies $\kappa_A^2 > \kappa_B^2$ and $P_-^{-1} = \kappa_A + \kappa_B > 4\pi^2/\Lambda^2$. The existence of a minimal, critical coupling to realize spontaneous symmetry breaking is a characteristic property of the NJL model. On the other hand, the consistency requirement $M_\psi/\Lambda \lesssim 1$ implies an upper bound on the coupling, $\xi \equiv \Lambda^2(\kappa_A+\kappa_B)/(4\pi^2) \lesssim (1-\ln 2)^{-1} \simeq 3.25$, see also Fig. 3 below. Note that if the underlying $Sp(2N)$ gauge theory confines, it necessarily breaks $SU(4)$ into $Sp(4)$ as a consequence of the anomaly matching discussed in Sec. II B, because the fermions ψ cannot form baryons. This means that the true strong dynamics has to correspond to a supercritical value of $\kappa_A + \kappa_B$. This conclusion holds for the ψ sector in isolation, but it may not be the case when a colored X sector will be added in Sec. IV, and baryons become possible, see the discussion in Sec. IV A. Note also that, in the NJL large-N approximation, the mass gap M_ψ and the fermion condensate,

$$\frac{1}{2}\langle(\psi^a\psi^b) + (\bar\psi^a\bar\psi^b)\rangle \equiv \langle\Psi\Psi\rangle\Sigma_0^{ab}, \qquad \langle\Psi\Psi\rangle = \frac{1}{\sqrt{N_f^\psi}}\langle S_0^\psi\rangle, \quad (3.18)$$

corresponding to the tadpole in Fig. 1, are trivially related:

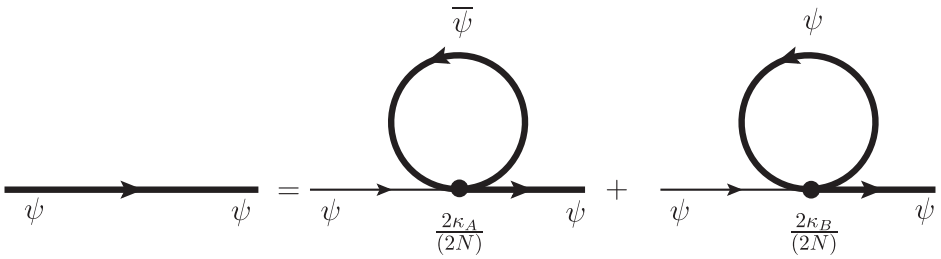

FIG. 1. Graphical illustration of the mass gap equation, in the leading $1/N$-approximation. Thick and thin lines represent dressed and bare fermion propagators, respectively.

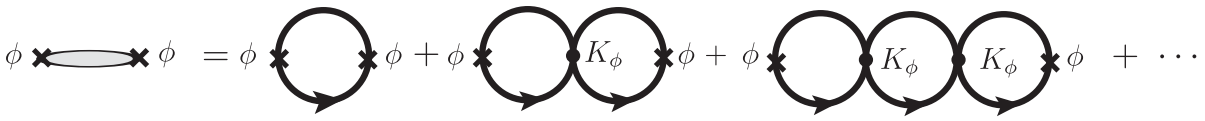

FIG. 2. Resummation of leading $1/N$ graphs for a mesonic two-point correlator, corresponding to a composite meson exchange.

$$\langle \Psi\Psi \rangle \equiv -2(2N) M_\psi \tilde{A}_0(M_\psi^2) = -\frac{N}{\kappa_A + \kappa_B} M_\psi. \quad (3.19)$$

We have also indicated the direct relation between the quark condensate and the vacuum expectation value $\langle S_0^\psi \rangle$ of the singlet scalar density, at this level of NJL approximation, with S_0^ψ defined in Eq. (2.6).

B. Masses of scalar resonances

The masses and the couplings of the composite mesonic resonances can be computed, at first order in $1/N$, by performing the resummation of the dominant large-N graphs contributing to the two-point functions with the appropriate quantum numbers, according to a well-known procedure [22,24,25,66,68]. The resummation takes the form of a geometric series, as illustrated in Fig. 2. For the two-point functions defined in Eqs. (2.8) and (2.9), the outcome of this procedure translates into the generic formula

$$\bar{\Pi}_\phi(q^2) \equiv \frac{\tilde{\Pi}_\phi(q^2)}{1 - 2K_\phi \tilde{\Pi}_\phi(q^2)}, \quad (3.20)$$

where K_ϕ are combinations of the four-fermion couplings in Eq. (3.14). The expressions of K_ϕ and of the one-loop correlators $\tilde{\Pi}_\phi(q^2)$ have been collected in Table II. They involve the one-loop two-point function $\tilde{B}_0(q^2, M_\psi^2)$ defined in Appendix B. In this section, we will discuss the scalar and pseudoscalar channels, while the spin-one channels will be discussed in Sec. III D.

Before starting this discussion, we would like to make a few remarks on the resummed correlators, some of which being also relevant for the spin-one channels.

(i) Expression (3.20) is not applicable in this simple form in the pseudoscalar channel, $\phi = G^{\hat{A}}, \eta'$, due to the fact that, at one loop, the axial two-point function also receives a longitudinal part, which will then mix with the pseudoscalar two-point function when the resummation in Fig. 2 is performed. For the time being, we can ignore these aspects, which will be treated in detail in Sec. III E, and, in the meantime, we proceed with the general discussion of masses and couplings on the basis of Eq. (3.20).

(ii) The corresponding resonance masses M_ϕ are determined by the poles of the resummed propagators,

$$1 - 2K_\phi \tilde{\Pi}_\phi(q^2 = M_\phi^2) = 0. \quad (3.21)$$

In order to discuss some general features of this type of equation, let us point out that the functions $\tilde{\Pi}_\phi(q^2)$ can be defined in the cut complex q^2-plane, where the cut lies on the real positive axis and starts at $q^2 = 4M_\psi^2$. The cut results from a logarithmic branch point, so that the functions $\tilde{\Pi}_\phi(q^2)$ become multi-valued through analytic continuation across the cut. These properties simply reflect those of the function $\tilde{B}_0(q^2, M_\psi^2)$ itself. In general, Eq. (3.21) has solutions for complex values of q^2, lying on the second Riemann sheet, which are interpreted as resonances, generated dynamically through the resummation procedure.

TABLE II. The couplings K_ϕ and the expressions of the one-loop spin-0 and spin-1 two-point functions. We also give the expression of the mixed (one-loop) pseudoscalar-longitudinal axial correlator, that enters in the analysis of both the quintuplet and singlet sectors. The explicit calculation of the correlators $\tilde{\Pi}_\phi(q^2)$ is detailed in Appendix C.

ϕ	K_ϕ	$\tilde{\Pi}_\phi(q^2)$
$G^{\hat{A}}$ η'	$2(\kappa_A + \kappa_B)/(2N)$ $2(\kappa_A - \kappa_B)/(2N)$	$\tilde{\Pi}_P(q^2) = (2N)[\tilde{A}_0(M_\psi^2) - \frac{q^2}{2}\tilde{B}_0(q^2, M_\psi^2)]$
$S^{\hat{A}}$ σ	$2(\kappa_A - \kappa_B)/(2N)$ $2(\kappa_A + \kappa_B)/(2N)$	$\tilde{\Pi}_S(q^2) = (2N)[\tilde{A}_0(M_\psi^2) - \frac{1}{2}(q^2 - 4M_\psi^2)\tilde{B}_0(q^2, M_\psi^2)]$
V_μ^A	$-2\kappa_D/(2N)$	$\tilde{\Pi}_V(q^2) = \frac{1}{3}(2N)[-2M_\psi^2\tilde{B}_0(0, M_\psi^2) + (q^2 + 2M_\psi^2)\tilde{B}_0(q^2, M_\psi^2)]$
$A_\mu^{\hat{A}}$ a_μ	$-2\kappa_D/(2N)$ $-2\kappa_C/(2N)$	$\tilde{\Pi}_A(q^2) = \frac{1}{3}(2N)[-2M_\psi^2\tilde{B}_0(0, M_\psi^2) + (q^2 - 4M_\psi^2)\tilde{B}_0(q^2, M_\psi^2)]$ $\tilde{\Pi}_A^L(q^2) = -2(2N)M_\psi^2\tilde{B}_0(q^2, M_\psi^2)$
$A_\mu^{\hat{A}} - G^{\hat{A}}$ $a_\mu - \eta'$		$\tilde{\Pi}_{AP}(q^2) = -(2N)M_\psi\tilde{B}_0(q^2, M_\psi^2)$

(iii) Other solutions to Eq. (3.21) than poles on the second sheet are possible. For instance, there can exist a critical value $K_\phi^{\rm crit}$, such that if the coupling K_ϕ satisfies $K_\phi \geq K_\phi^{\rm crit} > 0$, then Eq. (3.21) possesses (in addition) a real solution $0 \leq M_\phi \leq 2M_\psi$ [69], corresponding to a two-fermion bound state. As we will see below, this situation arises in the singlet pseudoscalar channel (and also in the vector channel, but this time for $K_\phi \leq K_\phi^{\rm crit} < 0$). As K_ϕ moves towards $K_\phi^{\rm crit}$ from above, the bound-state mass moves from zero towards the value $2M_\psi$. When $K_\phi < K_\phi^{\rm crit}$, this solution of Eq. (3.21) moves back towards the origin, but now on the real axis of the second Riemann sheet, and thus becomes a "virtual-state" solution [69].

(iv) Another aspect concerning the solutions of Eq. (3.21) is intimately connected to the fact that, in order to make this equation meaningful, it has been necessary to introduce a regularization for the function $\tilde{B}_0(q^2, M_\psi^2)$. As a consequence, there are solutions corresponding to real, but negative, values of q^2, $q^2 = -M_{\text{gh-}\phi}^2 \gtrsim -3\Lambda^2$. These "ghost" singularities[5] of the functions $\bar{\Pi}_\phi(q^2)$ occur quite far from the physical region, and have only a small influence on, for instance, the values of the resonance masses. When determining the latter, we thus systematically discard them. But they have to be taken into account when considering more global properties of the functions $\bar{\Pi}_\phi(q^2)$, like the spectral sum rules of Sec. II D. These will be discussed within the framework of the NJL approximation below, in Sec. III G.

(v) From a practical point of view, resonance solutions to Eq. (3.21) will not be determined by looking for poles on the second sheet, but rather by solving a real equation as follows. We rewrite the denominator of Eq. (3.20) as $1-2K_\phi\tilde{\Pi}_\phi(q^2)=c_0^\phi(q^2)+c_1^\phi(q^2)q^2$, where the q^2 dependence of the coefficients $c_{0,1}^\phi(q^2)$ comes from the loop function $\tilde{B}_0(q^2, M_\psi^2)$ only, see table II. The meson mass is then defined implicitly by

$$M_\phi^2 = \text{Re}[g_\phi(M_\phi^2)],$$
$$g_\phi(q^2) \equiv -\frac{c_0^\phi(q^2)}{c_1^\phi(q^2)}. \tag{3.22}$$

The value M_ϕ obtained this way remains a good approximation to the mass given by the real part of the resonance pole, as long as the imaginary part of $g_\phi(M_\phi^2)$ remains small,

$$\left|\frac{\text{Im}[g_\phi(M_\phi^2)]}{\text{Re}[g_\phi(M_\phi^2)]}\right| < 1. \tag{3.23}$$

Indeed, the solution of Eq. (3.22) may be larger than the threshold, $M_\phi^2 > 4M_\psi^2$, so that the loop function $\tilde{B}_0(M_\phi^2, M_\psi^2)$ develops an imaginary part. This may happen in the case of the $Sp(4)$-singlet pseudoscalar state, see Eq. (3.26), and it always happens in the case of the nonsinglet scalar state, see Eq. (3.28). This imaginary part corresponds to the unphysical decay of a meson into two constituent fermions, and reflects the well known fact that the NJL model does not account for confinement. In what follows, it will be understood that resonance masses are defined as the solutions of Eq. (3.22) and, in order to define a consistency condition for the NJL approximation to be reliable, we will require that Eq. (3.23) holds. Note also that, when extracting the expressions of the pole masses, it will be often convenient to take advantage of the gap equation (3.16), in order to obtain a simpler form of the solutions.

After these general considerations, we now turn to the analysis of the scalar and pseudoscalar channels of the model. The functions $\tilde{\Pi}_{S/P}(q^2)$ correspond to the one-loop estimates of the two-point functions $\Pi_{S/P}(q^2)$ defined in Eq. (2.8). Notice that one needs $K_\phi \propto 1/N$, in order for the $1/N$-expansion to be well defined. Indeed, according to Sec. III A (see also Table II), we have $K_{\sigma,G} = 2(\kappa_A + \kappa_B)/(2N)$ and $K_{S,\eta'} = 2(\kappa_A - \kappa_B)/(2N)$.

Let us consider first the pseudoscalar channels, ignoring, for the time being, the issue of mixing with the longitudinal part of the axial correlator. After taking the traces and evaluating the momentum integral, the pseudoscalar two-point correlator in the $SU(4)$ sector takes the form

$$\tilde{\Pi}_P(q^2) = (2N)\left[\tilde{A}_0(M_\psi^2) - \frac{q^2}{2}\tilde{B}_0(q^2, M_\psi^2)\right]. \tag{3.24}$$

In the case of the Goldstone states $G^{\hat{A}}$, Eq. (3.21) becomes

$$\begin{aligned} &1 - 4\frac{(\kappa_A+\kappa_B)}{2N}\tilde{\Pi}_P(M_G^2) \\ &= 1 - 4(\kappa_A+\kappa_B)\left[\tilde{A}_0(M_\psi^2) - \frac{M_G^2}{2}\tilde{B}_0(M_G^2, M_\psi^2)\right] \\ &= 2M_G^2(\kappa_A+\kappa_B)\tilde{B}_0(M_G^2, M_\psi^2) = 0, \end{aligned} \tag{3.25}$$

and the term proportional to $\tilde{A}_0$ cancels out upon using the mass-gap equation, Eq. (3.16), a well-known feature of the standard NJL model [22,24]. As a consequence, one is left with an exactly massless inverse propagator, $M_G = 0$, as it should be for the Goldstone boson state.

A similar computation for the $Sp(4)$-singlet pseudoscalar η', using the information provided by Table II, leads to

[5]These pathologies are absent if the Pauli-Villars regularization is adopted [70], but they reappear in another guise.

$$M_{\eta'}^2 = g_{\eta'}(M_{\eta'}^2) = \frac{2\tilde{A}_0(M_\psi^2)}{\tilde{B}_0(M_{\eta'}^2, M_\psi^2)}\left(1 - \frac{P_+}{P_-}\right) = -\frac{\kappa_B}{\kappa_A^2 - \kappa_B^2}\frac{1}{\tilde{B}_0(M_{\eta'}^2, M_\psi^2)}, \tag{3.26}$$

where we have again used Eq. (3.16). In the above equation and in the following expressions of the resonance masses, it is implicitly assumed that only the real part of $g_\phi(M_\phi^2)$ is taken into account, according to Eq. (3.22). Note that the constraint $\kappa_A^2 > \kappa_B^2$, needed for the existence of a nontrivial solution of the gap equation, also ensures that $M_{\eta'}^2$ is positive. As it will be discussed in subsection V E, a similar but stronger constraint holds when the colored sector is introduced. To roughly estimate the expected range for $M_{\eta'}$, one may notice that $\tilde{B}_0(q^2, M_\psi^2)$ is real and has a rather moderate q^2 dependence for $q^2 \ll 4M_\psi^2$, so that if $M_{\eta'}^2$ lies in this range, one can use the approximate expression

$$M_{\eta'}^2 \simeq -\frac{\kappa_B}{\kappa_A^2 - \kappa_B^2}\frac{1}{\tilde{B}_0(0, M_\psi^2)} \simeq \frac{4}{\xi}\frac{\kappa_B/\kappa_A}{1 - \kappa_B/\kappa_A}\frac{\Lambda^2}{\ln(\Lambda^2/M_\psi^2) - 1}, \tag{3.27}$$

where the expression for $\tilde{B}_0(0, M_\psi^2)$ is given in Eq. (B3). Thus $M_{\eta'}$ may become arbitrarily small for $\kappa_B/\kappa_A \to 0$, as the extra $U(1)_\psi$ symmetry is restored when $\kappa_B = 0$, and η' turns into the associated Goldstone boson. However, $M_{\eta'}$ rapidly increases with κ_B/κ_A to become of order Λ. Note that, in the large-N limit, one expects $M_{\eta'}^2 \sim 1/N$, as for the η' mass in QCD [71]. This indicates that the four-fermion couplings, normalized as in Eq. (3.1), should scale as $\kappa_B/\kappa_A \sim 1/N$. Large-$N$ arguments indicate that κ_A is N independent, as the associated four-fermion operator is generated from the hypercolor current-current interaction (for details see Appendix D 1). Therefore, the correct scaling is reproduced for $\kappa_B = \bar{\kappa}_B/(2N)$, with an N-independent $\bar{\kappa}_B$, and the associated four-fermion operator, induced by the hypercolor anomaly, scales as $1/N^2$.

For the scalar channels, the two-point function is to be found in Table II, and the corresponding scalar resonance masses are

$$M_\sigma^2 = 4M_\psi^2,$$
$$M_S^2 = 4M_\psi^2 + M_{\eta'}^2\frac{\tilde{B}_0(M_{\eta'}^2, M_\psi^2)}{\tilde{B}_0(M_S^2, M_\psi^2)} \simeq M_\sigma^2 + M_{\eta'}^2, \tag{3.28}$$

where one recognizes the same relation $M_\sigma = 2M_\psi$, as in the standard NJL model for QCD with two flavors. The relation $M_S^2 \simeq M_{\eta'}^2 + M_\sigma^2$ holds again if one can neglect the difference between the function $\tilde{B}_0(p^2, M_\psi^2)$ evaluated at $p^2 = M_{\eta'}^2$ and at $p^2 = M_S^2$.

We stress that all previous expressions for the spectrum of spin-zero resonances hold in the pure chiral limit, where the $SU(4)/Sp(4)$ Goldstone bosons $G^{\hat{A}}$, including the Higgs, are massless. Eventually, they will receive a nonzero effective potential, radiatively induced by the SM gauge and Yukawa couplings, which break explicitly the $SU(4)$ symmetry. In particular, the top quark Yukawa coupling is generically expected to destabilize the vacuum, and to trigger EWSB, see Refs. [27,28] for reviews. This implies that the masses of some resonances, obtained in the NJL large-N approximation, may receive corrections of order $\mathcal{O}(m_{\rm top}^2/\Lambda^2)$. These represent typically mild corrections for the non-Goldstone resonances, whose masses $\sim\Lambda$ are significantly larger than the electroweak scale. Thus, the qualitative features of the spectrum of meson resonances are not expected to depart from those exhibited here, once the effect of the explicit symmetry-breaking couplings is added to the picture. One should also remember that, in any case, the NJL large-N approximation already constitutes a limitation to the precision that can be achieved. The radiative contribution to the pseudo-Goldstone Higgs mass, induced from the external electroweak gauge fields, is given in Eq. (A7) (see also the general discussion in Sec. II E). However, this contribution plays a secondary role in EWSB: since it is positive, it cannot destabilize the $Sp(4)$-invariant vacuum, and it should be overcome by the one from the top Yukawa coupling [27,28].

In the traditional NJL literature [22,24,25,66], the resonance masses are determined from the resummed scattering amplitudes for $\psi\psi \to \psi\psi$ in the various channels. These amplitudes involve the same couplings K_ϕ and functions $\tilde{\Pi}_\phi(p^2)$ as in Eq. (3.20). Moreover, they also allow to define couplings between the elementary fermions and the resonances. The interested reader will find a brief discussion of these issues, not directly related to our main purposes, in Appendix C.

C. Vector interactions of fermion bilinears

Let us now consider vector bilinears, in order to study spin-one resonances. There are two independent four-fermion vector-vector operators, that can be written as

$$\mathcal{L}_{\rm vect}^{\psi} = \frac{\kappa_C'}{2N}(\bar{\psi}_a\bar{\sigma}^\mu\psi^a)(\bar{\psi}_b\bar{\sigma}_\mu\psi^b) + \frac{\kappa_D'}{2N}(\bar{\psi}_a\bar{\sigma}^\mu\psi^b)(\bar{\psi}_b\bar{\sigma}_\mu\psi^a), \tag{3.29}$$

where the coupling constants κ_C' and κ_D' are real. It turns out that consistent (nontachyonic) spin-one resonance masses are obtained for $\kappa_{C,D}' > 0$, in the same way as for the NJL vector interaction in QCD. Applying the $SU(4)$ Fierz identity given by Eq. (D22), the Lagrangian can be rewritten in the 'physical' channels, corresponding to definite $Sp(4)$ representations,

$$\mathcal{L}^{\psi}_{\rm vect} = \frac{\kappa_C}{2N}(\bar\psi T^0_\psi \bar\sigma^\mu \psi)^2 + \frac{\kappa_D}{2N}(\bar\psi T^A \bar\sigma^\mu \psi)^2 + \frac{\kappa_D}{2N}(\bar\psi T^{\hat A} \bar\sigma^\mu \psi)^2, \tag{3.30}$$

where $\kappa_D = 2\kappa'_D$, $\kappa_C = 8\kappa'_C + 2\kappa'_D$, and contracted flavor indexes are understood, as well as summations over generator labels A and $\hat A$. Introducing auxiliary vector fields, the vector sector Lagrangian takes the form

$$\begin{aligned}\mathcal{L}^{\psi}_{\rm vect} = &-a_\mu(\bar\psi T^0_\psi \bar\sigma^\mu \psi) - V^A_\mu(\bar\psi T^A \bar\sigma^\mu \psi) - A^{\hat A}_\mu(\bar\psi T^{\hat A} \bar\sigma^\mu \psi) \\ &- \frac{N}{2\kappa_C} a^\mu a_\mu - \frac{N}{2\kappa_D}(V^A_\mu V^{A\mu} + A^{\hat A}_\mu A^{\hat A\mu}),\end{aligned} \tag{3.31}$$

with vectors $V^A_\mu \sim 10_{Sp(4)}$, and axial vectors $(a_\mu, A^{\hat A}_\mu) \sim (1+5)_{Sp(4)}$. Their transformation properties are summarized in Table I. This Lagrangian defines the strength of the four-fermion interactions in the three physical channels mediated by a_μ, V^A_μ and $A^{\hat A}_\mu$.

We remark that additional spin-one resonances can be associated to the fermion bilinear $(\psi^a \sigma^{\mu\nu} \psi^b) \sim 10_{Sp(4)}$, or to its conjugate. However, one can check that the corresponding four-fermion interactions vanish because of Lorentz and/or $SU(4)$ invariance. Therefore, to describe these resonances one should consider higher-dimensional operators. Although such an exercise is feasible with analogous NJL techniques, it goes beyond the scope of this paper.

In general, the couplings κ_C and κ_D are additional free parameters with respect to those in the spin-zero sector, and in the following we will provide expressions for the vector masses and couplings as functions of these couplings. However, κ_C and κ_D may be related to the scalar sector coupling κ_A, if one assumes that the low-energy effective interactions, between two hypercolor-singlet fermion bilinears, originate from a one-hypergluon exchange current-current interaction, as determined by the underlying hypercolor gauge interaction. This may be justified in the large-N approximation (or equivalently 'ladder' approximation for the current-current interaction) and it proves to be a reasonably good approximation in the NJL-QCD case [66,72]. Under such an assumption, one can apply Fierz identities for Weyl, as well as for $SU(4)$ and $Sp(2N)$, indices, as detailed in Appendix D, in order to relate the coefficients of the various four-fermion operators. We obtain that the vector couplings of Eq. (3.30) are simply related to the scalar coupling of Eq. (3.14) by

$$\kappa_A = \kappa_C = \kappa_D. \tag{3.32}$$

An analogous relation holds in the NJL-QCD case [66], where the couplings of the scalar-scalar and vector-vector interactions are identical. We will use Eq. (3.32) as a benchmark for numerical illustration, however one should keep in mind that the true dynamics may appreciably depart from this naive relation.

D. Masses of vector resonances

The vector meson masses can be computed, at leading order in the $1/N$ expansion, similarly to the scalar meson channels, from the resummed two-point functions, and the geometric series illustrated in Fig. 2 now leads, in this approximation, to the following expressions for the vector or axial two-point correlators $\Pi_{V,A}(p^2)$ defined in Eq. (2.7),

$$\bar\Pi_{V/A}(q^2) \equiv -\frac{\tilde\Pi_{V/A}(q^2)}{q^2[1 - 2K_{V/A}\tilde\Pi_{V/A}(q^2)]}, \tag{3.33}$$

We have introduced one-loop correlators $\tilde\Pi_{V/A}(q^2)$ with a normalization that is more convenient for our purposes, so that $\tilde\Pi_{V/A}(q^2) \equiv -q^2\Pi_{V/A}(q^2)|_{1-\rm loop}$. Similarly, for the one-loop axial longitudinal part we have $\tilde\Pi^L_A(q^2) \equiv q^2\Pi^L_A(q^2)|_{1-\rm loop}$, where $\Pi^L_A(q^2)$ is defined in Eq. (2.18). More precisely, upon taking the traces over spinor indices, flavor and hypercolor, the one-loop two-point vector and axial correlators take the form,

$$\begin{aligned}\tilde\Pi^{\mu\nu,AB}_V(q) &= \tilde\Pi_V(q^2) T^{\mu\nu}\delta^{AB}, \\ \tilde\Pi^{\mu\nu,\hat A\hat B}_A(q) &= [\tilde\Pi_A(q^2) T^{\mu\nu} + \tilde\Pi^L_A(q^2) L^{\mu\nu}]\delta^{\hat A\hat B},\end{aligned} \tag{3.34}$$

where the transverse and longitudinal projectors are defined as

$$T^{\mu\nu} = \eta^{\mu\nu} - \frac{q^\mu q^\nu}{q^2}, \qquad L^{\mu\nu} = \frac{q^\mu q^\nu}{q^2}, \tag{3.35}$$

and where the expressions of the functions $\tilde\Pi_{V/A}(q^2)$ and $\tilde\Pi^L_A(q^2)$ are given in Table II. One should be cautious to adopt a regularization that preserves $SU(4)$ current conservation for the one-loop correlators, which is not the case with the standard NJL cutoff regularization. There are various ways to deal with this well-known problem [24], the simplest being to use dimensional regularization for the intermediate stages of the calculation. In this way the one-loop vector correlator is automatically transverse. In the final expression for the correlators, the formally divergent loop function $\tilde B_0$ can be written as a function of the $D = 4$ cutoff Λ, see Eq. (B4). The latter is then interpreted as the physical cutoff of the NJL model.

As compared to the two-point axial correlator in the massless limit, defined by Eq. (2.7), and as already mentioned in Sec. III B, the one-loop expression (3.34) also exhibits a longitudinal part. This is a specific trait of the NJL model, where the dynamically generated mass M_ψ acts here like an explicit symmetry-breaking term. We will come back later on the manner this longitudinal piece is

taken care of. For the time being, one may notice that the transverse part of the two-point axial correlator reproduces the expected physical features. Indeed, the resummed function $\bar{\Pi}_A(q^2)$ exhibits the massless pole[6] due to the contribution of the Goldstone bosons, but it also has a pole from the axial-vector state $A_\mu^{\hat{A}}$. This second pole mass is extracted from Eq. (3.21), by injecting the coupling[7] and the transverse part of the correlator, $\tilde{\Pi}_A(q^2)$. One obtains

$$M_A^2 = -\frac{3}{4\kappa_D \tilde{B}_0(M_A^2, M_\psi^2)} + 2M_\psi^2 \frac{\tilde{B}_0(0, M_\psi^2)}{\tilde{B}_0(M_A^2, M_\psi^2)} + 4M_\psi^2. \tag{3.36}$$

The pole mass equation for the axial vector singlet a_μ is obtained with the replacements $\kappa_D \to \kappa_C$ and $M_A \to M_a$.

The V_μ^A pole mass can likewise be extracted from Eq. (3.21), with the replacements $K_\phi \to K_V = -2\kappa_D/(2N)$ and $\tilde{\Pi}_\phi(p^2) \to \tilde{\Pi}_V(p^2)$. This leads to

$$M_V^2 = -\frac{3}{4\kappa_D \tilde{B}_0(M_V^2, M_\psi^2)} + 2M_\psi^2 \frac{\tilde{B}_0(0, M_\psi^2)}{\tilde{B}_0(M_V^2, M_\psi^2)} - 2M_\psi^2. \tag{3.37}$$

In estimating the sizes of the spin-one resonance masses, note that $\tilde{B}_0(p^2, M_\psi^2)$ is real for $0 \le p^2 \le 4M_\psi^2$, and negative in the physically relevant range of $0 < M_\psi^2 < \Lambda^2$, with $|\tilde{B}_0(p^2, M_\psi^2)| \ge |\tilde{B}_0(0, M_\psi^2)|$. The term proportional to $1/\kappa_D$ on the right-hand side of Eqs. (3.37) and (3.36) is positive for $\kappa_D > 0$, and gives the dominant contribution to $M_{V,A}$ for, roughly, $\kappa_D M_\psi^2 \lesssim 4\pi^2$, that is $(M_\psi/\Lambda)^2 \lesssim 1/\xi$ when one takes $\kappa_D \simeq \kappa_A \gg \kappa_B$. By neglecting the difference between $\tilde{B}_0(M_V^2, M_\psi^2)$ and $\tilde{B}_0(M_A^2, M_\psi^2)$, we obtain the usual NJL relation between the axial and vector masses,

$$M_A^2 \simeq M_V^2 + 6M_\psi^2. \tag{3.38}$$

When one adopts the exact self-consistent pole mass definitions, M_A is somewhat below the prediction of Eq. (3.38), by typically 5–10%. Also, the singlet mass M_a is equal to M_A when $\kappa_D = \kappa_C$ as in Eq. (3.32). As already mentioned in the general considerations at the beginning of Sec. III B, depending on the values of the couplings, one may have resonance masses satisfying $M_\phi^2 > 4M_\psi^2$, in which case $\tilde{B}_0(M_\phi^2, M_\psi^2)$ develops an imaginary part. Indeed, this is always the case for M_A, as one reads off Eq. (3.38). In such cases, the resonance mass is obtained upon solving Eq. (3.22), and we consider that the NJL predictions remain sensible as long as the width Γ_ϕ of the resonance, defined in Eq. (3.23), does not exceed its mass.

E. Goldstone decay constant and pseudoscalar-axial mixing

A key parameter of the composite sector is the Goldstone boson decay constant F_G, the analogous of F_π in QCD. We recall that, when the Higgs is a composite pseudo-Goldstone boson, the electroweak precision parameters, such as S, T (see Sec. III H), and the Higgs couplings receive corrections of order $(v/f)^2$ with respect to their SM value, where $v \simeq 246$ GeV and $f \equiv \sqrt{2}F_G$. Here f is the Goldstone decay constant in the normalization that is generally adopted in the composite Higgs literature.[8] Thus, f is the physical scale most directly constrained by precision measurements, $f \gtrsim (0.5\text{–}1)$ TeV, the exact bound depending on the spontaneous symmetry breaking pattern, as well as on the flavor representations of the spin-one and spin-one-half composite resonances coupled to the SM fields. Therefore, it will be convenient to express all the resonance masses in units of f, and in the following we will adopt the more conservative bound $f \gtrsim 1$ TeV.

The decay constant F_G, as defined by Eq. (2.22), can most directly be extracted from the two-point axial transverse correlator, introduced in Eq. (2.7), through the residue of the Goldstone boson pole. Identifying this correlator in the NJL approximation with the resummed correlator defined by Eq. (3.33) and using the explicit expression in Table II, one obtains

$$\begin{aligned} F_G^2 &= \lim_{q^2 \to 0} [-q^2 \bar{\Pi}_A(q^2)] \\ &= \frac{\tilde{\Pi}_A(0)}{1 - 2K_A \tilde{\Pi}_A(0)} = \frac{\tilde{F}_G^2}{1 - 2K_A \tilde{F}_G^2} = g_A(0) \tilde{F}_G^2, \end{aligned} \tag{3.39}$$

where we have defined the axial coupling form factor

$$g_A(q^2) \equiv [1 - 2K_A \tilde{\Pi}_A^L(q^2)]^{-1} = \left[1 + \frac{4\kappa_D}{2N} \tilde{\Pi}_A^L(q^2)\right]^{-1} \tag{3.40}$$

[6] As expected, such a massless pole does not occur in $\bar{\Pi}_V(q^2)$, defined in Eq. (3.33), since, as can be inferred from Table II, $\tilde{\Pi}_V(q^2)$ vanishes for $q^2 = 0$.

[7] Note the relative minus sign between the four-fermion couplings in the Lagrangian of Eq. (3.30) $K_A = -2\kappa_D/(2N)$, and the couplings $K_{V,A}$ that enter in the denominator of the resummed correlators in Eq. (3.33). This follows from the proper definition of the argument of the associated geometric series.

[8] The relation $f \equiv \sqrt{2}F_G$ follows from our definitions of F_G, see Eq. (2.22), and of the Goldstone matrix U, see Eq. (2.32). After the gauging of the SM group, the covariant derivative acting on the Goldstone bosons reads $D_\mu U = \partial_\mu U - i\mathcal{V}_\mu U - iU\mathcal{V}_\mu^\dagger$, where the external source $\mathcal{V}_\mu$ is defined by Eq. (A6). This determines the nonlinear corrections to the electroweak precision parameters in terms of v/f.

and the one-loop decay constant

$$\tilde{F}_G^2 \equiv \tilde{\Pi}_A(0) = -2(2N)M_\psi^2 \tilde{B}_0(0, M_\psi^2) = \tilde{\Pi}_A^L(0). \quad (3.41)$$

At this point, one should remark that $\tilde{F}_G$ would be the complete NJL result for the Goldstone decay constant only if one would consider the scalar sector in isolation, i.e. by switching off the axial vector coupling κ_D. However, since by definition the Goldstone boson couples to the axial current, a nonzero κ_D implies a nontrivial mixing of the pseudoscalar and axial vector channels, that affects the expression of the decay constant. In order to take into account this effect and to define consistently F_G, one needs to consider the resummed transverse axial-vector correlator $\bar{\Pi}_A(q^2)$ of Eq. (3.33), as shown in (3.39) above. This equation gives the complete NJL approximation for F_G, which should be matched with its experimental value, once it becomes available, as is the case of F_π in the NJL approximation of QCD [24,66].

The behavior of F_G is illustrated in Fig. 3, as a function of the dimensionless coupling ξ. Combining the definition of ξ in Eq. (3.17) with the explicit form of $\tilde{B}_0(0, M_\psi^2)$ given in Eq. (B3), one obtains

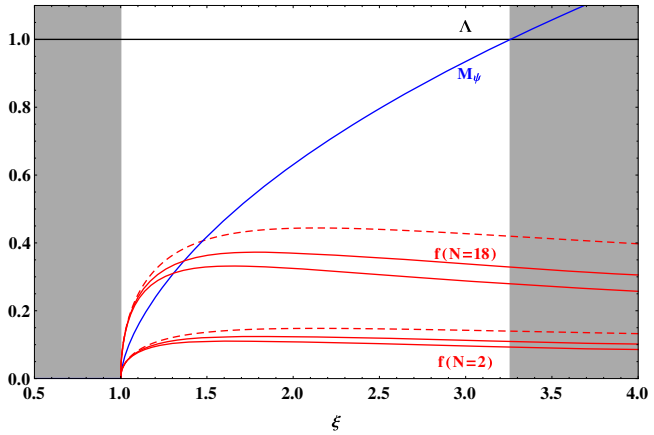

FIG. 3. The mass gap M_ψ and the Goldstone decay constant $f = \sqrt{2}F_G$, in units of the cutoff Λ, as a function of the dimensionless coupling $\xi \equiv (\kappa_A + \kappa_B)\Lambda^2/(4\pi^2)$. For $\xi \leq 1$ there is no spontaneous symmetry breaking, $M_\psi = 0$, while for $\xi \geq (1 - \ln 2)^{-1} \sim 3.25$ one has $M_\psi \gtrsim \Lambda$ and the NJL description is no longer reliable. The decay constant f is proportional to $\sqrt{N}$, where $Sp(2N)$ is the hypercolor gauge group. In the complete model including a colored sector (see Sec. IV), one finds that $N \geq 2$ is required to allow for fermion-trilinear top partners, and $N \leq 18$ is needed to preserve hypercolor asymptotic freedom [8]. One further needs $N \leq 6$ to avoid Landau poles in the SM gauge couplings below 100 TeV (see Sec. III F). The red dashed line indicates the nonresummed decay constant $\tilde{f} = \sqrt{2}\tilde{F}_G$, while the upper (lower) red solid line corresponds to the resummed f, for $\kappa_D = \kappa_A$ and $\kappa_B = 0$ ($\kappa_B = \kappa_A$).

$$\tilde{F}_G^2 = \frac{N}{4\pi^2}\Lambda^2\left(\frac{\xi - 1}{\xi} - \frac{M_\psi^2}{\Lambda^2 + M_\psi^2}\right). \quad (3.42)$$

Closely above the critical coupling, $\xi = 1$, the mass gap is much smaller than the cutoff, $M_\psi \ll \Lambda$, and $\tilde{F}_G$ grows rapidly with ξ. As $\xi - 1$ becomes of order one, the mass gap approaches the cutoff, $M_\psi \lesssim \Lambda$, while $\tilde{F}_G$ stops growing and remains below the cutoff by a factor of a few, $\tilde{f} \equiv \sqrt{2}\tilde{F}_G \simeq \sqrt{N}\Lambda/10$. The resummed F_G, see Eq. (3.39), is smaller, as K_A is negative. In Fig. 3 we assumed Eq. (3.32) to hold, so that $K_A = -4\pi^2\xi/[N\Lambda^2(1 + \kappa_B/\kappa_A)]$, which leads to $f \simeq (0.6\text{–}0.8)\tilde{f}$.

As already mentioned at several places in this section, a nonvanishing axial-vector coupling $\kappa_D \neq 0$ implies a nontrivial mixing between the pseudoscalar and the axial longitudinal channel. Therefore, the definition of the resummed pseudoscalar correlator $\bar{\Pi}_P(q^2)$ in Eq. (3.20) should be appropriately generalized in order to account for this mixing. In the process, we will also define a resummed axial longitudinal correlator $\bar{\Pi}_A^L(q^2)$, we will recover consistency relations among the Goldstone decay constants, and determine more precisely the properties of the non-Goldstone pseudoscalar η'. We discuss first the quintuplet $G - A^\mu$ mixing, while the similar analysis of the singlet $\eta' - a^\mu$ mixing is presented at the end of this section.

The mixing phenomenon is best described using a matrix formalism, so that we are led to consider

$$\mathbf{K}_G = \begin{pmatrix} K_G & 0 \\ 0 & K_A \end{pmatrix},$$
$$\Pi(q^2) = \begin{pmatrix} \tilde{\Pi}_P(q^2) & \sqrt{q^2}\tilde{\Pi}_{AP}(q^2) \\ \sqrt{q^2}\tilde{\Pi}_{AP}(q^2) & \tilde{\Pi}_A^L(q^2) \end{pmatrix}. \quad (3.43)$$

Explicit expressions for all the entries of these matrices can be found in Table II. Notice the appearance of $\tilde{\Pi}_{AP}(q^2)$, the one-loop expression of the mixed correlator $\Pi_{AP}(q^2)$ introduced in Eq. (2.15), and of the one-loop longitudinal axial correlator $\tilde{\Pi}_A^L(q^2)$ defined in Eq. (3.34). Note that, consistently with the normalization of $\tilde{\Pi}_A^L(q^2)$ in Eq. (3.34), the matrix $\mathbf{\Pi}(q^2)$ has been defined so that all its entries have the same dimensions, whence the factor of $\sqrt{q^2}$ in front of $\tilde{\Pi}_{AP}(q^2)$. The resummed large-N two-point matrix correlator $\bar{\mathbf{\Pi}}_G$ in this basis is then given by

$$\bar{\mathbf{\Pi}}_G \equiv \mathbf{\Pi} + \mathbf{\Pi}(2\mathbf{K}_G)\mathbf{\Pi} + \cdots = (\mathbb{1} - 2\mathbf{\Pi}\mathbf{K}_G)^{-1}\mathbf{\Pi}, \quad (3.44)$$

which is the analog of Eqs. (3.20) and (3.33). From Eqs (3.43), (3.44) one then obtains

$$\bar{\mathbf{\Pi}}_G(q^2) \equiv \begin{pmatrix} \bar{\Pi}_G(q^2) & \sqrt{q^2}\bar{\Pi}_{AG}(q^2) \\ \sqrt{q^2}\bar{\Pi}_{AG}(q^2) & q^2\bar{\Pi}_A^L(q^2) \end{pmatrix} = \frac{1}{D_G(q^2)} \begin{pmatrix} \tilde{\Pi}_P(q^2)[1-2K_A\tilde{\Pi}_A^L(q^2)] + 2K_A q^2\tilde{\Pi}_{AP}^2(q^2) & \sqrt{q^2}\tilde{\Pi}_{AP}(q^2) \\ \sqrt{q^2}\tilde{\Pi}_{AP}(q^2) & \tilde{\Pi}_A^L(q^2)[1-2K_G\tilde{\Pi}_P(q^2)] + 2K_G q^2\tilde{\Pi}_{AP}^2(q^2) \end{pmatrix}, \quad (3.45)$$

with

$$D_G \equiv \det(\mathbb{1} - 2\mathbf{\Pi}\mathbf{K}_G) = (1-2K_G\tilde{\Pi}_P)(1-2K_A\tilde{\Pi}_A^L) - 4K_G K_A q^2\tilde{\Pi}_{AP}^2 = 2(\kappa_A+\kappa_B)q^2\tilde{B}_0(q^2, M_\psi^2). \quad (3.46)$$

The last expression in this equation is obtained after using the gap-equation (3.16) and the relation $\tilde{\Pi}_{AP}^2(q^2) = -(1/2)(2N)\tilde{B}_0(q^2, M_\psi^2)\tilde{\Pi}_A^L(q^2)$. Using the relevant expressions in Table II, gives explicitly

$$\bar{\Pi}_G(q^2) = \frac{1}{2}(2N)\frac{2\tilde{A}_0(M_\psi^2)g_A^{-1}(q^2) - q^2\tilde{B}_0(q^2, M_\psi^2)}{D_G(q^2)}, \qquad \bar{\Pi}_{AG}(q^2) = \frac{\tilde{\Pi}_{AP}(q^2)}{D_G(q^2)}, \qquad \bar{\Pi}_A^L(q^2) = 0. \quad (3.47)$$

Note in particular that the *resummed* longitudinal axial correlator $\bar{\Pi}_A^L(q^2)$ vanishes identically, thus consistently recovering the conservation of the axial current in the exact chiral limit, in spite of the nonzero mass gap, which induces a nonvanishing longitudinal axial correlator at the one-loop level, $\tilde{\Pi}_A^L \propto M_\psi^2$. Also the resummed mixed correlator $\bar{\Pi}_{AG}(q^2)$ satisfies the relation (2.16), which shows that it is entirely saturated by the Goldstone-boson pole.

Now one can extract the NJL prediction for the Goldstone constants F_G and G_G, defined by Eqs. (2.22) and (2.23), respectively. The residue of $\bar{\Pi}_G(p^2)$ with respect to the Goldstone boson pole gives the pseudoscalar decay constant,

$$G_G^2 = -\lim_{q^2\to 0} q^2\bar{\Pi}_G(q^2) = -\frac{(2N)}{8(\kappa_A+\kappa_B)^2\tilde{B}_0(0, M_\psi^2)}g_A^{-1}(0). \quad (3.48)$$

Next, the residue of $\bar{\Pi}_{AG}(q^2)$ determines $F_G G_G$,

$$F_G G_G = -\lim_{q^2\to 0} q^2\bar{\Pi}_{AG}(q^2) = \frac{(2N)}{2}\frac{M_\psi}{(\kappa_A+\kappa_B)} = 2(2N)M_\psi\tilde{A}_0(M_\psi^2), \quad (3.49)$$

that satisfies Eq. (2.24), by taking the expression for $\langle S_0^\psi\rangle$ derived from Eq. (3.19). Combining Eqs. (3.48) and (3.49), and using the gap equation, one consistently recovers the very same expression of F_G in Eq. (3.39), as obtained from the resummed axial transverse correlator. Note that, if one had computed G_G in the limit of vanishing axial-vector coupling, $\kappa_D = 0$, by taking the residue of $\bar{\Pi}_P$ in Eq. (3.20), one would have missed the (inverse) axial form factor $g_A(0)$, see Eq. (3.48). Such a correction is important e.g. when analysing the possible saturation of the scalar spectral sum rules, which will be discussed in Sec. III G.

Obviously, a similar pseudoscalar-axial mixing mechanism also affects the singlet sector of the model, as soon as the axial singlet coupling κ_C is nonvanishing. The resummed correlator matrix for the singlet sector, $\bar{\mathbf{\Pi}}_{\eta'}$, is defined in complete analogy with Eq. (3.44), by taking the same one-loop correlator matrix $\mathbf{\Pi}$, but replacing the couplings, $K_G \to K_{\eta'}$ and $K_A \to K_a$ (i.e. $\kappa_D \to \kappa_C$), respectively, for the pseudoscalar and axial-vector channels, according to Table II. One main consequence of the mixing is that the pseudoscalar singlet mass $M_{\eta'}$ is modified with respect to Eq. (3.26), which holds for the pseudoscalar sector "in isolation." The η' mass rather corresponds to the pole of the determinant

$$D_{\eta'} \equiv \det(\mathbb{1} - 2\mathbf{\Pi}\mathbf{K}_{\eta'}) = (1-2K_{\eta'}\tilde{\Pi}_P)g_a^{-1} - 4K_{\eta'}K_a q^2\tilde{\Pi}_{AP}^2 = 8\kappa_B\tilde{A}_0(M_\psi^2)g_a^{-1} + 2(\kappa_A-\kappa_B)q^2\tilde{B}_0(q^2, M_\psi^2), \quad (3.50)$$

where we defined an axial singlet form factor,

$$g_a(q^2) = \left[1 + \frac{4\kappa_C}{2N}\tilde{\Pi}_A^L(q^2)\right]^{-1}, \quad (3.51)$$

in complete analogy with Eq. (3.40) for the nonsinglet sector. Therefore, Eq. (3.26) gets modified ("renormalized") by the (inverse) axial singlet form factor,

$$M_{\eta'}^2 = -\frac{\kappa_B}{\kappa_A^2-\kappa_B^2}\frac{1}{\tilde{B}_0(M_{\eta'}^2, M_\psi^2)}g_a^{-1}(M_{\eta'}^2), \quad (3.52)$$

which is the final expression that we will use in numerical illustrations of the mass spectrum in the next subsection.

F. The mass spectrum of the resonances

The resonance masses have to be proportional to the unique independent energy scale of the theory, which is conveniently choosen as $f \equiv \sqrt{2}F_G$, defined in Eq. (3.39), as explained above. In order to fix the ideas, one can take f just above the lower bound imposed by electroweak precision tests, which is conservatively given by $f = 1$ TeV. Since the resonance masses are N independent and $f \sim \sqrt{N}$, in principle the resonances become lighter and lighter in the large-N limit. However, if the model is augmented with colored fermions to provide top partners, as we will do in Sec. IV, the $Sp(2N)$ asymptotic freedom is lost (at one loop) for $N \geq 19$ [8]. Moreover, these colored fermions are also charged under $U(1)_Y$, resulting in Landau poles in the SM gauge couplings (α_1 and α_3) possibly too close to the condensation scale of the strong sector. A naive one-loop estimation of the running of the SM gauge couplings in presence of the hypercolor fermions leads to the appearance of Landau poles around 100 (500) TeV for $N = 6$ (5) while for $N = 4$, the Landau poles appear above 4×10^3 TeV. Then, a more reasonable interval for the number of hypercolors is $2 \leq N \leq 6$. For the numerical illustration, we take the conservative value $N = 4$.

The resonance masses are a function of the couplings $\kappa_{A,B,C,D}$ of the four-fermion operators. For the numerical illustration, we will assume Eq. (3.32) to hold, $\kappa_C = \kappa_D = \kappa_A$, and we will trade the two remaining, independent couplings for the dimensionless parameters $\xi \equiv (\kappa_A + \kappa_B)\Lambda^2/(4\pi^2)$ and κ_B/κ_A.

Let us describe the main feature of the mass spectrum. Since we work in the chiral limit approximation, the resonances are complete multiplets of the unbroken $Sp(4)$ symmetry, and the Goldstone bosons $G_{\hat{A}}$ are massless. In the spin-zero sector, there are three independent massive states: the singlet scalar σ and the five-plet scalar $S_{\hat{A}}$, see Eq. (3.28), as well as the singlet pseudoscalar η', see Eq. (3.26). The latter is the would-be Goldstone boson of the anomalous $U(1)_\psi$; therefore, $M_{\eta'}$ vanishes when this symmetry is restored, that is when $\kappa_B/\kappa_A \to 0$. In the spin-one sector, there are two independent masses: the singlet axial vector a^μ and the five-plet axial vector $A^\mu_{\hat{A}}$ are mass-degenerate as we assume $\kappa_C = \kappa_D$, with mass given by Eq. (3.36), while the ten-plet vector $V^\mu_{\hat{A}}$ has a different mass, see Eq. (3.37). Even though we neglect the mass splitting among the different electroweak components, in view of collider searches it is important to keep in mind the electroweak charges of the resonances, that are fixed by the decomposition of the $Sp(4)$ representations under the $SU(2)_w \times U(1)_Y$ gauged subgroup:

$$\begin{aligned} 1_{Sp(4)} &= 1_0, \\ 5_{Sp(4)} &= (2_{1/2} + \text{H.c.}) + 1_0, \\ 10_{Sp(4)} &= 3_0 + (2_{1/2} + \text{H.c.}) + (1_1 + \text{H.c.}) + 1_0. \end{aligned} \tag{3.53}$$

In Fig. 4 we display the five independent resonance masses, $M_{\sigma,\eta',S,V,A}$, as a function of ξ, for two representative values of κ_B/κ_A. While $M_\sigma = 2M_\psi$ grows over the entire range for ξ, the other four masses follow a different pattern: they appear to be several times larger than f when ξ is very close to one (see the discussion in the next paragraph), then they steeply decrease to reach a minimum value $\sim(2\text{–}3)f$ for an intermediate value of ξ, and finally they grow roughly linearly for $\xi \gtrsim 1.5$. We recall the two approximate mass relations, $M_S \simeq (M_\sigma^2 + M_{\eta'}^2)^{1/2}$ and $M_A \simeq (M_V^2 + 3M_\sigma^2/2)^{1/2}$, that hold neglecting pole mass differences in the loop form

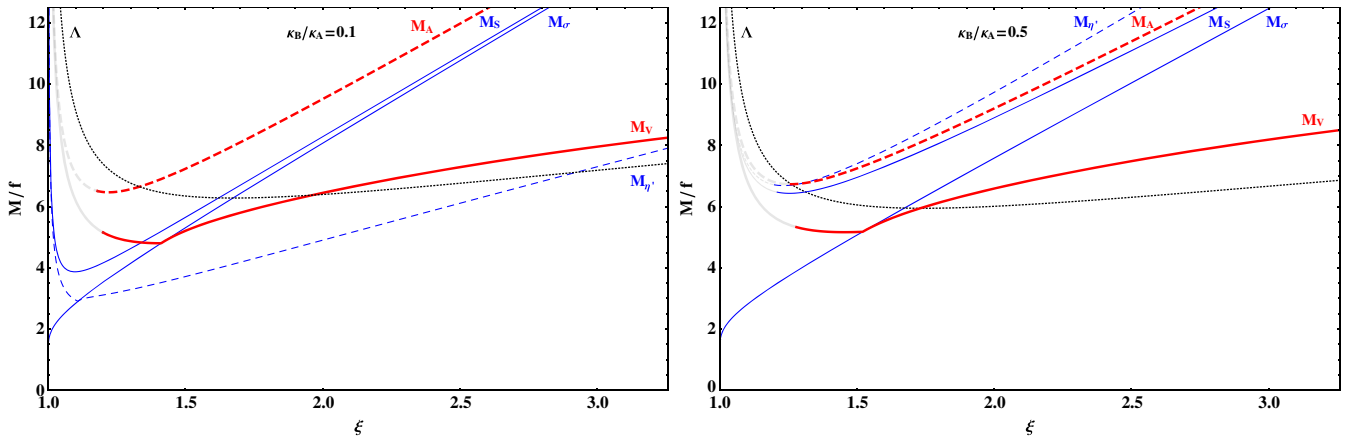

FIG. 4. The masses of the electroweak resonances in units of the Goldstone decay constant f, for $N = 4$ (the masses scale with $1/\sqrt{N}$), as a function of the coupling ξ, for $\kappa_B/\kappa_A = 0.1$ (left-hand panel) and $\kappa_B/\kappa_A = 0.5$ (right-hand panel). We displayed the full physical range for ξ, according to Fig. 3. Each curve is shaded when the corresponding pole mass equation develops a large, unphysical imaginary part, $|\text{Im}[g_\phi(M_\phi^2)]/\text{Re}[g_\phi(M_\phi^2)]| > 1$. The dotted line is the cutoff of the constituent fermion loops.

factor. As a consequence, one has always $M_A > M_S > M_\sigma$, with a similar asymptotic value at large ξ. On the contrary, M_V decreases until it becomes degenerate with M_σ, then it grows with a weaker slope. Finally, $M_{\eta'}$ may also become smaller than M_σ at large values of ξ, but only for a sufficiently small value of κ_B/κ_A. For example, taking $f = 1$ TeV, $N = 4$ and $\kappa_B/\kappa_A = 0.1$, the resonance masses for two representative values of ξ are

$$\begin{aligned} &\xi = 1.3: \quad M_A \simeq 6.6 \text{ TeV}, \quad M_V \simeq 4.9 \text{ TeV}, \quad M_S \simeq 4.6 \text{ TeV}, \quad M_\sigma \simeq 4.1 \text{ TeV}, \quad M_{\eta'} \simeq 3.3 \text{ TeV}, \\ &\xi = 2.0: \quad M_A \simeq 9.5 \text{ TeV}, \quad M_V \simeq 6.4 \text{ TeV}, \quad M_S \simeq 8.3 \text{ TeV}, \quad M_\sigma \simeq 8.1 \text{ TeV}, \quad M_{\eta'} \simeq 4.9 \text{ TeV}. \end{aligned} \tag{3.54}$$

In general, electroweak resonances lighter than $\simeq 4f \simeq 4$ TeV are possible in two cases: the scalar σ becomes light when one approaches the critical coupling $\xi = 1$, where the mass gap vanishes; the pseudoscalar η' becomes light as κ_B/κ_A tends to zero, where the anomalous $U(1)_\psi$ symmetry is restored. These two singlet states, together with the SM singlet Goldstone boson $G^{\hat{3}}$, may be observed as the lightest scalar resonances at the LHC, beside the 125 GeV Higgs boson. In Sec. V E we will discuss the mixing of σ and η' with the analogous singlet states of the color sector, a feature that will induce corrections to their masses.

A comment is in order on the region close to the critical coupling. In the limit $\xi \to 1$, one finds that $M_\sigma/f \sim [-\log(\xi - 1)]^{-1/2}$ vanishes, while the other resonance masses diverge relatively to f, $M_{V,A,S,\eta'}/f \sim (\xi - 1)^{-1/2}$. The lightness of σ may be interpreted as the signal that scale invariance is recovered below $\xi = 1$, while all other resonances decouple in this limit. However, we should remark that, for some of these heavy resonances, the NJL computation of their masses cannot be trusted close to the critical coupling, because the pole of the resummed propagator develops a large, unphysical imaginary part. Recall, from the general discussion at the beginning of Sec. III B, that the curves in Fig. 4 are the solution of Eq. (3.22),[9] where the imaginary part of $g_\phi(M_\phi^2)$ has been neglected. The curves in Fig. 4 are shaded when $|\mathrm{Im}[g_\phi(M_\phi^2)]/\mathrm{Re}[g_\phi(M_\phi^2)]| > 1$, where we consider that the corresponding result cannot be trusted anymore. This happens when $\xi \lesssim (1.2\text{–}1.3)$, for the vector and axial-vector resonances, with masses $M_{V/A}$ close to the cutoff of the NJL model.

Let us also comment on the complementary limit where ξ is so large that M_ψ/Λ becomes of order one, as illustrated in Fig. 3. In this case Fig. 4 shows that the resonances become heavier than Λ (except for η', if κ_B/κ_A is small enough). This is not necessarily problematic: while the mass M_ψ of constituent fermions in the loops need to be smaller than the loop cutoff Λ, external mesons heavier than Λ do not harm the consistency of the NJL approximation. Indeed, in QCD the NJL model predicts rather accurately resonance masses twice as large as the cutoff. Nonetheless, we notice that, for $M_\phi \sim \Lambda$, the value of the two-point function $\tilde{B}_0(M_\phi^2, M_\psi^2)$ becomes sensitive to the regularization chosen, defined in Appendix B, as the cutoff-dependent finite terms become sizeable. As a consequence, we observe that the mass values in this region may vary up to a few 10% in different regularization schemes. This is an intrinsic theoretical uncertainty of the NJL approximation.

The resonance masses in units of $f \equiv \sqrt{2}F_G$ may be compared with recent lattice studies of the same model [73,74], which provide scalar and vector masses in the same units.[10] Actually, the lattice simulations performed to date for this model are available only for an underlying $SU(2)$ gauge theory, thus equivalent to the special case $Sp(2)$ of our more general $Sp(2N)$ study. Let us recall that the meson masses scale as $M_\phi/f \sim 1/\sqrt{N}$, where the scaling originates solely from f (this statement holds for a fixed value of the ratio κ_B/κ_A). Therefore, the mass values illustrated for $N = 4$ in Fig. 4 get enhanced by a factor 2 for $N = 1$, and these rescaled values can be directly compared with the lattice results.

The lattice prediction for the vector masses in the chiral limit is $M_V/f = 13.1 \pm 2.2$, $M_A/f = 14.5 \pm 3.6$ [73]. The latter results, although affected with relatively large uncertainties, indicate a more moderate $V - A$ mass splitting than is generally expected from the NJL model, see Eq. (3.38), unless M_ψ is rather small, which corresponds in the NJL framework to rather small values of ξ. More precisely, typically the previous central lattice values can be (approximately) matched for $\xi \simeq 1.1$, therefore not far above the critical NJL coupling value, where on the other hand the NJL calculation becomes less reliable, as already explained above, since entering the ξ range where the V and A width both become relatively large. But accounting for the lattice uncertainties, the above values are also easily matched alternatively for rather large ξ values, where the NJL prediction is also more reliable: for example for $N = 1$ and $\xi = 1.6$ $[\xi = 1.9]$, $M_V/f|_{NJL} \simeq 11 [\simeq 12.5]$,

[9]The function $\mathrm{Re}\tilde{B}_0(q^2, M_\psi^2)$ develops a cusp at $q^2 = 4M_\psi^2$. Through the definition of the masses M_ϕ adopted here, this cusp naturally shows up in Fig. 4 (and in Fig. 7 below) as soon as the value of a resonance mass goes through $2M_\psi$. In practice, this only occurs for M_V and $M_{\eta'}$, at the cross-over from a bound state to a genuine resonance.

[10]Our normalization of f, see footnote 8, appears consistent with what is called F_{PS} in the notations of Ref. [73] thus we compare our NJL predictions in units of f directly with their numbers, assuming that the same normalization has been used in those lattice calculations.

$M_A/f|_{NJL} \simeq 15.3[\simeq 18]$. [NB recall that the V and A masses are mildly dependent on κ_B, which enters only indirectly through the mass gap. One should also keep in mind that the Fierz-induced relation (3.32) is assumed for the axial and vector coupling κ_D in Fig. 4, and since the dominant contribution to the V, A masses scales as $1/\kappa_D$, a somewhat smaller (larger) κ_D would induce somewhat larger (smaller) V, A masses, for a fixed value of ξ]. At least one may tentatively conclude from this comparison that intermediate ξ values, say $1.2 \lesssim \xi \lesssim 1.6$ approximately, as well as very large $\xi > 2$, appear more disfavored.

Concerning the lightest scalar masses, Ref. [74] provides the very recent lattice estimates $M_\sigma/f = 19.2(10.8)$, $M_{\eta'}/f = 12.8(4.7)$, and $M_S/f = 16.7(4.9)$, in the chiral limit (where the scalar nonsinglet S is called a_0 in Ref. [74]). Compared with Fig. 4 (rescaled for $N = 1$) and combined with the results for the V and A masses, ξ values very close to 1 appear disfavored by the σ mass, even when taking its lowest lattice value above, because in this region the NJL prediction for M_σ is much smaller than M_V, as it is clear from $M_\sigma = 2M_\psi$ (see also Fig. 4). The NJL (approximate) relation $M_S^2 \simeq M_\sigma^2 + M_{\eta'}^2$ [see Eq. (3.28)], can be fulfilled within the large lattice uncertainties, although the rather high lattice central value of M_σ is in tension with this relation. So putting all together it may indicate that relatively large values of $\xi \simeq 1.6$–2, well above the NJL critical coupling, are more favored by lattice results. The η' pseudoscalar mass, in the NJL model, is very sensitive to the ratio κ_B/κ_A, see Eq. (3.27). Modulo the large lattice uncertainties, the comparison with lattice results appears to indicate intermediate values for this ratio, $\kappa_B/\kappa_A \simeq 0.2$–$0.4$, such that $M_{\eta'}$ is comparable with M_V.

In conclusion the comparison of NJL and lattice results appears roughly consistent, at least the lattice results may be matched for some definite values of the NJL parameters ξ and κ_B/κ_A, with no strong tensions. But it appears still an essentially qualitative comparison at the present stage, given both the intrinsic NJL uncertainties amply discussed previously, as well as the still relatively large lattice systematic uncertainties, specially for the scalar resonances: so unfortunately it cannot be taken yet as giving tight constraints on the effective NJL model parameters. Note also that other recent lattice simulations of composite Higgs model resonances are available in the literature (see e.g. [75,76]), but are based on different gauge symmetries and/or global symmetry breaking pattern, thus not directly comparable with our results.

G. Comparison with spectral sum rules

Several authors [68,70,77] have addressed the issue of spectral sum rules, discussed in general terms in Sec. II D, in the context of the NJL approximation applied to QCD. In this section, we will study them in the context of the NJL approximation to the underlying $Sp(2N)$ gauge dynamics of the present composite Higgs framework. The aim will be to check whether these sum rules provide additional constraints on the parameters of the model, namely ξ and κ_B/κ_A.

It seems only natural to identify the spectral densities appearing in the sum rules displayed in Eqs. (2.13) and (2.14) with the discontinuities of the resummed NJL two-point correlators[11] discussed in the preceding subsections, i.e.

$$\mathrm{Im}\Pi_{V/A}(t) = \lim_{\epsilon\to 0^+} \frac{\bar\Pi_{V/A}(t+i\epsilon) - \bar\Pi_{V/A}(t-i\epsilon)}{2i}, \qquad (3.55)$$

or, in the singlet scalar and pseudoscalar channels,

$$\mathrm{Im}\Pi_{S^0/P^0}(t) = \lim_{\epsilon\to 0^+} \frac{\bar\Pi_{\sigma/\eta'}(t+i\epsilon) - \bar\Pi_{\sigma/\eta'}(t-i\epsilon)}{2i}, \qquad (3.56)$$

and analogous relations between $\mathrm{Im}\Pi_{S/P}(t)$ and $\bar\Pi_{S/P}(t)$. Before discussing the sum rules of Sec. II D under these identifications, let us recall that the sum rules themselves follow from the short-distance properties, which reflect the properties of the underlying $Sp(2N)$ gauge dynamics, of the two-point functions under consideration, and from general properties of quantum field theories, here essentially invariance under the Poincaré group and the spectral property. The latter allow to extend the definitions of the functions $\Pi_\phi(t)$ to functions in the complex t plane, with all singularities (poles and branch points) confined to the positive real axis. The former then allow to write down unsubtracted dispersion relations for the appropriate combinations of two-point correlators, from which the sum rules follow. The necessity to introduce a regularization (here the cutoff Λ), in order to render the one-loop correlators $\tilde\Pi_\phi(t)$ finite, and to perform the resummation shown in Fig. 2, leads to functions $\bar\Pi_\phi(t)$ that will in general not respect all the required properties. For instance, with the choice of regularization adopted in the present study, ghost poles on the *negative* real q^2-axis will appear, as discussed at the beginning of Sec. III B. This situation is well known in the context of the NJL approximation applied to QCD, where it has been examined quite extensively by the authors of Ref. [70], and we refer the reader to this article for additional details.

[11] At the level of one-loop two-point correlators, the spectral sum rule (2.19) is trivially satisfied, provided one identifies m with M_ψ, due to the identity $\tilde\Pi_V(q^2) - \tilde\Pi_A(q^2) = -\tilde\Pi_A^L(q^2)$. The identities

$$\tilde\Pi_S(q^2) - \tilde\Pi_P(q^2) = \tilde\Pi_S(q^2) - \tilde\Pi_{\eta'}(q^2) = \tilde\Pi_\sigma(q^2) - \tilde\Pi_G(q^2) = 2(2N)M_\psi^2 \tilde B_0(q^2, M_\psi^2)$$

allow only for the difference of the two last sum rules in Eq. (2.14), involving $\tilde\Pi_{S-\eta'} - \tilde\Pi_{\sigma-G}$, to be satisfied at one-loop. The sum rule involving Π_{S-P} is not expected to hold, since this correlator does not constitute an order parameter for $SU(4)/Sp(4)$, see footnote 3.

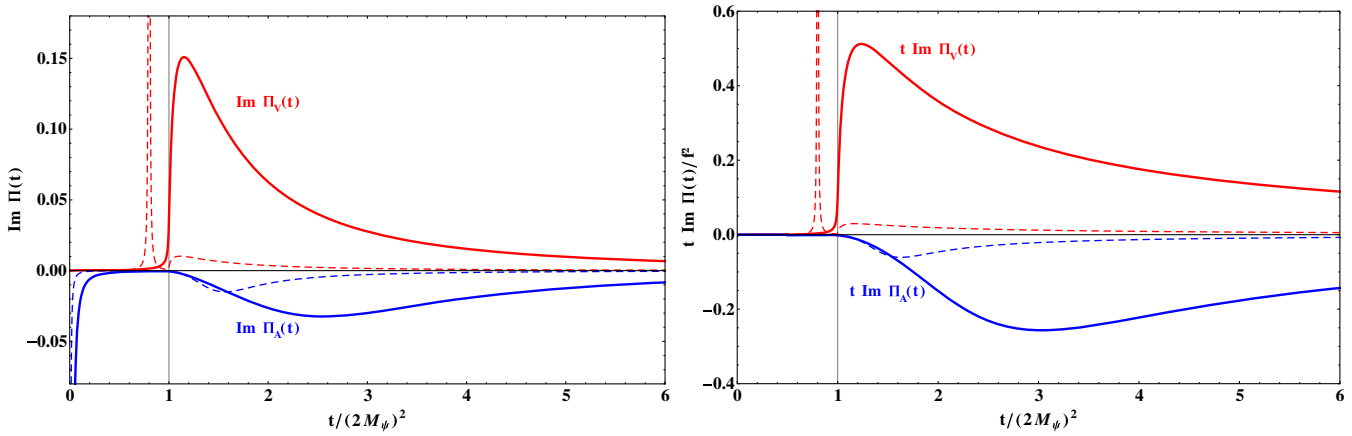

FIG. 5. The figure on the left shows the spectral functions $\mathrm{Im}\Pi_V(t)$ (upper curves, in red) and $-\mathrm{Im}\Pi_A(t)$ (lower curves, in blue), as a function of $t/(2M_\psi)^2$. The plotted quantities are dimensionless and scale like N. The solid and dashed lines correspond to $\xi = 1.3$ and $\xi = 2$, respectively. The value of the parameter κ_B/κ_A has been taken equal to 0.1 in all cases. The narrow vector bound state below the continuum starting at $t = (2M_\psi)^2$ (materialized on the figures by the vertical line) is present in $\mathrm{Im}\Pi_V(t)$ when $\xi = 2$, but disappears for smaller values of ξ. The pion pole appears clearly in $\mathrm{Im}\Pi_A(t)$, but the axial-vector resonance has a mass that is always greater that $4M_\psi^2$, and therefore a narrow subthreshold peak never occurs. The figure on the right likewise shows the functions $t\mathrm{Im}\Pi_V(t)$ and $t\mathrm{Im}\Pi_A(t)$. The latter are in units of f^2 and consequently are N independent.

The spectral densities resulting from the identifications in Eqs. (3.55) and (3.56) are shown in Figs. 5 and 6 (in order to make the figure more readable, we have kept ϵ in the definitions (3.55) and (3.56) very small, but finite). It is most instructive to analyze them in conjunction with the spectrum of the mesonic resonances, as given in Fig. 4, and with the general discussion at the beginning of Sec. III B. Figure 5 shows the vector and axial spectral functions for two different values of the parameter ξ. In the axial case, one recognizes the contribution from the pion pole at $t = 0$, and no other narrow bound state. Only a rather broad resonance peak appears above the $t = 4M_\psi^2$ threshold, where the continuum starts. This is in agreement with Fig. 4, which shows that M_A is always greater than $M_\sigma = 2M_\psi$. In the vector channel, a narrow bound state appears below the $2M_\psi$ threshold for $\xi = 2$, but is absent (it has moved to the real axis on the second Riemann sheet) for $\xi = 1.3$, and is replaced by a resonance peak. Again, this agrees with Fig. 4, where one sees that M_V becomes greater than $2M_\psi$ when ξ takes values below ~ 1.4.

For the nonsinglet scalar spectral density, shown on the left panel of Fig. 6, there is no narrow bound state lying below the threshold of the continuum, whatever the value of

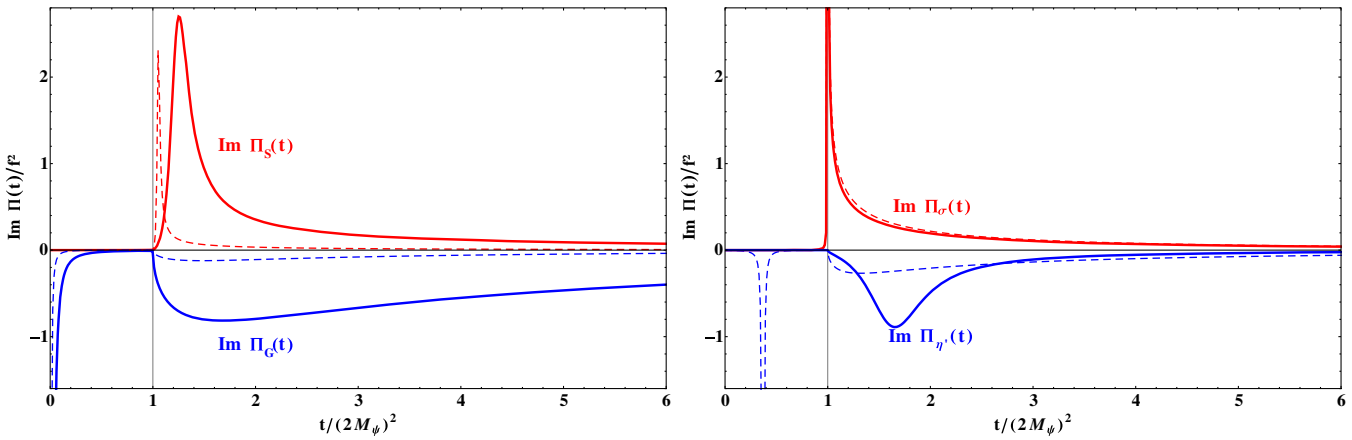

FIG. 6. The left-hand panel shows the nonsinglet spectral functions $\mathrm{Im}\Pi_S(t)/10$ (upper curves, in red) and $-\mathrm{Im}\Pi_G(t)$ (lower curves, in blue), as functions of $t/(2M_\psi)^2$, for $\kappa_B/\kappa_A = 0.1$, and for $\xi = 1.3$ (solid lines) and $\xi = 2$ (dashed lines). In the right-hand panel we fix $\xi = 2$ and show the singlet spectral functions $\mathrm{Im}\Pi_\sigma(t)$ (dashed red) and $-\mathrm{Im}\Pi_{\eta'}(t)$ (dashed blue) for $\kappa_B/\kappa_A = 0.1$, as well as $\mathrm{Im}\Pi_\sigma(t)$ (solid red) and $-\mathrm{Im}\Pi_{\eta'}(t)/20$ (solid blue) for $\kappa_B/\kappa_A = 0.5$. The narrow η' bound state is present only for the smallest value of κ_B/κ_A. A narrow σ pole appears in all cases right at the threshold $t = 4M_\psi^2$. Note that the spectral functions are all expressed in units of f^2, such that they are dimensionless and have no N dependence.

ξ. However, the larger the value of ξ, the more the resonance peak moves closer to the threshold. The shape of $\mathrm{Im}\Pi_S(t)$ is also sensitive to κ_B/κ_A. In the pseudoscalar nonsinglet channel, only the massless pion pole shows up, and $\mathrm{Im}\Pi_P(t)$ is not sensitive to the value of κ_B/κ_A. The singlet scalar spectral density, shown on the right panel of Fig. 6, presents a narrow peak at the threshold, for any value of ξ and κ_B/κ_A. In the pseudoscalar singlet channel, the features of the spectral function become also sensitive to this second parameter, as can already be inferred upon comparing the two panels of Fig. 4. In particular, a narrow subthreshold bound state is only present for smaller values of κ_B/κ_A.

An illustration of the two Weinberg-type sum rules of Eq. (2.13), as well as the sum rules of Eq. (2.14), is provided by Fig. 7. The integrals compared there, as functions of the coupling ξ and for two values of κ_B/κ_A, run over the whole positive t-axis, which means that, for the sake of illustration, the NJL description has been kept even beyond its expected range of validity. Of course, it is certainly difficult to ascribe any physical meaning to the spectral densities for values of, say, $t/\Lambda^2 \gtrsim 2$ [note that, for ξ close to the critical coupling, one has $2M_\psi \ll \Lambda$; therefore, the NJL description holds up to a large value of $t/(2M_\psi)^2$]. Beyond this value of t, the NJL description ceases to be appropriate, and we have to assume that the underlying $Sp(2N)$ gauge dynamics takes over. However, from the experience with QCD [78], it is expected that the matching between the two regimes is not very smooth. Keeping this proviso in mind, we show, on the left-hand panel of Fig. 7, the ratio of the integrals $\int dt\,\mathrm{Im}\Pi_V(t)$ and $\int dt\,\mathrm{Im}\Pi_A(t)$, as well as the ratio of the integrals $\int dtt\mathrm{Im}\Pi_V(t)$ and $\int dtt\mathrm{Im}\Pi_A(t)$. Similarly, the right-hand panel shows the ratios of the integrals $\int dt\,\mathrm{Im}\Pi_{\eta'}(t)$ and $\int dt\,\mathrm{Im}\Pi_S(t)$, and of the integrals $\int dt\,\mathrm{Im}\Pi_G(t)$ and $\int dt\,\mathrm{Im}\Pi_\sigma(t)$. If the sum rules were satisfied exactly for all values of ξ, all these curves would be a constant equal to one. This is obviously not the case. The general trend is that the departure from the sum rules is more important for larger values of ξ. This is in line with Fig. 4, from which we infer that the continuum, corresponding to $\sqrt{t} > 2M_\psi$, starts close to the cutoff Λ when $\xi \gtrsim 1.5$; therefore, the NJL description becomes questionable soon after the threshold. On the right-hand panel of Fig. 7 we also show the ratio of the integrals $\int dt\,\mathrm{Im}\Pi_G$ and $\int dt\,\mathrm{Im}\Pi_S$. Since $\Pi_{S\text{-}P}$ is not an order parameter of the $SU(4)$ spontaneous breaking (see footnote 3), there is no corresponding sum rule, and indeed this ratio deviates significantly from unity, already for lower values of ξ.

In view of the difficulties to interpret the meaning of the sum rules, expressed in terms of the spectral densities provided by the NJL description through Eqs. (3.55) and (3.56), one may consider an alternative approach, at least when $\mathrm{Im}\tilde{\Pi}_\phi(M_\phi^2)$ vanishes or is sufficiently small so that it can be neglected. This happens, for instance, for the Goldstone state, or for $\tilde{\Pi}_V(M_V^2)$ when there is a subthreshold vector bound state. In that case each correlator exhibits a single real pole, or narrow resonance [except for $\bar{\Pi}_A(q^2)$, which exhibits both the Goldstone pole and the axial-meson resonance pole, the latter being not very narrow, though], and one can saturate the sum rules with these narrow states. Introducing, similarly to F_G and to G_G in Eqs. (2.22) and (2.23), respectively, decay constants defined as

$$\begin{aligned}\langle 0|\mathcal{J}_\mu^A(0)|V^B(p;\lambda)\rangle &\equiv f_V M_V \epsilon_\mu^{(\lambda)}(p)\delta^{AB},\\ \langle 0|\mathcal{J}_\mu^{\hat{A}}(0)|A^{\hat{B}}(p;\lambda)\rangle &\equiv f_A M_A \epsilon_\mu^{(\lambda)}(p)\delta^{\hat{A}\hat{B}},\end{aligned} \tag{3.57}$$

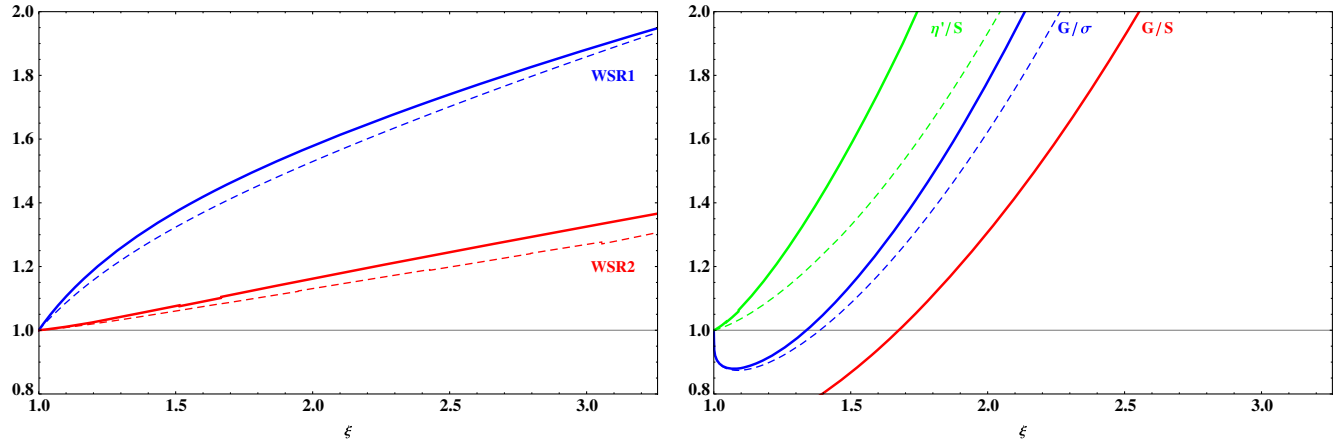

FIG. 7. Left panel: the ratio of the integrals, taken over the whole positive t-axis, $\int dt\mathrm{Im}\Pi_V(t)/\int dt\mathrm{Im}\Pi_A(t)$ (blue, upper curves) and $\int dtt\mathrm{Im}\Pi_V(t)/\int dtt\mathrm{Im}\Pi_A(t)$ (red, lower curves), as a function of the parameter ξ, and for $\kappa_B/\kappa_A = 0.1$ (solid lines) and $\kappa_B/\kappa_A = 0.5$ (dashed lines). Right panel: the ratio of the integrals, taken over the whole positive t-axis, $\int dt\mathrm{Im}\Pi_{\eta'}(t)/\int dt\mathrm{Im}\Pi_S(t)$ (green, upper curves), $\int dt\mathrm{Im}\Pi_G(t)/\int dt\mathrm{Im}\Pi_\sigma(t)$ (blue, middle curves) and $\int dt\mathrm{Im}\Pi_G(t)/\int dt\mathrm{Im}\Pi_S(t)$ (red, lower curve), as a function of the parameter ξ, for $\kappa_B/\kappa_A = 0.1$ (solid lines) and $\kappa_B/\kappa_A = 0.5$ (dashed lines, not shown in the G/S case). Note that the above ratios are independent from N.

where $\epsilon_\mu^{(\lambda)}(p)$ is the polarization vector associated to V or A, with $\sum_\lambda \epsilon_\mu^{(\lambda)}(p)\epsilon_\nu^{(\lambda)*}(p) = -(\eta_{\mu\nu} - p_\mu p_\nu/M_{V,A}^2)$, as well as

$$\begin{aligned}\langle 0|\mathcal{S}^{\hat{A}}|S^{\hat{B}}(p)\rangle &= G_S\delta^{\hat{A}\hat{B}},\\ \langle 0|\mathcal{S}^0|\sigma(p)\rangle &= G_\sigma,\\ \langle 0|\mathcal{P}^0|\eta'(p)\rangle &= G_{\eta'},\end{aligned} \tag{3.58}$$

the sum rules become, in this narrow-width, single-resonance approximation,

$$\begin{aligned}f_V^2M_V^2 - f_A^2M_A^2 - F_G^2 &= 0,\\ f_V^2M_V^4 - f_A^2M_A^4 &= 0,\end{aligned} \tag{3.59}$$

and

$$G_\sigma^2 - G_G^2 = 0, \qquad G_S^2 - G_{\eta'}^2 = 0. \tag{3.60}$$

Now, taking the various expressions of the meson masses, decay constants, as obtained from the NJL large-N approximation above, one can check to which extent these Weinberg-type and scalar sum rules are actually saturated by the first resonance from each of the available spectra. To proceed, one may first rewrite the *resummed* two-point correlators of Eq. (3.33) in the pole-dominance form: from Eqs. (3.33) and (3.57), the residues of the vector and axial-vector channels are defined by

$$\begin{aligned}f_{V/A}^2M_{V/A}^2 &= \lim_{q^2\to M_{V,A}^2}(q^2 - M_{V/A}^2)\bar{\Pi}_{V/A}(q^2)\\ &= \frac{-1}{(2K_{V/A})^2}\left[M_{V/A}^2\frac{\mathrm{d}\tilde{\Pi}_{V/A}(q^2)}{\mathrm{d}q^2}\bigg|_{q^2=M_{V/A}^2}\right]^{-1},\end{aligned} \tag{3.61}$$

where in the second equality, we have expanded the denominator of $\bar{\Pi}_{V/A}(q^2)$ around the complex pole $M_{V/A}^2$ and used Eq. (3.21). Similarly to the definition of the resonance masses in Eq. (3.22), one should however adopt a prescription to deal with the unphysical imaginary parts, NJL artifacts of the lack of confinement properties. We adopt the following prescription: (i) the residues are evaluated at the real pole masses $M_{V,A}^2 = \mathrm{Re}[g_{V,A}(M_{V,A}^2)]$ defined by Eq. (3.22), and (ii) we similarly define $f_{V,A}^2$ by the real parts of their right-hand-side expressions in Eq. (3.61). Of course, in the range of parameter space where the left-over imaginary contributions in Eqs. (3.61) become large, it puts a definite limit on the reliability of the NJL calculation, as will be specified below. According to this prescription, we obtain explicitly for the vector decay constant,

$$\begin{aligned}f_V^2 = &-\frac{3(2N)}{16\kappa_D^2M_V^4}\\ &\times\mathrm{Re}\left[\frac{1}{\tilde{B}_0(M_V^2,M_\psi^2) + (M_V^2+2M_\psi^2)\tilde{B}_0'(M_V^2,M_\psi^2)}\right].\end{aligned} \tag{3.62}$$

The axial decay constant f_A^2 is obtained in a similar way by making the following replacements $M_V \to M_A$ and $(M_V^2 + 2M_\psi^2) \to (M_A^2 - 4M_\psi^2)$ in the previous equation.

Similarly, for the spin zero channels, the residues are defined by

$$\begin{aligned}G_\phi^2 &\equiv -\lim_{q^2\to M_\phi^2}(q^2 - M_\phi^2)\bar{\Pi}_\phi(q^2)\\ &= \frac{1}{(2K_\phi)^2}\left[\frac{\mathrm{d}\tilde{\Pi}_\phi(q^2)}{\mathrm{d}q^2}\bigg|_{q^2=M_\phi^2}\right]^{-1}.\end{aligned} \tag{3.63}$$

From Eqs. (3.20) and (3.58), the scalar decay constants are explicitly given by

$$G_{\sigma,S}^2 = -\frac{1}{2(2N)K_{\sigma,S}^2}\mathrm{Re}\left[\frac{1}{\tilde{B}_0(M_{\sigma,S}^2,M_\psi^2) + (M_{\sigma,S}^2 - 4M_\psi^2)\tilde{B}_0'(M_{\sigma,S}^2,M_\psi^2)}\right], \tag{3.64}$$

while for the pseudoscalar decay constants we obtain

$$G_{G,\eta'}^2 = -\frac{1}{2(2N)K_{G,\eta'}^2}\mathrm{Re}\left[\frac{g_{A,a}^{-1}(M_{G,\eta'}^2)}{\tilde{B}_0(M_{G,\eta'}^2,M_\psi^2) + M_{G,\eta'}^2\tilde{B}_0'(M_{G,\eta'}^2,M_\psi^2)}\right], \tag{3.65}$$

where the axial-vector pseudoscalar mixing (see Sec. III E) brings the factor $g_{A,a}^{-1}(M_{G,\eta'}^2)$ for G and η', respectively.

Generally, we cannot expect the sum rules in the narrow width approximation to be very well satisfied, both because of the already discussed inherent approximations of the NJL framework, and also since the narrow width approximation itself is not justified in a substantial part of the parameter range, as we will examine more precisely below.

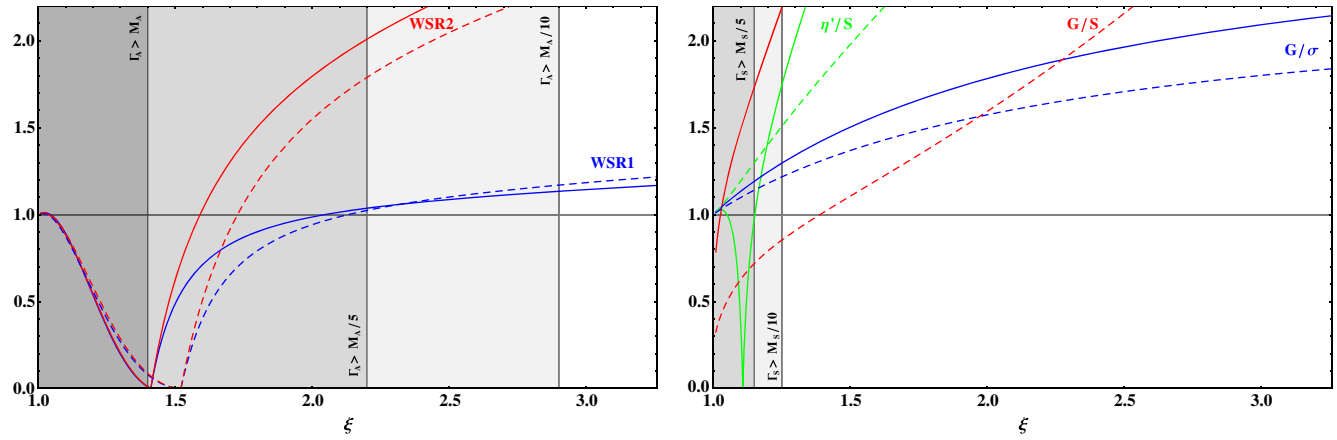

FIG. 8. Left panel: the two ratios $(f_V^2 M_V^2)/(F_G^2 + f_A^2 M_A^2)$ (WSR1, blue lines) and $(f_V^2 M_V^4)/(f_A^2 M_A^4)$ (WSR2, red lines) as functions of the coupling ξ, for $\kappa_B/\kappa_A = 0.1$ (solid lines) and $\kappa_B/\kappa_A = 0.5$ (dashed lines). Right panel: the analog for scalar sum rules. Also indicated are the values of the most relevant resonance widths, calculated from Eq. (3.66) for $\kappa_B/\kappa_A = 0.1$.

To be more specific, we will use the standard definition of the width,

$$M_\phi \Gamma_\phi = \frac{\mathrm{Im}\tilde{\Pi}_\phi(M_\phi^2)}{\mathrm{Re}\tilde{\Pi}'_\phi(M_\phi^2)}, \tag{3.66}$$

with $\tilde{\Pi}'_\phi(q^2)$ denoting the derivative of $\tilde{\Pi}_\phi(q^2)$ with respect to q^2. By evaluating explicitly Eq. (3.66) for the relevant resonances one may control the range of validity of the narrow width approximation.

Before a precise illustration of the deviations from the sum rules relations in Eqs. (3.59) and (3.60) in the parameter space of the model, it is instructive to examine more closely the NJL expressions of the involved quantities, Eqs. (3.62), (3.37) and (3.36). Namely, let us assume momentarily that we could crudely neglect the q^2 dependence of $\tilde{B}_0$, i.e. taking $\tilde{B}_0(M_V^2, M_\psi^2) \simeq \tilde{B}_0(M_A^2, M_\psi^2) \equiv \tilde{B}_0$ (therefore, taking also its derivative to vanish, $\tilde{B}'_0(q^2) \simeq 0$). Within this approximation, the second sum rule in Eq. (3.59) is immediately satisfied, see Eq. (3.62), while for the first sum rule, one can write, after some simple algebra,

$$\begin{aligned} f_V^2 M_V^2 - f_A^2 M_A^2 &\simeq f_V^2 (6M_\psi^2)\left[1 + \mathcal{O}\left(\frac{M_\psi^2}{M_V^2}\right)\right] \\ &\simeq -F_G^2\left[1 + \mathcal{O}\left(\frac{M_\psi^2}{M_V^2}\right)\right], \end{aligned} \tag{3.67}$$

where in the first equality we used the fact that the relation in Eq. (3.38) becomes exact in this approximation, and in the last equality we used Eqs. (3.62) and (3.37) in the same approximation, and identified F_G^2 from its expression in Eq. (3.41). This simple exercise shows explicitly and rather intuitively where the bulk of deviations from the Weinberg sum rules (WSR) comes from: one infers that the sum rules in Eq. (3.59) will, in general, not be satisfied, since the quantities they involve are the pole masses, $M_V^2 = \mathrm{Re}[M_V^2(M_V^2)]$ and $M_A^2 = \mathrm{Re}[M_A^2(M_A^2)]$, the Goldstone decay constant $F_G^2 = F_G^2(0)$, and the vector decay constants $f_{V,A}^2$ in Eq. (3.62), actually evaluated at the different V, A pole masses and involving also the nonvanishing derivative $\tilde{B}'_0(M_{V/A}^2)$. Accordingly since the relevant expressions like Eq. (3.62) are to be evaluated at *different* values of q^2, this implies not quite negligible differences in $\tilde{B}_0(q^2)$, and in its derivative. Only to the extent that they display a rather mild q^2 dependence will the narrow-width version (3.59) of the sum rules approximatively hold[12] Moreover, the crudely neglected terms $\mathcal{O}(M_\psi^2/M_V^2)$ in Eq. (3.67) are actually not so negligible, the less when ξ increases, just as M_A^2/M_V^2 also increases with ξ. Thus, we generally expect stronger deviations from Eq. (3.59) for larger ξ values.

In order to illustrate more precisely the deviations from the Weinberg-like sum rules of Eq. (3.59), taking now the "exact" expressions of $f_{V/A}, M_{V/A}$ according to our NJL calculations and prescriptions above, we consider the two ratios

$$\mathrm{WSR}_1 \equiv \frac{f_V^2 M_V^2}{F_G^2 + f_A^2 M_A^2}, \qquad \mathrm{WSR}_2 \equiv \frac{f_V^2 M_V^4}{f_A^2 M_A^4}, \tag{3.68}$$

which would both equal unity if the sum rules were satisfied in their narrow-width versions. Similarly, for the scalar sum rules we consider the two ratios G_G^2/G_σ^2 and $G_{\eta'}^2/G_S^2$. The behavior of these ratios with respect to ξ and κ_B/κ_A are illustrated in the left and right panels of Fig. 8 for the Weinberg and scalar sum rules, respectively. We also indicate some specific values of the relevant resonance widths, calculated from Eq. (3.66) for the reference value $\kappa_B/\kappa_A = 0.1$. The corresponding shaded regions thus indicate approximately the range where the narrow width

[12]We note that those finding and observations are qualitatively similar to the WSR results for the NJL model applied to low energy QCD in ref. [78], although those authors used somewhat different approximations than ours.

approximation can be trusted or not. Note that the V and A widths are very weakly sensitive to the values of κ_B/κ_A, so that the indicated ranges are also approximately valid for $\kappa_B/\kappa_A = 0.5$. In contrast the η' and S widths grow rapidly with κ_B, such that the indicated limit $\Gamma_S/M_S = 1/5$ ($\Gamma_S/M_S = 1/10$) is pushed, for $\kappa_B/\kappa_A = 0.5$, towards larger values of ξ, $\xi \simeq 1.7$ ($\xi \simeq 2$, respectively).

The two sum rules of Eq. (3.59) are actually reasonably satisfied in some specific ranges of ξ, respectively, either for intermediate values $1.6 \lesssim \xi \lesssim 2$, or for ξ very close to 1. Conversely the deviations appear maximal in the range $\xi \simeq 1.2-1.6$ and again for very large ξ. Most of these features can be understood more intuitively with the help of the above analysis. The intermediate range, where the deviations are the smallest, corresponds to a range where, at the same time, the narrow width approximation is well justified, and the relevant pole-mass differences are still moderate such that the relevant q^2 arguments of $\tilde{B}_0(q^2, M_\psi^2)$ are not very different. Then for very large values of ξ, while the A width is becoming smaller, one enters the regime of increasingly large differences in the relevant $\tilde{B}_0(M_{A/V}^2, M_\psi^2)$ functions, thus increasing the deviations, although the first WSR remains relatively well satisfied. The second WSR sum rule shows more rapidly increasing and important deviations for larger values of ξ, as intuitively expected since the fourth power of the masses enhances the increasing M_A/M_V ratio. The WSR values are not very sensitive to the ratio κ_B/κ_A, but depend mostly on ξ: a larger κ_B value essentially shifts the values of the sum rules in Fig. 8, as it implies larger values of $\kappa_A + \kappa_B$. Conversely for decreasing values of ξ, the narrow width approximation becomes totally unreliable, say for $\xi \lesssim 1.6$ in the case of Γ_A, where, correspondingly, the deviations are seen to be maximal. Moreover, when approaching (from below) the threshold $M_V^2 = 4M_\psi^2$, Γ_V is vanishing, but $\mathrm{Re}[\tilde{B}_0'(M_V^2, M_\psi^2)]$ tends toward infinity, so that $f_V^2 \to 0$, see Eq. (3.62). This happens around $\xi \simeq 1.4$ (1.5) for $\kappa_B/\kappa_A = 0.1$ (0.5). This peculiar feature can be understood as follow. When moving towards the threshold from below, the residue of the vector resonance, $f_V^2 M_V^2$, tends to zero, because its contribution to the spectral function is progressively transferred from the subthreshold to the continuum part of the spectral function. Since in the pole dominance approximation one only considers the lightest resonances, just below the threshold, the continuum contribution is not included within Eq. (3.62); therefore, the crossing of the threshold appears problematic in our NJL approximation. Of course, this pathological behavior is not present in Fig. 7, where we consider the complete two-point functions, which include also the continuum contributions. Finally, very close to the critical coupling $\xi \simeq 1$, although both $\Gamma_{V,A}$ are large, the mass gap in this region is relatively very small, $M_\psi \ll \Lambda$, such that $M_A - M_V$ is minimal, and $F_G \simeq M_\psi$ is also relatively small. Thus taking the real contributions prescriptions according to Eq. (3.62), one is again very close to the ideal approximation discussed above, leading to Eq. (3.67).

From these results, if considering that the best possible matching of the Weinberg-type sum rules, established on more general dynamical grounds, may be more important than the possible limitations of the NJL model approximation (somewhat in the spirit of Ref. [78]), one could be tempted to infer some preferred range of ξ values, where both deviations are minimal (although as clear from the figure it is not possible to satisfy the two WSR exactly for the same value of ξ). However, given the limitations of the NJL dynamical approximation, partly responsible for the nonperfectly matched Weinberg-type sum rules, we consider this only as an indicative trend rather than a genuine dynamical constraint on the couplings.

Concerning next the scalar sum rules, note that the above relations in Eqs. (3.64) and (3.65) do not lead to $G_G^2(q^2) - G_\sigma^2(q^2) = 0$ and $G_{\eta'}^2(q^2) - G_S^2(q^2) = 0$, which would be valid only if all expressions were evaluated at the same value of q^2. This is due to the pseudoscalar axial mixing, i.e. a term proportional to $g_{A,a}(q^2)$ does not vanish in the difference. In addition, for $G_G^2(q^2) - G_S^2(q^2)$, there is a term proportional to κ_B that indicates that this difference does not satisfy a convergent sum rule, consequently the discrepancy increases with κ_B. Indeed, as can be seen on Fig. 8, some of the scalar sum rules are approximately satisfied very close to $\xi = 1$, but are rapidly and badly invalidated for larger values of ξ, even though the narrow width approximation is justified in this region. This is mainly due to very large differences in the argument of the relevant functions $\tilde{B}_0(q^2, M_\psi^2)$, and also, as discussed above, due to the nonvanishing of κ_B. Note that, similarly to what is discussed above for the WSRs, the scalar sum rule associated to the η' may exhibit a pathological behavior, when the lightest resonances do not incorporate the dominant contributions. Indeed, the η' mass crosses the threshold for $\kappa_B/\kappa_A = 0.1$ and the associated ratio $G_{\eta'}^2/G_S^2$ tends to zero in this regime, which lies around $\xi = 1.1$.

In summary, the mismatch between the NJL predictions and the spectral sum rules resides in the gap between the contribution of the low-lying resonances and the full spectral functions. Given these limitations in the comparison of our results with the spectral sum rules, and since our interest is mostly the phenomenology of the lightest composite states, in the following we will keep studying the full range for the parameters ξ and κ_B/κ_A.

H. Evaluation of the oblique parameter S[13]

In the absence of explicit symmetry breaking effects, like, for instance, the coupling to the external electroweak gauge fields, the vacuum state $|\mathrm{vac}\rangle_0$ is left invariant by the

[13]We thank Alex Pomarol for encouraging us to estimate the ultraviolet correction to S in the present model.

$Sp(4)$ subgroup of the $SU(4)$ flavor symmetry defined by the generators T^A satisfying Eq. (2.2), where Σ_e stands for Σ_0 as given in Eq. (3.6). After electroweak symmetry breaking through misalignment, the vacuum state becomes $|\mathrm{vac}\rangle_v$. It is left invariant by a different $Sp(4)$ subgroup, whose generators $T^A_v = U_v T^A U_v^\dagger$ now satisfy[14]

$$T^A_v \Sigma_v + \Sigma_v (T^A_v)^T = 0, \tag{3.69}$$

with Σ_v and the $SU(4)$ transformation U_v given by

$$\Sigma_v = U_v \Sigma_0 U_v^T,$$
$$U_v = e^{i\sqrt{2}\langle h\rangle T^{\hat{1}}/f} = \cos\left(\frac{\langle h\rangle}{2f}\right) + 2\sqrt{2} i \sin\left(\frac{\langle h\rangle}{2f}\right) T^{\hat{1}}. \tag{3.70}$$

The expression of the transformation U_v conveys the information that the Higgs field $G^{\hat{1}}$ takes a vev $\langle h\rangle$. The shift in the oblique parameter S [79] induced by the composite electroweak sector is given by

$$\Delta S = 16\pi \left.\frac{d\Pi^{(v)}_{3Y}(q^2)}{dq^2}\right|_{q^2=0}, \tag{3.71}$$

where the two-point correlator $\Pi^{(v)}_{3Y}(q^2)$ has the following expression (cf. Appendix A 1)

$$\Pi^{(v)}_{3Y}(q^2)\left(\eta_{\mu\nu} - \frac{q_\mu q_\nu}{q^2}\right) = \frac{i}{2}\int d^4x e^{iq\cdot x}{}_v\langle \mathrm{vac}|T\{(J^4_\mu(x) - J^3_\mu(x))(J^4_\nu(0) + J^3_\nu(0))\}|\mathrm{vac}\rangle_v. \tag{3.72}$$

Expressing the generators T^3 and T^4 in terms of T^A_v and $T^{\hat{A}}_v$, $T^3 = \cos(\langle h\rangle/f) T^3_v - \sin(\langle h\rangle/f) T^{\hat{2}}_v$, $T^4 = T^4_v$, leads to[15]

$$\Delta S = 8\pi \frac{v^2}{f^2}\frac{d}{dq^2}(q^2 \Pi_{V\text{-}A}(q^2))|_{q^2=0}, \qquad \frac{v}{f} = \sin\left(\frac{\langle h\rangle}{f}\right). \tag{3.73}$$

Notice that the Goldstone pole at $q^2 = 0$ does not contribute to this expression. The corresponding shift in the oblique parameter T vanishes, due to custodial symmetry.

[14]Similarly, the generators of the coset space $SU(4)/Sp(4)$ corresponding to this new orientation of the $Sp(4)$ subgroup are given by $T^{\hat{A}}_v = U_v T^{\hat{A}} U_v^\dagger$, and satisfy $T^{\hat{A}}_v \Sigma_v - \Sigma_v (T^{\hat{A}}_v)^T = 0$.

[15]One can repeat the same exercice when in addition the singlet Goldstone boson $G^{\hat{3}}$ takes a vev $\langle \eta\rangle$. This will leave the expression for ΔS unchanged, the relation between v and the two vev's being given by

$$\frac{v}{f} = \frac{\langle h\rangle}{\sqrt{\langle h\rangle^2 + \langle \eta\rangle^2}} \sin\left(\frac{\sqrt{\langle h\rangle^2 + \langle \eta\rangle^2}}{f}\right).$$

In the NJL approximation the resummed correlator $\bar{\Pi}_{V-A}(q^2)$ is defined according to Eq. (3.33), that implies

$$\Delta S_{\mathrm{NJL}} = \frac{2N}{9\pi}\frac{v^2}{f^2}\left[\frac{1}{2} + g_A^2(0) - \frac{3}{2}\left(\frac{1}{1+x_\psi} - \ln\frac{1+x_\psi}{x_\psi}\right) \times (1 - g_A^2(0))\right] = \frac{2N}{6\pi}\frac{v^2}{f^2}(1 + \mathcal{O}(x_\psi)), \tag{3.74}$$

where $x_\psi \equiv M_\psi^2/\Lambda^2$, the axial form factor $g_A(q^2)$ is defined in Eq. (3.40), and its value at $q^2 = 0$ reads

$$\frac{1}{g_A(0)} = 1 - \frac{\kappa_D/\kappa_A}{1 + \kappa_B/\kappa_A} 2x_\psi \left(1 - x_\psi \ln\frac{1+x_\psi}{x_\psi}\right)^{-1} \times \left(\frac{1}{1+x_\psi} - \ln\frac{1+x_\psi}{x_\psi}\right). \tag{3.75}$$

The left panel of Fig. 9 shows the variation of ΔS_{NJL} as a function of ξ, that is in one-to-one correspondence with x_ψ, according to Eq. (3.17). As expected, ΔS_{NJL} decreases when the strong sector decouples, i.e. with the increase of f. More precisely, for $\xi \to 1$ we have $x_\psi \to 0$ and $\Delta S_{\mathrm{NJL}} \simeq 2N/(6\pi)(v^2/f^2)$. As ξ increases, the factor $(1 - g_A^2(0))$ becomes nonzero, and ΔS_{NJL} first grows moderately, and then decreases as x_ψ approaches one. In the range of parameter space where the narrow-width approximation applies, one may saturate the above correlator with the first light resonances, see Eq. (A8) with $q^2 = -Q^2$, and in this case one obtains [50,79] $\Delta S_{\mathrm{NJL}} \simeq 8\pi(v^2/f^2)(f_V^2 - f_A^2)$.

The composite sector will also modify the couplings of the Higgs boson to the electroweak gauge bosons by a factor $\sqrt{1 - v^2/f^2}$. This modification will upset the cancellation of logarithmic divergences in the gauge-boson self-energies, and induce model independent shifts in both S and T [81]. These contributions from low energies are given by [27,28]

$$\Delta S_{\mathrm{IR}} = \frac{1}{6\pi}\frac{v^2}{f^2}\ln\left(\frac{\mu}{M_h}\right), \qquad \Delta T_{\mathrm{IR}} = -\frac{3}{8\pi}\frac{1}{\cos^2\theta_W}\frac{v^2}{f^2}\ln\left(\frac{\mu}{M_h}\right) = -\frac{9}{4}\frac{\Delta S_{\mathrm{IR}}}{\cos^2\theta_W}, \tag{3.76}$$

One finds $\Delta S_{\mathrm{IR}} = (0.045, 0.022, 0.014)$ and $\Delta T_{\mathrm{IR}} = (-0.17, -0.08, -0.05)$, for $f = (0.5, 0.75, 1)$ TeV, if the cutoff scale is taken equal to $4\pi F_G = 2\sqrt{2}\pi f$, leading to non-negligible contributions. Notice that Goldstone boson loops contribute to the low-q^2 end of the $\Pi_{V\text{-}A}(q^2)$ function, but only at subleading order in the $1/N$ expansion. The NJL approximation only provides leading-order contributions, and thus cannot remove this subleading (in the $1/N$ expansion) cutoff dependence in ΔS_{IR} and ΔT_{IR}.

The right panel of Fig. 9 shows the combined contributions from Eqs. (3.74) and (3.76) to the S and T

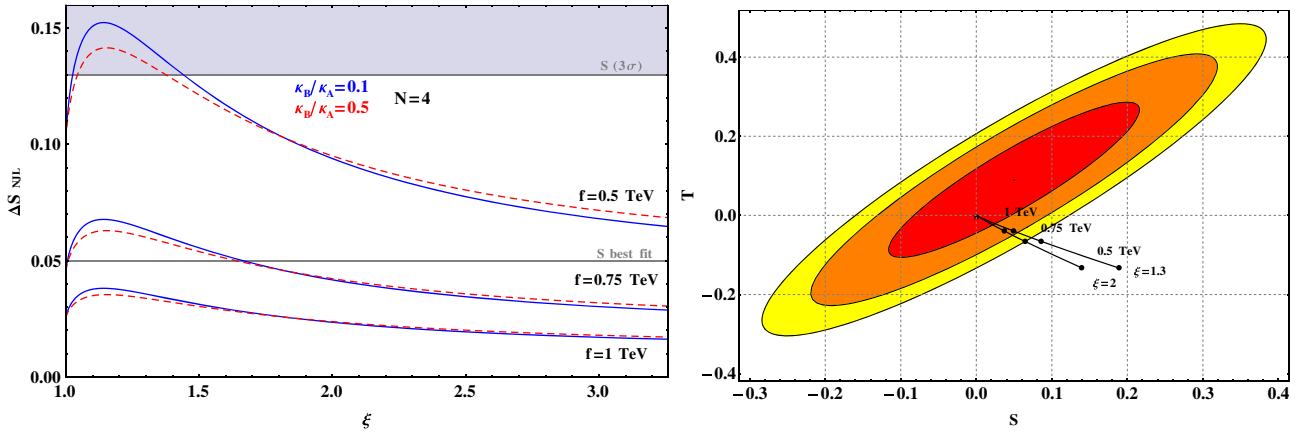

FIG. 9. On the left, the contribution to the S parameter from the composite electroweak sector in the NJL approximation [see Eq. (3.74)] as a function of the dimensionless coupling ξ, and for three representative values of f, $f = (0.5, 0.75, 1)$ TeV. The value of the parameter κ_B/κ_A has been taken equal to 0.1 (solid blue curves) and to 0.5 (dashed red curves), while the number of hypercolors is fixed to $N = 4$ and the vector coupling is given by $\kappa_D = \kappa_A$. The best fit for S is indicated by the horizontal line at 0.05 and the region above the 3σ limit, assuming $T = 0$, is shaded. On the right, the preceding UV contribution, evaluated in the NJL approximation, as well as the IR contributions coming from the nonlinear realization of the EWSB (i.e. $\Delta S_{\rm NJL} + \Delta S_{\rm IR}$ and $\Delta T_{\rm IR}$), as a function of f. The black dots correspond to $f = 0.5$, 0.75 and 1 TeV, and the curves stand for two representative values, $\xi = 1.3$ and $\xi = 2$, with $\kappa_B/\kappa_A = 0.1$, $N = 4$ and $\kappa_D = \kappa_A$. The 68% (red), 95% (orange) and 99% (yellow) C.L. ellipses in the $S - T$ plane are extracted from the fit of Ref. [80]. As stressed in the text, one expects in general additional contributions, which could significantly impinge on the values of S and T.

parameters as a function of f, for different values of ξ and of κ_B/κ_A. When linear couplings between the top quark and the fermions of the strong sector are introduced, one expects in general additional contributions, which could significantly affect the S and T parameters. These fermionic contributions, as well as other order $1/N$ corrections than $\Delta S_{\rm IR}$ and $\Delta T_{\rm IR}$, are beyond the scope of this paper. The right panel of Fig. 9 thus displays only a specific kind of contributions, and does by no means constitute a complete prediction of the model under discussion as far as S and T are concerned.

IV. ADDING THE COLORED SECTOR

An appealing way to couple the SM fermions to the composite Higgs is to introduce a linear coupling between each SM fermion and a composite fermion resonance with the same quantum numbers. Such an approach, known as fermion partial compositeness [26,82], is especially attractive in the case of the top quark: relatively light composite top partners allow to induce the required, large top Yukawa coupling. In order for the composite sector to contain partners for the top (and possibly the other SM quarks), one needs to introduce constituent fermions X^f that are charged under the color group $SU(3)_c$. It is not possible to construct a "baryon" (a hypercolor invariant spin-1/2 bound state) if X^f transforms under the fundamental, pseudoreal representation of $Sp(2N)$. Following [8], we rather assume that X^f transforms under the two-index, real representation of $Sp(2N)$ that is antisymmetric, $X^f_{ij} = -X^f_{ji}$, and traceless, $X^f_{ij}\Omega_{ji} = 0$. This irreducible representation has dimension $(2N+1)(N-1)$. In order to embed a $SU(3)_c$ triplet-antitriplet pair, one has to introduce six such fermions, $f = 1, \ldots, 6$. Then, the theory acquires a flavor symmetry $SU(6) \supset SU(3)_c$, with $X^f \sim 6_{SU(6)} = (3+\bar{3})_{SU(3)_c}$. The addition of such an X sector modifies several results that we have derived for the ψ sector in isolation, because the underlying $Sp(2N)$ gauge dynamics connects the two sectors in a highly nontrivial way, as we now describe.

Once both types of fermions ψ^a and X^f are in presence, the flavor symmetry group becomes $G = SU(4) \times SU(6) \times U(1)$, where $U(1)$ is the nonanomalous linear combination of the two axial symmetries $U(1)_\psi$ and $U(1)_X$, which separately are both anomalous with respect to $Sp(2N)$. The current corresponding to the $U(1)_\psi$ transformations and its divergence were already given in Eqs. (3.4) and (3.5), respectively. In the case of the $U(1)_X$ transformations, the corresponding expressions read [a sum over the flavor indices is understood, gauge and spinor indices are omitted]

$$\mathcal{J}^0_{X\mu} = \frac{1}{2}[(\bar{X}\bar{\sigma}_\mu X) - (X\sigma_\mu \bar{X})], \tag{4.1}$$

$$\partial^\mu \mathcal{J}^0_{X\mu} = 4\sqrt{3} m_X \mathcal{P}^0_X + 2(N-1)\frac{N_f^X g_{HC}^2}{32\pi^2} \times \sum_{I=1}^{N(2N+1)} \epsilon_{\mu\nu\rho\sigma} G^{I,\mu\nu}_{HC} G^{I,\rho\sigma}_{HC}, \tag{4.2}$$

where the factor $N_f^X = 3$ accounts for the number of flavors in the X sector. In the above, $\bar{X}$, as defined in Table III below,

TABLE III. The transformation properties of the elementary fermions, the spin-0 and spin-1 fermion bilinears, in the color sector of the model. Spinor indexes are understood, and brackets stand for a hypercolor-invariant contraction of the $Sp(2N)$ indexes.

	Lorentz	$Sp(2N)$	$SU(6)$	$SO(6)$
X^f_{ij}	$(1/2,0)$	$\square_{ij}$	6^f	6
$\bar{X}_{fij} \equiv \Omega_{ik} X^\dagger_{fkl} \Omega_{lj}$	$(0,1/2)$	$\square_{ij}$	$\bar{6}_f$	6
$M^{fg}_c \sim (X^f X^g)$	(0,0)	1	21^{fg}	$20' + 1$
$\bar{M}_{cfg} \sim (\bar{X}_f \bar{X}_g)$	(0,0)	1	$\bar{21}_{fg}$	$20' + 1$
$a^\mu_X \sim (\bar{X}^f \bar{\sigma}^\mu X_f)$	$(1/2,1/2)$	1	1	1
$(V^\mu_c, A^\mu_c)^g_f \sim (\bar{X}_f \bar{\sigma}^\mu X^g)$	$(1/2,1/2)$	1	35^f_g	$15 + 20'$

transforms under the $Sp(2N)$ gauge group in the same way as X, and the gauge-invariant bilinear fermion contractions between X and X are defined as

$$(X^f X^g) \equiv X^f_{ij} \Omega_{jk} X^g_{kl} \Omega_{li} = \mathrm{tr}(X^f \Omega X^g \Omega). \tag{4.3}$$

Contractions like $(\bar{X}_f \bar{X}_g)$ and $(\bar{X}_f X^g)$ are defined in the same way. For later use we have also introduced a flavor independent mass term for the X fermions,

$$\mathcal{L}^X_m = -2\sqrt{3} m_X \mathcal{S}^0_X, \tag{4.4}$$

with

$$\mathcal{S}^0_X = \frac{1}{2}[(\bar{X} T^0_X \Sigma^c_0 \bar{X}) + (X \Sigma^c_0 T^0_X X)],$$
$$\mathcal{P}^0_X = \frac{1}{2i}[(\bar{X} T^0_X \Sigma^c_0 \bar{X}) - (X \Sigma^c_0 T^0_X X)], \tag{4.5}$$

in agreement with the general definitions given in Eq. (2.6) and the normalization adopted there for the singlet scalar and pseudoscalar densities, that is $T^0_X = \mathbb{1}/(2\sqrt{3})$. Note that the singlet contraction of two fermions in the (anti)fundamental of $SU(6)$ is realized through the matrix

$$\Sigma^c_0 = \begin{pmatrix} 0 & \mathbb{1}_3 \\ \mathbb{1}_3 & 0 \end{pmatrix}, \tag{4.6}$$

which determines the $SU(6)/SO(6)$ vacuum direction. The two conditions in Eq. (2.2) are satisfied with $\Sigma_\epsilon = \Sigma^c_0$ and the $SU(6)$ generators T^F and $T^{\hat{F}}$ defined in Appendix A 2.

Examining the respective $U(1)_\psi$ and $U(1)_X$ anomaly coefficients, it is easily seen that the combination of the two axial singlet currents given by

$$\mathcal{J}^0_\mu = \ell(\square)\mathcal{J}^0_{X\mu} - \frac{3}{2}\ell(\square\!\square)\mathcal{J}^0_{\psi\mu} = \frac{3}{2}\ell(\square\!\square)\left(\psi^a \sigma_\mu \overline{\psi}_a\right) - \ell(\square)\left(X^f \sigma_\mu \overline{X}_f\right) \ , \tag{4.7}$$

is free from the gauge anomaly,

$$\partial^\mu \mathcal{J}^0_\mu = 4\sqrt{3} m_X \mathcal{P}^0_X, \tag{4.8}$$

where the Dynkin index $\ell(r)$ of the representation r of the gauge group $Sp(2N)$ gives the normalization of the $Sp(2N)$ generators $T^I(r)$ in this representation,

$$\mathrm{tr}[T^I(r) T^J(r)] = \frac{1}{2}\ell(r)\delta^{IJ} \ , \qquad \ell(\square) = 1 \ , \qquad \ell(\square\!\square) = 2(N-1) \ . \tag{4.9}$$

Consequently, the axial singlet transformation of *both* the ψ and X fermions, with charges satisfying

$$q_\psi = -3(N-1) q_X, \tag{4.10}$$

is a true symmetry of the theory, even at the quantum level, in the limit where m_X vanishes.

The introduction of fermions in the two-index antisymmetric representation of the $Sp(2N)$ gauge group has another consequence. The first coefficient of the β-function of the gauge coupling g_{HC} now reads

$$b_0 = \frac{11}{3} C_2(\mathrm{adj}) - \frac{4}{3}\sum_{i=\psi,X} N^i_f \ell(r_i)$$
$$= \frac{2}{3}(11 - 4N^X_f)\left[N + 1 - 2\frac{4N^X_f - N^\psi_f}{4N^X_f - 11}\right]. \tag{4.11}$$

Therefore, as soon as $N^X_f \geq 3$, b_0 stays positive and asymptotic freedom is preserved (at one loop) only if the number of colors N is bounded from above,

$$N < 2\frac{4N^X_f - N^\psi_f}{4N^X_f - 11} - 1 \quad [N^X_f \geq 3], \tag{4.12}$$

which, in the case at hand ($N_f^\psi = 2$ and $N_f^X = 3$), means $N \leq 18$. This upper bound prevents us from considering the limit $N \to \infty$ at the level of the fundamental hypercolor theory once the sector of X fermions has been introduced. Notice, however, that independently from the existence of this upper bound on N, the anomalous contribution on the left-hand side of Eq. (4.2) would not vanish in the 't Hooft limit $N \to \infty$, with Ng_{HC}^2 staying constant. Despite the absence of a well-defined large-N limit at the level of the fundamental theory, it remains useful to keep the naive counting in powers of $1/N$ at the level of the NJL description of the dynamics, since it allows, for instance, to identify contributions which will be numerically suppressed even for already moderate values of N. Therefore, when, in the sequel, we mention or use the $1/N$ expansion, it will thus always be understood that it refers to the NJL context.

A. The pattern of flavor symmetry breaking

Concerning the pattern of spontaneous symmetry breaking, there are now two possible fermion bilinears that may form a condensate. A nonzero $\langle \psi^a \psi^b \rangle$ would break $SU(4) \times U(1)$ to $Sp(4)$, with NGBs transforming as $(5+1)_{Sp(4)}$. A nonzero $\langle X^f X^g \rangle$ would break $SU(6) \times U(1)$ to $SO(6)$, with NGBs in the representation $(20'+1)_{SO(6)} = (8+6+\bar{6}+1)_{SU(3)_c}$. Light colored scalars are phenomenologically problematic because of the strong bounds from collider searches. An important contribution to their mass is induced by gluon loops, as discussed in Sec. II E, in Appendix A 2 and in Sec. V B. Another possibility to lift the colored NGBs from the low energy spectrum is to introduce the mass term (4.4), which explicitly breaks $SU(6) \times U(1)$ to $SO(6)$. Alternatively, if $SU(6)$ does not undergo spontaneous breaking, colored NGBs would be absent. However, we will show below that the matching of anomalies would then require massless, colored fermions, that again call for a large radiative mass or for $m_X \neq 0$.

Since we have adopted the same fermion content as in Ref. [8], let us stress some differences with respect to the discussion of flavor symmetries in that paper. First, the nonanomalous axial $U(1)$ symmetry was not discussed: we will show that it has several phenomenological consequences. Second, the color triplet and antitriplet components of X^f were treated separately, and the global symmetry was identified with $SU(3) \times SU(3) \times U(1)_V$, broken by a mass term to $SU(3)_c \times U(1)_V$. However, these are just maximal subgroups of the complete global symmetry $SU(6)$, and of the complete unbroken subgroup $SO(6)$, respectively. The pattern is different from QCD, because there quarks and antiquarks transform under different representations of the gauge group, while here the six copies of X^f transform in the same way under $Sp(2N)$. Note that $U(1)_V$ was introduced in Ref. [8] in order to provide top partners with the appropriate SM hypercharge, but remarkably enough such a symmetry is automatically present, as one of the unbroken generators within $SO(6)$.

Once both the elementary fermions ψ^a and X^f are introduced, one can form several baryons. As a consequence, the anomaly matching condition provides nontrivial constraints on the spontaneous symmetry breaking, as discussed in Sec. II B. If one denotes by V the conserved currents associated to the H_m generators, and by A the conserved currents associated to the generators of the coset G/H_m (see Sec. II A), one needs only consider the anomaly matching constraints that arise from the $\langle VVA \rangle$ correlators. Then, to each fermion transforming in the representation r of G is associated an anomaly coefficient $A(r)$, which is defined by

$$2\mathrm{tr}[T^{\hat{A}}(r)\{T^B(r), T^C(r)\}] = A(r) d^{\hat{A}BC}, \qquad (4.13)$$

where $T^A(r)$ and $T^{\hat{A}}(r)$ are the generators of H_m and of G/H_m, respectively, in the representation r, and $d^{\hat{A}BC}$ is an invariant tensor that depends on G. The generators of the fundamental representation r_0 are normalized as in Eq. (4.9), and its anomaly coefficient is fixed to $A(r_0) = 1$. The anomaly matching condition can be written as

$$\sum_i n_i A(r_i) = \sum_i n_i' A(r_i), \qquad (4.14)$$

where the left-hand (right-hand) sum runs over the representations of the constituent (composite) fermions, and n_i (n_i') are their multiplicities. If this equality cannot be satisfied, then G necessarily undergoes spontaneous symmetry breaking.

In the model under investigation, the possible trilinear baryons consist of

$$\begin{aligned} \Psi^{abf} &= (\psi^a \psi^b X^f), \qquad & \Psi_f^{ab} &= (\psi^a \psi^b \bar{X}_f), \\ \Psi_b^{af} &= (\psi^a \bar{\psi}_b X^f), \qquad & \Psi^{fgh} &= (X^f X^g X^h), \\ & & \Psi_h^{fg} &= (X^f X^g \bar{X}_h), \end{aligned} \qquad (4.15)$$

plus their conjugates, where the brackets stand for a spin-1/2, hypercolor-singlet contraction (multiple, independent contractions of this kind may be possible). Each Ψ decomposes in several irreducible representations (r_4, r_6) of $SU(4) \times SU(6)$, each corresponding to an independent baryon state: for example $\Psi^{abf} \sim [(6,6) + (10,6)]$. In addition, exotic baryons are also possible, formed by a larger, odd number of constituent fermions.

Let us begin with the $SU(4)^3$ anomaly. As ψ lies in the fundamental representation of $SU(4)$, its anomaly coefficient is $A_4(4) = 1$. The $SU(4)$ representations contained in $\psi^a \psi^b$ or $\psi^a \bar{\psi}_b$ have coefficients $A_4(1) = A_4(6) = A_4(15) = 0$ and $A_4(10) = 8$. Therefore, the anomaly matching between ψ and the trilinear baryons Ψ reads

$$2N \cdot A_4(4) = 2N = \sum_{(r_4,r_6)} n_{(r_4,r_6)} A_4(r_4) \cdot \dim(r_6) = n_{(10,6)} 6 \cdot 8, \quad (4.16)$$

where the sum runs over the various massless baryon states, and $n_{(r_4,r_6)}$ are their multiplicities. One can generalize the result to include exotic baryons: in full generality, hypercolor invariance requires the total number of ψ and $\bar{\psi}$ fermions to be even; then, in order to obtain a fermion, one needs that the total number of X and $\bar{X}$ is odd. One can check [83] that (i) the anomaly coefficient of any $SU(4)$ representation, contained in $4 \times \cdots \times 4$ an even number of times, is a multiple of 8, and (ii) the dimension of any $SU(6)$ representation, contained in $6 \times \cdots \times 6$ an odd number of time, is a multiple of 2. As a consequence, the right-hand side of Eq. (4.16) generalizes to a multiple of $2 \cdot 8$, and the matching is possible only for $N = 8n$, with n integer. An example with $N = 8$ is provided by one exotic baryon $(\psi\psi XXX) \sim (10, 20)$ plus three copies of $(\bar{\psi}\,\bar{\psi}\,X) \sim (\bar{10}, 6)$. In summary, for $N \neq 8n$ $SU(4)$ necessarily spontaneously breaks to $Sp(4)$ and the corresponding NGB decay constant F_G is nonzero. Strictly speaking, the other order parameters, such as the condensate $\langle\psi\psi\rangle$, may still vanish, for instance if a discrete symmetry subgroup leaves the vacuum invariant but not the $(\psi\psi)$ operator [84]. This is, however, a rather unlikely situation to happen [85], and we will assume that the spontaneous symmetry breaking of the $SU(4)$ flavor group (towards its $Sp(4)$ subgroup) is due to the formation of a nonvanishing $\langle\psi\psi\rangle$ condensate. This corresponds actually to the dynamical situation described by the NJL framework, where $SU(4)$ order parameters like the condensate are proportional to F_G.

Next, let us consider the $SU(6)^3$ anomaly. The crucial observation is that there are baryons, contained either in $(\psi\bar{\psi}X)$ or $(XX\bar{X})$, that transform under the representation (1,6). These states have evidently the same anomaly coefficient $A_6(6) = 1$ as the constituent fermion X; therefore, the matching is trivially possible for any value of N,

$$(2N+1)(N-1) \cdot A_6(6) = \sum_{(r_4,r_6)} n_{(r_4,r_6)} \dim(r_4) \cdot A_6(r_6) = n_{(1,6)} 1 \cdot A_6(6) + \cdots, \quad (4.17)$$

where the ellipsis stands for the contribution from larger representations, which are not relevant in the present context. As a consequence, from the point of view of the anomaly condition, the spontaneous breaking of $SU(6)$ is not a necessity, and in particular it allows the possibility that $\langle XX\rangle = 0$. However, the mass inequalities mentioned in Sec. II C require, in the case where massless baryons are present in the bound state spectrum, massless spin-zero bound states, coupled to the currents associated with the generators of the $SU(6)/SO(6)$ coset, which is tantamount to the spontaneous breaking of $SU(6)$ towards $SO(6)$.

Note that the massless baryons required by anomaly matching carry color and are phenomenologically excluded. Once these baryons are made heavy by explicit symmetry breaking, there are no exact NGBs either, and again one cannot tell whether the dynamics breaks spontaneously $SU(6)$ or not. Indeed, in either case an explicit symmetry breaking mass term $m_X XX$ is required for specular reasons: in the unbroken phase, one needs it to give a sufficiently large mass to the colored baryons; in the broken phase, the mass term is necessary to make the colored NGBs sufficiently heavy. Ref. [86] argues that the mass of the top partners can be controlled by the parameter m_X, if one assumes to be in the unbroken phase.

Finally, one should consider the anomalies involving the nonanomalous $U(1)$. The anomaly for $U(1)SU(6)^2$ is easily matched for any N, by the same set of baryons that matches the $SU(6)^3$ anomaly. We also proved that the other anomalies involving $U(1)$, that is $U(1)SU(4)^2$ and $U(1)^3$, can be matched for any N as well, but using a different set of baryons in each case. It is highly nontrivial to match all $U(1)$ anomalies at the same time, and thus preserve this symmetry from spontaneous breaking. As we have already argued though, it is quite unlikely that the spontaneous breaking of the $SU(4)$ flavor symmetry happens without, at the same time, also triggering the spontaneous breaking of the $U(1)$ symmetry.

In the following sections, we will apply the NJL techniques to the complete model including the electroweak and the color sector. In particular, we will study the mass gap equations that determine $\langle\psi\psi\rangle$ and $\langle XX\rangle$ in terms of the coefficients of the four-fermion operators. For $N \neq 8n$, only the phase $\langle\psi\psi\rangle \neq 0$ of the NJL model should be considered as a good approximation of the full dynamics, while $\langle XX\rangle$ is not constrained by the matching of anomalies. For $N = 8n$, both condensates may or may not vanish.

B. Sum rules and pseudoscalar decay constants in the flavor-singlet sector

As a last point to be discussed in this section, let us recall that in Sec. II D we introduced the spectral sum rules for a simple group G that undergoes spontaneous breaking. That discussion applies to the ψ sector alone, with coset $SU(4)/Sp(4)$, as well as to the X sector in isolation, with coset $SU(6)/SO(6)$. In the complete model, one can also construct correlation functions involving simultaneously the two sectors and that are order parameters for the whole symmetry group $SU(4) \times SU(6) \times U(1)$, i.e. involving also the nonanomalous axial singlet transformations. This leads to additional sum rules that may constrain the resonance spectrum. At the level of two-point functions, the relevant order parameters involving the two sectors are

$$\Pi^{\psi X}_{S^0}(q^2) = i\int d^4x e^{iq\cdot x}\langle \mathrm{vac}|T\{\mathcal{S}^0_\psi(x)\mathcal{S}^0_X(0)\}|\mathrm{vac}\rangle,$$
$$\Pi^{\psi X}_{P^0}(q^2) = i\int d^4x e^{iq\cdot x}\langle \mathrm{vac}|T\{\mathcal{P}^0_\psi(x)\mathcal{P}^0_X(0)\}|\mathrm{vac}\rangle. \tag{4.18}$$

From them we derive two additional spectral sum rules, valid in the limit where m_X vanishes:

$$\int_0^\infty dt\,\mathrm{Im}\Pi^{\psi X}_{S_0}(t) = 0, \qquad \int_0^\infty dt\,\mathrm{Im}\Pi^{\psi X}_{P_0}(t) = 0, \tag{4.19}$$

which, respectively, constrain the spectrum of scalar and pseudoscalar singlets resonances.

One could examine the realization of these sum rules in the NJL framework, similarly to what we did for the electroweak sector in Sec. III G, for instance investigating whether the first low-lying resonances in each channel saturate them. Here we rather describe some of the expected features in general terms, independently from the NJL approximation. In the singlet pseudoscalar channel, we expect two states. The first one is the Goldstone boson η_0 produced by the spontaneous breaking of the nonanomalous axial $U(1)$ symmetry. The second one is a massive pseudoscalar state η', which corresponds to the second Goldstone boson that would be present in the absence of the gauge anomaly in the divergences of the $U(1)_\psi$ and $U(1)_X$ currents. These states both couple to the (partially) conserved $U(1)$ current, defined in Eq. (4.7) above,

$$\langle \mathrm{vac}|\mathcal{J}^0_\mu(0)|\eta_0(p)\rangle = iF_{\eta_0}p_\mu,$$
$$\langle \mathrm{vac}|\mathcal{J}^0_\mu(0)|\eta'(p)\rangle = iF_{\eta'}p_\mu. \tag{4.20}$$

In the limit where m_X vanishes, F_{η_0} remains nonzero and $F_{\eta'}\sim\mathcal{O}(m_X)$, whereas for the masses $M^2_{\eta_0}\sim\mathcal{O}(m_X)$ while $M^2_{\eta'}$ does not vanish. Of course, there are also couplings to the individual, nonconserved, $U(1)_\psi$ and $U(1)_X$ currents, defined in Eqs. (3.4) and (4.1), respectively,

$$\langle \mathrm{vac}|\mathcal{J}^0_{\psi\mu}(0)|\eta_0(p)\rangle = iF^\psi_{\eta_0}p_\mu,$$
$$\langle \mathrm{vac}|\mathcal{J}^0_{\psi\mu}(0)|\eta'(p)\rangle = iF^\psi_{\eta'}p_\mu,$$
$$\langle \mathrm{vac}|\mathcal{J}^0_{X\mu}(0)|\eta_0(p)\rangle = iF^X_{\eta_0}p_\mu,$$
$$\langle \mathrm{vac}|\mathcal{J}^0_{X\mu}(0)|\eta'(p)\rangle = iF^X_{\eta'}p_\mu. \tag{4.21}$$

According to the expressions given in Eqs. (3.4), (4.1), and (4.7), these four decay constants are related to the ones in the preceding equation through $F_{\eta_0,\eta'} = F^X_{\eta_0,\eta'} - 3(N-1)F^\psi_{\eta_0,\eta'}$. Both η_0 and η' states also couple to the singlet pseudoscalar densities,

$$\langle \mathrm{vac}|\mathcal{P}^0_\psi(0)|\eta_0(p)\rangle = G^\psi_{\eta_0},$$
$$\langle \mathrm{vac}|\mathcal{P}^0_\psi(0)|\eta'(p)\rangle = G^\psi_{\eta'},$$
$$\langle \mathrm{vac}|\mathcal{P}^0_X(0)|\eta_0(p)\rangle = G^X_{\eta_0},$$
$$\langle \mathrm{vac}|\mathcal{P}^0_X(0)|\eta'(p)\rangle = G^X_{\eta'}, \tag{4.22}$$

and through Eq. (4.8) the two following relations hold:

$$F_{\eta_0}M^2_{\eta_0} = 4\sqrt{3}m_X G^X_{\eta_0}, \qquad F_{\eta'}M^2_{\eta'} = 4\sqrt{3}m_X G^X_{\eta'}. \tag{4.23}$$

Although they do not lead to sum rules, it is both interesting and useful to consider two-point correlators involving the axial singlet current and the singlet pseudoscalar densities, defined in analogy to Eq. (2.15) for the nonsinglet case,

$$\Pi^\psi_{A^0P^0}(q^2)q_\mu = \int d^4x e^{iq\cdot x}\langle \mathrm{vac}|T\{\mathcal{J}^0_\mu(x)\mathcal{P}^0_\psi(0)\}|\mathrm{vac}\rangle,$$
$$\Pi^X_{A^0P^0}(q^2)q_\mu = \int d^4x e^{iq\cdot x}\langle \mathrm{vac}|T\{\mathcal{J}^0_\mu(x)\mathcal{P}^0_X(0)\}|\mathrm{vac}\rangle. \tag{4.24}$$

$\Pi^\psi_{A^0P^0}(q^2)$ and $\Pi^X_{A^0P^0}(q^2)$ are order parameters of $SU(4)\times U(1)$ and of $SU(6)\times U(1)$, respectively, and in the limit where the current $\mathcal{J}^0_\mu(x)$ is conserved they are both saturated by the massless η_0 pole, as in Eq. (2.16). In the presence of the mass m_X, this is no longer true, and the Ward identities give

$$q^2\Pi^\psi_{A^0P^0}(q^2) = 4\sqrt{3}m_X\Pi^{\psi X}_{P^0}(q^2) - 6(N-1)\langle\mathcal{S}^0_\psi\rangle,$$
$$q^2\Pi^X_{A^0P^0}(q^2) = 4\sqrt{3}m_X\Pi^X_{P^0}(q^2) + 2\langle\mathcal{S}^0_X\rangle. \tag{4.25}$$

These lead, in particular, to the constraints

$$4\sqrt{3}m_X\Pi^{\psi X}_{P^0}(0) = 6(N-1)\langle\mathcal{S}^0_\psi\rangle,$$
$$4\sqrt{3}m_X\Pi^X_{P^0}(0) = -2\langle\mathcal{S}^0_X\rangle, \tag{4.26}$$

as well as

$$F_{\eta_0}G^\psi_{\eta_0} = 6(N-1)\langle\mathcal{S}^0_\psi\rangle + \mathcal{O}(m_X),$$
$$F_{\eta_0}G^X_{\eta_0} = -2\langle\mathcal{S}^0_X\rangle + \mathcal{O}(m_X), \tag{4.27}$$

which provide useful cross-checks for the NJL calculation.

C. Effective couplings induced by the hypercolor gauge anomaly

In order to study, in the NJL framework, the anomalous divergence of Eq. (4.2), induced by the $Sp(2N)$ hypercolor gauge interaction, let us first discuss the X sector in isolation. The sector of gauge configurations with unit winding number now induces $2(N-1)$ fermionic zero

modes per flavor (in the present case, $N_f^X = 3$) for the Dirac operator corresponding to the X and $\bar{X}$ fermions (the uninteresting case $N = 1$ is, of course, discarded). Through the index theorem, these zero modes induce a violation of the $U(1)_X$ charge by $12(N-1)$ units, which, as already discussed in Sec. III A for the electroweak sector, has to be reproduced by the effective 't Hooft vertex. In the case of an $Sp(4)$ gauge group ($N = 2$), it is straightforward to construct an operator $\mathcal{O}_X$ that induces this violation of the invariance under $U(1)_X$, while at the same time preserving the invariance under the $SU(6)$ flavor group:

$$\mathcal{O}_X = -\frac{1}{6!}\epsilon_{f_1\cdots f_6}\epsilon_{g_1\cdots g_6}(X^{f_1}X^{g_1})\cdots(X^{f_6}X^{g_6}) = -\det(X^f X^g), \tag{4.28}$$

where the determinant is taken in the six-dimensional flavor space. For $N > 2$ and only 6 Weyl fermions at our disposal, one obvious extension of the above operator satisfying the required properties would consist in taking $\mathcal{O}_X^{N-1}$. One should, however, be aware that, on the one hand, this simple procedure might not comply with the properties of the 't Hooft vertex as arising from the Grassmann integration over the fermionic collective coordinates,[16] and, on the other hand, that the 't Hooft vertex could also involve derivatives of the fermion fields. An example where this second feature is known to happen is provided by the case of an $SU(2) \simeq Sp(2)$ gauge group with fermions in the adjoint representation [90]. Delving more deeply into these issues would, however, lead us too far astray. Moreover, dealing with a term involving derivatives of the fermion fields is beyond the NJL framework as it is usually understood. From the point of view of the latter, the term $\mathcal{O}_X^{N-1}$, possessing all the required symmetry properties, is quite appropriate, and henceforth we will assume that at the level of the NJL approach, it provides the required description of the explicit breaking of the $U(1)_X$ symmetry by quantum effects.

The preceding discussion considered the $SU(6)$ sector in isolation and, apart from some subtle aspects due to the representation of the gauge group under which the X fermions transform, has essentially paralleled the related discussion for the $SU(4)$ sector in Sec. III A. We will now bring the two sectors together and, as was already the case for the discussion of the anomaly matching conditions in Sec. IV A, we will find that when acting together the two sectors unravel new features. Indeed, the structure of anomaly-driven effective terms is actually different, as one should take into account that a combination of $U(1)_X$ and $U(1)_\psi$ transformations, as given in Eq. (4.10), remains nonanomalous. This drastically changes the form of appropriate effective interactions generalizing the 't Hooft terms usually being given by a (flavor) determinant, since ψ and X are not in the same representation. Combining this information with the discussion above and in Sec. III A, the lowest dimensional operator that breaks both $U(1)_\psi$ and $U(1)_X$ axial singlet symmetries, while preserving the $U(1)$ symmetry generated by the combination (4.7), reads

$$\mathcal{L}_{\psi X} = A_{\psi X}\frac{\mathcal{O}_\psi}{(2N)^2}\left[\frac{\mathcal{O}_X}{[(2N+1)(N-1)]^6}\right]^{(N-1)} + \text{H.c.}, \tag{4.29}$$

with $\mathcal{O}_X$ defined in Eq. (4.28) and $\mathcal{O}_\psi$ the antisymmetric four-fermion operator in Eq. (3.1),

$$\mathcal{O}_\psi = -\frac{1}{4}\epsilon_{abcd}(\psi^a\psi^b)(\psi^c\psi^d). \tag{4.30}$$

The constant $A_{\psi X}$ can be taken real and positive by adjusting the phase of ψ. Its normalization in Eq. (4.29) has been conveniently chosen in order to compensate the different powers of N contained in the condensates, see Eqs. (3.19) and (5.4). This normalization, with an N-independent coefficient $A_{\psi X}$, would reproduce the correct behavior of the $U(1)_{\psi,X}$ anomaly in the large-N limit, would the latter exist, see the discussion around Eqs. (4.11) and (4.12). Indeed, Eq. (4.2) shows that the effect of the anomaly would not vanish in this limit, as $(N-1)g_{HC}^2 \sim (N-1)/N \sim 1$. As we will see in Sec. V E, a trace of this feature appears in the mass of the η', which is proportional to $A_{\psi X}$, $M_{\eta'}^2 \sim A_{\psi X}[1 + \mathcal{O}(1/N)]$.

After formation of the two condensates $\langle\psi\psi\rangle$ and $\langle XX\rangle$, the interaction (4.29) will generate effective four-fermion interactions for ψ and X, as well as a mixed $\psi\psi XX$ term, upon replacing appropriate number of fermion bilinears by their respective condensate (i.e. closing the loops). To identify these four-fermion interactions, relevant for the computation of the meson spectrum, let us first consider for simplicity the $SU(6) \to SO(6)$ sector. The fermion bilinear can be decomposed as

$$(X^f X^g) \equiv 2(T_X^0\Sigma_0^c)^{gf}(X\Sigma_0^c T_X^0 X) + 2(T^{\hat{F}}\Sigma_0^c)^{gf}(X\Sigma_0^c T^{\hat{F}} X), \tag{4.31}$$

in terms of the $SO(6)$ singlet and the two-index symmetric traceless components. Then, taking into account combinatorial factors, the operator of Eq. (4.28) can be decomposed as[17]

$$\mathcal{O}_X = \frac{1}{27}[(X\Sigma_0^c T_X^0 X)^6 - 3(X\Sigma_0^c T_X^0 X)^4(X\Sigma_0^c T^{\hat{F}} X)(X\Sigma_0^c T^{\hat{F}} X) + \cdots], \tag{4.32}$$

[16] Useful introductions to instantons are provided by Refs. [87–89].

[17] The coefficient of $(X\Sigma_0^c T_X^0 X)^6$ in $\det(X^f X^g)$ is $2^6\det(\Sigma_0^c T_X^0) = -1/27$, and the coefficient of $(X\Sigma_0^c T_X^0 X)^4(X\Sigma_0^c T^{\hat{F}} X)(X\Sigma_0^c T^{\hat{G}} X)$ is $2^6\det(\Sigma_0^c T_X^0)(2\sqrt{3})^2\frac{1}{2}[\mathrm{tr}(T^{\hat{F}})\mathrm{tr}(T^{\hat{G}}) - \mathrm{tr}(T^{\hat{F}}T^{\hat{G}})] = \frac{1}{9}\delta^{\hat{F}\hat{G}}$.

where a sum over the $SU(6)$ generators $T^{\hat{F}}$ belonging to the $SU(6)/SO(6)$ coset is understood. For the $SU(4) \to Sp(4)$ sector, the similar appropriate decomposition into $Sp(4)$-invariant bilinears reads

$$\mathcal{O}_\psi = (\psi\Sigma_0 T^0_\psi \psi)(\psi\Sigma_0 T^0_\psi \psi) - (\psi\Sigma_0 T^{\hat{A}}\psi)(\psi\Sigma_0 T^{\hat{A}}\psi). \tag{4.33}$$

Next we insert the results (4.32) and (4.33) into the full effective Lagrangian Eq. (4.29), and obtain

$$\begin{aligned}\mathcal{L}_{\psi X} = \frac{A_{\psi X}}{(27)^{N-1}}\Bigg\{ &\left(\frac{\psi\Sigma_0 T^0_\psi\psi}{2N}\right)^2 \left[\frac{X\Sigma^c_0 T^0_X X}{(2N+1)(N-1)}\right]^{6(N-1)} \\ &- \left(\frac{\psi\Sigma_0 T^{\hat{A}}\psi}{2N}\right)^2 \left[\frac{X\Sigma^c_0 T^0_X X}{(2N+1)(N-1)}\right]^{6(N-1)} \\ &- 3(N-1)\left(\frac{\psi\Sigma_0 T^0_\psi\psi}{2N}\right)^2 \left[\frac{X\Sigma^c_0 T^0_X X}{(2N+1)(N-1)}\right]^{6(N-1)-2} \\ &\times \left[\frac{X\Sigma^c_0 T^{\hat{F}} X}{(2N+1)(N-1)}\right]^2 \Bigg\} + \cdots, \end{aligned} \tag{4.34}$$

where the ellipsis denotes other interaction terms, of no relevance for our purposes. The overall constant $A_{\psi X}$ remains arbitrary, but the ratio of the coefficients of the three effective $XXXX$, $\psi\psi\psi\psi$, and $\psi\psi XX$ terms are fixed. All effective couplings in the singlet and nonsinglet sectors are thus related to the unique coupling $A_{\psi X}$ in Eq. (4.29), times appropriate powers of the two condensates and combinatorial factors (see Sec. V A below).

V. SPECTRUM OF MESON RESONANCES IN PRESENCE OF THE COLORED SECTOR

In this section, we will compute the condensates and the masses of mesons, once the colored sector is added to the electroweak sector, including their mixing through Eq. (4.34). The two sectors share the same $Sp(2N)$ hypercolor gauge interaction; therefore, one can, in principle, relate the sizes of the effective four-fermion operators in the two sectors. One may assume, in particular, that the effective interactions between hypercolor-singlet fermion bilinears originate from $Sp(2N)$ current-current operators (see Appendix D). In this approximation one can link, to some extent, the couplings of the colored operators to the electroweak ones. In this way the mass gap and the spectrum in the $SU(6)$ sector are connected to the ones in the $SU(4)$ sector.

A. The mass gap in a theory with two sectors

Let us begin with the colored scalar operators, which are relevant for the mass gap and for the spin-zero mesons. Besides the anomalous operator (4.34), there is one more independent four-fermion operator that describes the dynamics in analogy with the electroweak sector Lagrangian in Eq. (3.1),

$$\begin{aligned}\mathcal{L}^X_{\rm scal} = &\frac{\kappa_{A6}}{(2N+1)(N-1)}(X^f X^g)(\bar{X}_f \bar{X}_g) \\ &- \frac{1}{2} m_X[(X\Sigma^c_0 X) + (\bar{X}\Sigma^c_0 \bar{X})], \end{aligned} \tag{5.1}$$

where the coupling constant κ_{A6} is real and its normalization by an inverse factor $(2N+1)(N-1)$ has been conveniently chosen to compensate for the factors of N induced by the trace over hypercolor in the X-fermion one-loop two-point functions (see Appendix C). In contrast with the electroweak sector, we also include in Eq. (5.1) an explicit symmetry-breaking mass m_X, already introduced in Eq. (4.4), which can be chosen real and positive by tuning the phase of X. Note that also $A_{\psi X}$ in Eq. (4.34) can be chosen real and positive, by tuning the phase of ψ. Such a mass term may be phenomenologically necessary to raise the masses of the colored pNGBs, in order to comply with direct collider detection limits [91]. More generally, a nonzero m_X leads to several qualitative effects that are worth to be explored. As the contraction over $Sp(2N)$ indices in Eq. (4.3) is symmetric in hypercolor space, the scalar bilinear $(X^f X^g)$ must be symmetric in flavor space, that is, it transforms as the 21_s representation of $SU(6)$, to be compared with $(\psi^a\psi^b)$, which transforms as the 6_a of $SU(4)$. Since $21_{SU(6)} = (1 + 20')_{SO(6)}$, one can rewrite the Lagrangian (5.1) in the physical basis, as

$$\begin{aligned}\mathcal{L}^X_{scal} = &\frac{2\kappa_{A6}}{(2N+1)(N-1)}[(X\Sigma^c_0 T^0_X X)(\bar{X}T^0_X\Sigma^c_0\bar{X}) \\ &+ (X\Sigma^c_0 T^{\hat{F}} X)(\bar{X}T^{\hat{F}}\Sigma^c_0\bar{X})] - \frac{1}{2} m_X[(X\Sigma^c_0 X) + (\bar{X}\Sigma^c_0\bar{X})], \end{aligned} \tag{5.2}$$

where $T^{\hat{F}}$ are the 20 broken generators spanning the $SU(6)/SO(6)$ coset.

Combining the effect of the operators in Eqs. (3.14), (4.34) and (5.2), one can derive a system of two coupled gap equations for the $SU(4)$ and $SU(6)$ sectors,

$$\begin{cases} 1 - 4(\kappa_A + \kappa_B)\tilde{A}_0(M^2_\psi) = 0, \\ 1 - 4(\kappa_{A6} + \kappa_{B6})\tilde{A}_0(M^2_X) - \frac{m_X}{M_X} = 0, \end{cases} \tag{5.3}$$

which determine the dynamical masses M_ψ and M_X as functions of the four couplings $\kappa_{A,B,A6,B6}$ and of the mass m_X. More precisely, when $m_X \neq 0$ the scale M_X is not entirely generated by the dynamics, see Fig. 12. Just as in the electroweak sector, M_ψ can be traded for $\langle\Psi\Psi\rangle$, see Eq. (3.19), the NJL dynamical mass M_X is also related to the condensate $\langle XX\rangle$ in the colored sector,

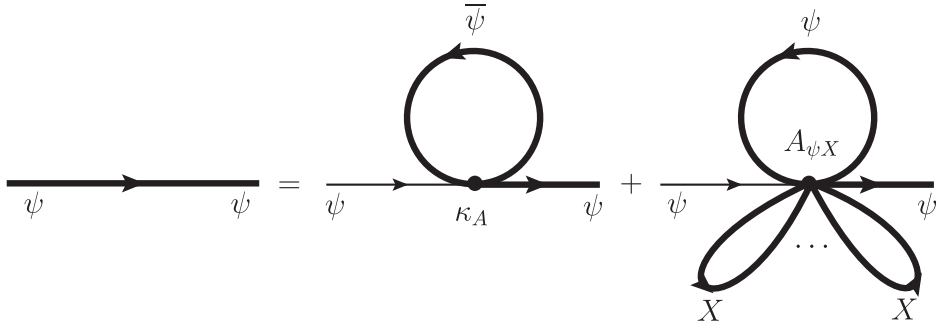

FIG. 10. Graphical illustration of the mass-gap equation in the ψ sector. The convention for the propagator lines are the same as in Fig. 1. The first term, proportional to κ_A, remains the same as in the electroweak sector in isolation. The second term, proportional to $A_{\psi X}$, is obtained by closing one loop of ψ fermions and $6(N-1)$ loops of X fermions in Eq. (4.34). The mass-gap equation in the X sector is obtained in an analogous way, with an additional term proportional to the explicit fermion mass m_X.

$$\langle XX\rangle \equiv \frac{1}{\sqrt{N_f^X}}\langle S_0^X\rangle = -2(2N+1)(N-1)M_X\tilde{A}_0(M_X^2), \tag{5.4}$$

where the factor $(2N+1)(N-1)$ comes from the trace over hypercolor. The two mass gap equations are coupled because the first operator in Eq. (4.34) induces both the κ_B and κ_{B6} terms in Eq. (5.3). These contributions are obtained by closing all but one fermion bilinears into a tadpole loop, as illustrated in Fig. 10 for the case of the ψ sector. This amounts to replacing each bilinear by the associated condensate, and to add a combinatorial factor 2 in κ_B, as one ψ-bilinear out of 2 is not closed, and $6(N-1)$ in κ_{B6}, as one X-bilinear out of $6(N-1)$ is not closed. Therefore, the anomalous terms in the gap equations are related to the original anomaly coefficient $A_{\psi X}$ by

$$\begin{aligned}\kappa_B &\equiv \frac{A_{\psi X}}{2\cdot 27^{N-1}}\left[\frac{4N_f^X\langle XX\rangle^2}{(2N+1)^2(N-1)^2}\right]^{3(N-1)}\frac{2}{2N}\\ &= [4M_X\tilde{A}_0(M_X^2)]^{6(N-1)}\frac{A_{\psi X}}{2N},\end{aligned} \tag{5.5}$$

$$\begin{aligned}\kappa_{B6} &\equiv \frac{A_{\psi X}}{2\cdot 27^{N-1}}\left[\frac{4N_f^\psi\langle\psi\psi\rangle^2}{(2N)^2}\right]\left[\frac{4N_f^X\langle XX\rangle^2}{(2N+1)^2(N-1)^2}\right]^{3(N-1)-1}\\ &\quad\times\frac{6(N-1)}{(2N+1)(N-1)}\\ &= \frac{4N}{2N+1}\frac{M_\psi^2}{M_X^2}\frac{\tilde{A}_0^2(M_\psi^2)}{\tilde{A}_0^2(M_X^2)}\kappa_B.\end{aligned} \tag{5.6}$$

The combinatorial factors will be essential, among other things, in order to recover the singlet Goldstone boson; see Sec. V E. The effective couplings $\kappa_{B,B6}$ are normalized such as to contribute to the gap equations (5.3) as for a single sector in isolation. However, since they are functions of both dynamical masses, $\kappa_{B,B6} = \kappa_{B,B6}(M_\psi^2, M_X^2)$, the two gap equations are actually coupled in a nontrivial way.

Let us analyze in some detail the system (5.3) of two coupled gap equations, because it is qualitatively different from the canonical NJL gap equation of QCD, and, to the best of our knowledge, it was not studied in the existing literature. It is convenient to take the effective coupling κ_B as the free parameter characterizing the effect of the hypercolor anomaly, that is, to express κ_{B6} as a function of κ_B according to Eq. (5.6). This choice makes it easier to compare with the electroweak sector in isolation, and it also simplifies the algebraic form of the solutions of Eq. (5.3). As we have seen in Sec. III A, the $SU(4)$ sector forms a condensate and a nonzero dynamical mass M_ψ is generated when $\xi \equiv (\kappa_A + \kappa_B)\Lambda^2/(4\pi^2)$ is above the critical value $\xi = 1$. Similarly, in the chiral limit $m_X = 0$, a nonzero dynamical mass M_X is generated when $\xi_c \equiv (\kappa_{A6} + \kappa_{B6})\Lambda^2/(4\pi^2) > 1$. Beyond that, the general resolution of the set of equations (5.3) coupled through Eq. (5.6) is very involved, especially for $m_X \neq 0$, and it can only be solved numerically. Still, it is instructive to consider a few special cases.

1. Case $m_X = 0$, $\kappa_B = 0$

When $\kappa_B = 0$, i.e. $A_{\psi X} = 0$, the two gap equations decouple. It is convenient to introduce dimensionless variables and functions in order to rewrite them in the form

$$\begin{cases} 1 - \xi_A\bar{A}(x_\psi) = 0, \\ 1 - \xi_{A6}\bar{A}(x_X) = 0, \end{cases} \tag{5.7}$$

where $x_{\psi,X} \equiv M_{\psi,X}^2/\Lambda^2$, $\xi_{A,A6} \equiv (\Lambda^2/4\pi^2)\kappa_{A,A6}$, and $\bar{A}(x) \equiv 1 - x\ln(1+1/x)$. The solutions of the two equations in (5.7) are simply related as

$$x_\psi(\xi_A) = x_X(\xi_{A6}). \tag{5.8}$$

The result is to restrict the range of the allowed values of $\xi|_{\kappa_B=0} = \xi_A$, as compared to the case of one sector in isolation. Indeed, imposing that both conditions $0 \le x_\psi(\xi_A) \le 1$ and $0 \le x_X(\xi_{A6}) \le 1$ be satisfied simultaneously requires

$$\max\left(1,\frac{\kappa_A}{\kappa_{A6}}\right) \le \xi \le \min\left(1,\frac{\kappa_A}{\kappa_{A6}}\right)\frac{1}{1-\ln 2} \qquad (\kappa_B = 0). \tag{5.9}$$

Hence, for $\kappa_A/\kappa_{A6} > 1$ the minimal value of ξ is larger than unity, whereas for $\kappa_A/\kappa_{A6} < 1$, the highest value allowed for ξ is reduced, see Fig. 12. These considerations do not depend explicitly on the value of N, although the actual values of κ_A and of κ_{A6}, being determined by the hypercolor dynamics, will depend on N.

Thus, although the two gap equations are decoupled, the presence of the second one impinges on the possible values allowed for the coupling of the second one, and vice-versa. This simply illustrates the fact that while the two gap equations may be decoupled, they nevertheless share the same effective-theory cutoff Λ.

2. Case $m_X = 0$, $\kappa_B \neq 0$

By treating κ_B as an extra free parameter, the first equation in the system (5.3) is formally identical to the gap equation for the electroweak sector in isolation, Eq. (3.17), with solution $x_\psi = x_\psi(\xi)$. Then, rewriting κ_{B6} as a function of κ_B according to Eq. (5.6), the second gap equation becomes a self-consistent relation for x_X, that depends on N, ξ, ξ_{A6}, and $\xi_B \equiv (\Lambda^2/4\pi^2)\kappa_B$:

$$\begin{cases} 1-\xi\bar{A}(x_\psi) = 0, \\ \mathcal{G}(x_X,\xi_{A6}) \equiv x_X\bar{A}(x_X)[1-\xi_{A6}\bar{A}(x_X)] = \dfrac{4N}{2N+1}\xi_B\dfrac{x_\psi(\xi)}{\xi^2}. \end{cases} \tag{5.10}$$

Note that the second equality assumes a consistent solution of the first equation, $x_\psi(\xi)$, which requires $1 < \xi < 1/(1-\ln 2)$. In practice we solve numerically the first equation for $x_\psi(\xi)$, then we use it as an input to solve numerically the second one for $x_X(\xi)$.

In Fig. 11 we plot $\mathcal{G}(x,\xi_{A6})$ as a function of x, for a few representative values of ξ_{A6}, as well as the right-hand side of the second equation in (5.10), for two values of N and ξ_B, assuming for simplicity two equal mass gaps, $x_\psi = x_X = x$. The intersection between the dashed and solid curves determines the solution $x_X = x_X(N,\xi,\xi_{A6},\xi_B)$. The function $\mathcal{G}(x,\xi_{A6})$ vanishes at $x = 0$ and, for any fixed value $0 < x < 1$, it decreases with ξ_{A6}. For $\xi_{A6} \le 1$, $\mathcal{G}(x,\xi_{A6})$ increases in the whole interval $0 \le x \le 1$, while for $\xi_{A6} > 1$ it decreases to negative values for small x, then increases as x moves towards unity, becoming positive before $x = 1$, as long as $\xi_{A6} < 1/(1-\ln 2)$. On the other hand, the function $x_\psi(\xi)/\xi^2$ satisfies $0 \le x_\psi(\xi)/\xi^2 \lesssim 1/10$ for $0 \le x \le 1$. Since $\xi_B \ge 0$, there is, therefore, no solution to the second equation in (5.10) in the interval $0 \le x_X \le 1$ when $\xi_{A6} \ge 1/(1-\ln 2)$. In contrast, for values $1 < \xi_{A6} < 1/(1-\ln 2)$ there is always a nontrivial solution with $x_X < 1$, as long as the right-hand side of the second equation in (5.10) is sufficiently small. Finally, for $0 < \xi_{A6} < 1$ the occurrence of a solution happens only for a sufficiently large ξ_B, also depending on N. The latter properties actually reflect the critical value $\xi_{A6} + \xi_{B6} > 1$, necessary in order to obtain a nontrivial mass-gap, here somewhat disguised by the change of variables. Note that for fixed values of N, ξ and ξ_B, the value of x_X increases with ξ_{A6}.

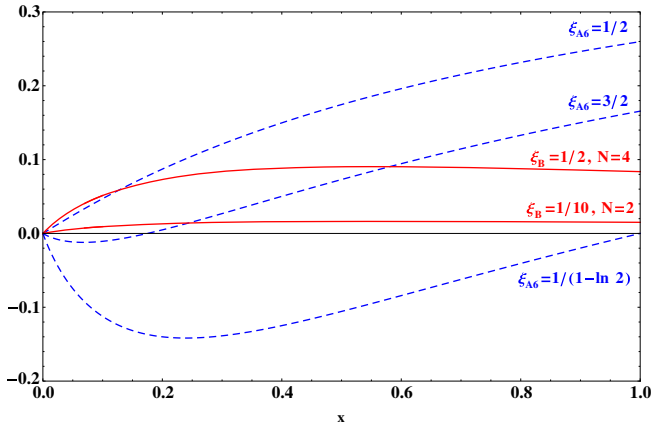

FIG. 11. Dotted curves: the function $\mathcal{G}(x,\xi_{A6})$ for three representative values of ξ_{A6} as indicated. Thick curves: right-hand side of the second equation in (5.10) for two values of N and ξ_B as indicated, and taking $x_\psi = x$.

One can make one more step in the analytical study of the two coupled gap equations. Moving the term proportional to ξ_B in the first equation of (5.10) to its right-hand side, one may now eliminate ξ_B between the two equations, and obtain

$$\mathcal{G}(x_\psi,\xi_A) = \left(\frac{1}{2}+\frac{1}{4N}\right)\mathcal{G}(x_X,\xi_{A6}). \tag{5.11}$$

A few simple remarks follow from this relation. First, if one of the masses, say M_X, has been determined as a function of ξ_A, ξ_{A6} and ξ_B, then the relation of M_ψ to M_X involves only ξ_A, ξ_{A6} and N, and not ξ_B. Second, this relation becomes rapidly independent of N as N increases. Third, the relatively simple Eq. (5.11) precisely gives the exact dependence of the ratio of the two mass gaps, M_X/M_ψ, as functions of the basic input parameters (although it is an implicit relation, due to the nonlinearity in the masses M_X, M_ψ), as illustrated for a few representative case in Fig. 12. More precisely, Eq. (5.11) may be trivially expressed as

$$\frac{M_\psi^2}{M_X^2} = \left(\frac{1}{2}+\frac{1}{4N}\right)\frac{\bar{A}^2(x_X)[1-\xi_{A6}\bar{A}(x_X)]}{\bar{A}^2(x_\psi)[1-\xi_A\bar{A}(x_\psi)]}. \tag{5.12}$$

This indeed shows that, as long as $M_\psi^2, M_X^2 \ll \Lambda^2$ [which implies $\bar{A}(x_X) \simeq \bar{A}(x_\psi)$ since $\bar{A}(x) \equiv 1 - x\ln(1+1/x) \simeq 1 + M^2/\Lambda^2\ln(\Lambda^2/M^2)$], one obtains $M_\psi < M_X$, at least for $\xi_A \simeq \xi_{A6}$. Indeed, the peculiar case of equal mass gaps, $x_\psi = x_X$, that is the one illustrated in Fig. 11, can only be

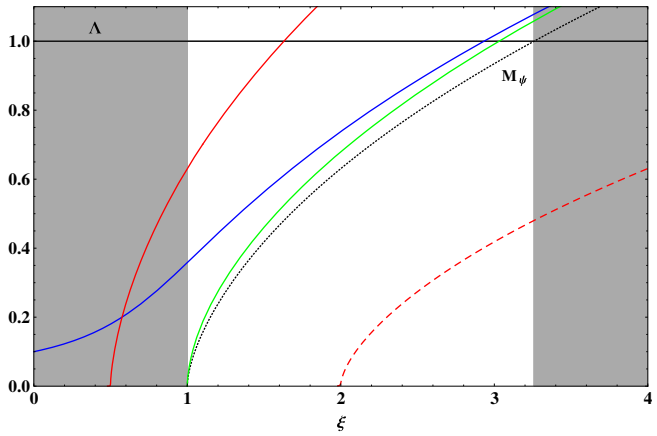

FIG. 12. Comparison between the mass gap M_ψ of the electroweak sector (black dotted line) and the mass gap M_X of the colored sector for few representatives cases. When $\kappa_{A6} = \kappa_A$, $m_X = 0$ and $\kappa_B/\kappa_A = 0$, the two dynamical masses are equal, $M_\psi = M_X$. To illustrate the behavior of M_X with respect to the free parameters of the theory (ξ, κ_B/κ_A, κ_{A6}/κ_A, m_X and N) we illustrate small departures from this particular case. The solid (dashed) red line corresponds to $\kappa_{A6} = 2(1/2)\kappa_A$ with $\kappa_B/\kappa_A = 0$, $m_X = 0$ and $N = 4$. In these cases, the critical coupling of the colored sector is, respectively, smaller or larger than the one in the electroweak sector ($\xi = 1$). Next, the solid blue (green) line corresponds to $\kappa_{A6} = \kappa_A$, $N = 4$ with $\kappa_B/\kappa_A = 0$ ($\kappa_B/\kappa_A = 0.1$) and $m_X = \Lambda/10$ ($m_X = 0$). In the case where there is an explicit symmetry-breaking mass m_X, there is no critical coupling in the colored sector as the lowest value of M_X is simply m_X. Finally note that M_X is almost independent of the number of hypercolor N.

obtained for significantly different values of ξ_A and ξ_{A6} (for instance when $N = 4$, $\xi_{A6} = 1/2$ and $\xi_B = 1/2$, one has $x_\psi = x_X \simeq 0.13$, that corresponds to $\xi_A \simeq 0.9$).

In the above considerations we have kept κ_A and κ_{A6} (equivalently, ξ_A and ξ_{A6}) arbitrary. Let us now examine more precisely a few typical situations concerning those parameters. When κ_{A6} is larger than κ_A, the $SU(6)$ sector first forms a condensate for $\xi < 1$ (see Fig. 12), and then $M_X > M_\psi$. In the opposite case where κ_{A6} is smaller than κ_A, the $SU(6)$ sector forms a condensate for a value $\xi > 1$, and $M_X < M_\psi$. If $\xi_{A6} \gg \xi_A$, the mass gap grows rather fast, so that one eventually obtains a very large $M_X \sim \Lambda$, and conversely a very large M_ψ if $\xi_{A6} \ll \xi_A$. Thus to obtain predictive calculations in both sectors from the NJL model, it requires that $\xi_A \sim \xi_{A6}$ are roughly of the same magnitude. In this way, there is a nonzero interval for the values of ξ where the NJL predictions can be trusted ($\xi, \xi_c > 1$ and $M_{\psi,X} < \Lambda$) in both sectors. Note that apart from these NJL consistency considerations, in principle no value of the ratio ξ_A/ξ_{A6} is theoretically excluded, but the case $M_\psi = 0$ and $M_X \neq 0$ evidently does not describe a composite Higgs model since then the spectrum of resonances does not contain a pNGB Higgs doublet. For $\xi_A = \xi_{A6}$, i.e. $\kappa_A = \kappa_{A6}$, and still for $m_X = 0$, the ratio M_X/M_ψ thus depends only of the value of κ_B and N, as given precisely by the relation in Eq. (5.12). When ξ_B is close to zero, one gets $M_\psi \simeq M_X$, since the two gap equations are almost decoupled. Next, when ξ_B increases, there is a complicated balance between the N, M_ψ and M_X dependence in Eq. (5.6), to determine κ_{B6}/κ_B, but the ratio M_X/M_ψ is consistently determined from the relatively simple relation in Eq. (5.12). This implies $\kappa_{B6} > \kappa_B$ and M_X slightly above M_ψ, with a M_X/M_ψ ratio that increases rather slowly with ξ_B, and is also a slowly increasing function of N. For instance for $N = 2$, $M_X/M_\psi \simeq 1.14$–1.21 for $\kappa_B/\kappa_A = 0.01$–0.5.

Finally, let us briefly discuss the most general case $m_X \neq 0$. The above considerations give of course only approximate relations, which however remains relatively good as long as m_X remains moderate, $m_X \ll M_X$. For $m_X \neq 0$ there is no critical coupling ξ_c in the $SU(6)$ sector, as the minimal value of M_X is obviously nonzero, being equal to m_X. A nonzero m_X evidently leads to $M_X > M_\psi$ for equivalent coupling values in the two sectors; see Fig. 12.

A couple of remarks are in order. In Sec. V E, we will see that the scalar singlet sector is consistent only for a very small value of κ_B/κ_A, see Eqs. (5.31) and (5.40). This is due to the requirement of vacuum stability, which is not apparent in the mass-gap equations (5.3). For example, this upper bound implies that a value $\xi_B = 1/2$, as illustrated in Fig. 11, is actually not possible. This in turns sets a lower bound on ξ_{A6}, in order to stay above the critical value, $\xi_{A6} + \xi_{B6} > 1$, and to obtain a nonzero value of M_X. Let us now comment on the dynamical relation between κ_B and the original anomalous parameter $A_{\psi X}$, given in Eq. (5.5), and which involves M_X and N. In the whole allowed range $1 < \xi < (1 - \ln 2)^{-1} \simeq 3.25$, even when $M_X \simeq \Lambda$ for large ξ, the factor in square brackets in Eq. (5.5) is small in Λ^3 units, essentially because of the loop-suppression, $4M_X\tilde{A}_0(M_X^2) \simeq (4 - 8) \times 10^{-3}\Lambda^3$ (with moderate dependence on κ_B/κ_A and N). This implies a strong suppression of the effective coupling ξ_B due to the large power $6(N - 1)$ in Eq. (5.5), even for the minimal value $N = 2$. Unfortunately, the original Lagrangian parameter $A_{\psi X}$ originates from nonperturbative dynamics that is not under control at the present stage, so that its size is essentially arbitrary, see also the discussion in subsection IV C after Eq. (4.28). Therefore, we can just remark that, whatever the actual size of $A_{\psi X}$, the corresponding value of κ_B is strongly suppressed by the dynamics. This may help to comply with the upper bound from vacuum stability on κ_B/κ_A, which behaves as $1/N$ for sufficiently large N, as we shall discuss in Sec. V E, because the effective coupling κ_B in Eq. (5.5) contains a power-N suppression factor.

B. Masses of colored scalar resonances

The scalar and pseudoscalar resonances associated to X-fermion bilinears transform under the flavor symmetry as $21_{SU(6)} = (1 + 20')_{SO(6)}$. In analogy with the ψ-fermion sector, we can define a matrix $\overline{M}_c$ in flavor space,

$$\overline{M}_c = \frac{1}{2} M_X \Sigma_0^c + (\sigma_X + i\eta_X)\Sigma_0^c T_X^0 + (S_c^{\hat{F}} + iG_c^{\hat{F}})\Sigma_0^c T^{\hat{F}}, \tag{5.13}$$

where the components σ_X (η_X) and $S_c^{\hat{F}}$ ($G_c^{\hat{F}}$) are, respectively, the $SO(6)$-singlet and twenty-plet (pseudo)scalars. The relevant operators for the computation of the spin-zero meson masses are those given in Eq. (5.2), plus the effective four-fermions operators ψ^4, X^4 and $\psi^2 X^2$, which are induced by the anomalous Lagrangian of Eq. (4.34), after spontaneous symmetry breaking,

$$\begin{aligned}\mathcal{L}_{\psi X}^{\text{eff}} = {} & \frac{\kappa_B}{2N}[(\psi\Sigma_0 T_\psi^0\psi)(\psi\Sigma_0 T_\psi^0\psi) \\ & - (\psi\Sigma_0 T^{\hat{A}}\psi)(\psi\Sigma_0 T^{\hat{A}}\psi) + \text{H.c.}] \\ & + \frac{\kappa_{B6}}{(2N+1)(N-1)}[(6N-7)(X\Sigma_0^c T_X^0 X)(X\Sigma_0^c T_X^0 X) \\ & - (X\Sigma_0^c T^{\hat{F}} X)(X\Sigma_0^c T^{\hat{F}} X) + \text{H.c.}] \\ & + \frac{\kappa_{\psi X}}{2N}[(\psi\Sigma_0 T_\psi^0\psi)(X\Sigma_0^c T_X^0 X) + \text{H.c.}],\end{aligned} \tag{5.14}$$

where κ_B and κ_{B6}, defined in Eq. (5.5) and (5.6), respectively, are the same couplings that appear in the gap equations. Note the factor $(6N-7)$ that multiples κ_{B6}, because here two X-fermion bilinears out of $6(N-1)$ are not closed into a loop, which implies a combinatorial factor $6(N-1)[6(N-1)-1]/2$. The additional coupling $\kappa_{\psi X}$ is defined by

$$\begin{aligned}\kappa_{\psi X} \equiv {} & \frac{A_{\psi X}}{27^{N-1}}\left[\frac{4N_f^\psi\langle\psi\psi\rangle^2}{(2N)^2}\right]^{\frac{1}{2}}\left[\frac{4N_f^X\langle XX\rangle^2}{(2N+1)^2(N-1)^2}\right]^{3(N-1)-\frac{1}{2}} \\ & \times \frac{2\cdot 6(N-1)}{(2N+1)(N-1)} = \frac{8\sqrt{6}N}{2N+1}\frac{M_\psi}{M_X}\frac{\tilde{A}_0(M_\psi^2)}{\tilde{A}_0(M_X^2)}\kappa_B,\end{aligned} \tag{5.15}$$

and it controls the mixing between the $Sp(4)$ and $SO(6)$ (pseudo)scalar singlets σ_ψ (η_ψ) and σ_X (η_X), which will be treated separately in Sec. V E. Note that all three effective couplings vanish if $\langle XX\rangle = 0$. When $\langle XX\rangle \neq 0$ both κ_{B6} and $\kappa_{\psi X}$ are fully determined as a function of M_ψ, M_X and κ_B. From Eqs. (5.2) and (5.14) one can derive the four-fermion couplings for each physical channel,

$$\begin{aligned}K_{\sigma_X(\eta_X)} &= 2\frac{[\kappa_{A6} \pm (6N-7)\kappa_{B6}]}{(2N+1)(N-1)}, \\ K_{S_c(G_c)} &= 2\frac{[\kappa_{A6} \mp \kappa_{B6}]}{(2N+1)(N-1)},\end{aligned} \tag{5.16}$$

For convenience, all the relevant four-fermion couplings for the X-sector spin-zero and spin-one mesons are collected in Table IV, together with the associated one-loop two-point functions.

We now calculate the masses of the scalar and pseudoscalar nonsinglet resonances $S_c^{\hat{F}}$ and $G_c^{\hat{F}}$. As already mentioned above, for the scalar and pseudoscalar singlet σ_X and η_X, there is a mixing with the corresponding

TABLE IV. The four-fermion couplings K_ϕ in the X sector, and the associated one-loop two-point functions $\tilde{\Pi}_\phi^X(q^2)$. The latter are related to the two-point functions of the ψ sector as follows: $\tilde{\Pi}_\phi^\psi(q^2) = \tilde{\Pi}_\phi(q^2, M_\psi^2, 2N)$ and $\tilde{\Pi}_\phi^X(q^2) = \tilde{\Pi}_\phi[q^2, M_X^2, (2N+1)(N-1)]$, where $\tilde{\Pi}_\phi(q^2, M_\psi^2, 2N)$ are defined in Table II. We also give the expression of the mixed (one-loop) pseudoscalar-longitudinal axial correlator, as well as those of the couplings mixing the singlet scalars of the two sectors, σ_ψ and σ_X, and the singlet pseudoscalars η_ψ and η_X. The explicit calculation of the correlators $\tilde{\Pi}_\phi^X(q^2)$ is detailed in Appendix C.

ϕ	K_ϕ	$\tilde{\Pi}_\phi^X(q^2)$
$G_c^{\hat{F}}$	$\frac{2(\kappa_{A6}+\kappa_{B6})}{(2N+1)(N-1)}$	$\tilde{\Pi}_P^X(q^2) = (2N+1)(N-1)[\tilde{A}_0(M_X^2) - \frac{q^2}{2}\tilde{B}_0(q^2, M_X^2)]$
η_X	$\frac{2[\kappa_{A6}-(6N-7)\kappa_{B6}]}{(2N+1)(N-1)}$	
$\eta_\psi - \eta_X$	$\frac{-\kappa_{\psi X}}{(2N)}$	
$S_c^{\hat{F}}$	$\frac{2(\kappa_{A6}-\kappa_{B6})}{(2N+1)(N-1)}$	$\tilde{\Pi}_S^X(q^2) = (2N+1)(N-1)[\tilde{A}_0(M_X^2) - \frac{1}{2}(q^2 - 4M_X^2)\tilde{B}_0(q^2, M_X^2)]$
σ_X	$\frac{2[\kappa_{A6}+(6N-7)\kappa_{B6}]}{(2N+1)(N-1)}$	
$\sigma_\psi - \sigma_X$	$\frac{\kappa_{\psi X}}{(2N)}$	
$V_c^{\mu F}$	$\frac{-2\kappa_{D6}}{(2N+1)(N-1)}$	$\tilde{\Pi}_V^X(q^2) = \frac{1}{3}(2N+1)(N-1)[-2M_X^2\tilde{B}_0(0, M_X^2) + (q^2 + 2M_X^2)\tilde{B}_0(q^2, M_X^2)]$
$A_c^{\mu\hat{F}}$	$\frac{-2\kappa_{D6}}{(2N+1)(N-1)}$	$\tilde{\Pi}_A^X(q^2) = \frac{1}{3}(2N+1)(N-1)[-2M_X^2\tilde{B}_0(0, M_X^2) + (q^2 - 4M_X^2)\tilde{B}_0(q^2, M_X^2)]$
a_X^μ	$\frac{-2\kappa_{C6}}{(2N+1)(N-1)}$	$\tilde{\Pi}_A^{XL}(q^2) = -2(2N+1)(N-1)M_X^2\tilde{B}_0(q^2, M_X^2)$
$A_c^{\mu\hat{F}} - G_c^{\hat{F}}$		$\tilde{\Pi}_{AP}^X(q^2) = -(2N+1)(N-1)M_X\tilde{B}_0(q^2, M_X^2)$
$a_X^\mu - \eta_X$		

resonances σ_ψ and η_ψ of the electroweak sector, so that the whole singlet sector will be treated separately in Sec. V E.

Concerning the nonsinglet pNGB G_c, we should also consider more generally a nontrivial pseudoscalar-axial vector mixing for nonvanishing vectorial four-fermion couplings, as we anticipate will be introduced below in Sec. V C, in analogy with the electroweak sector discussed in Sec. III E. With the additional explicit breaking mass term m_X of Eq. (5.1), the pseudoscalar axial-vector mixing formalism of Sec. III E can easily be generalized with explicitly m_X-dependent resummed matrix correlator $\bar{\mathbf{\Pi}}_{G_c}(m_X)$, the analogue of Eqs. (3.44) and (3.47) for the colored sector. Note that all of the one-loop two-point functions $\tilde{\Pi}(q^2, M_X^2) \equiv \tilde{\Pi}_\phi^X(q^2)$ of the $SU(6)$ sector can be obtained from those in table II with the following replacements: $M_\psi \to M_X$ and $(2N) \to (2N+1)(N-1)$ (see Appendix C for details). Accordingly the pNGB obviously gets a nonzero mass, whose expression is obtained from the zero of the determinant, analogous to (3.46) for the $SU(4)$ sector, as

$$\begin{aligned} D_{G_c} &= \frac{m_X}{M_X} g_{A_c}^{-1} + 2(\kappa_{A6} + \kappa_{B6})\tilde{B}_0(p^2, M_X^2)p^2 \\ &\equiv 2(\kappa_{A6} + \kappa_{B6})\tilde{B}_0(p^2, M_X^2)(p^2 - M_{G_c}^2). \end{aligned} \tag{5.17}$$

The calculation of the scalar $S_c^{\hat{F}}$ mass is simpler and follows the same derivation as for the scalar mass of the $SU(4)$ sector. Thus we obtain

$$\begin{aligned} M_{G_c}^2 &= -\left(\frac{m_X}{M_X}\right) \frac{g_{A_c}^{-1}(M_{G_c}^2)}{2(\kappa_{A6} + \kappa_{B6})\tilde{B}_0(M_{G_c}^2, M_X^2)}, \\ M_{S_c}^2 &= 4M_X^2 - \frac{8\kappa_{B6}\tilde{A}_0(M_X^2) + \frac{m_X}{M_X}}{2(\kappa_{A6} - \kappa_{B6})\tilde{B}_0(M_{S_c}^2, M_X^2)}. \end{aligned} \tag{5.18}$$

where as before the pole masses are defined as $M_{G_c}^2 = M_{G_c}^2(p^2 = M_{G_c}^2)$. Accordingly, similarly to M_η^2 in Eq. (3.52), when a nonvanishing colored sector vector coupling κ_{D6} is considered (see Sec. V C), the pseudoscalar Goldstone mass $M_{G_c}^2$ is renormalized by the (inverse) axial form factor $g_{A_c}^{-1}(p^2 \equiv M_{G_c}^2) \equiv 1 - 2K_{A_c}\tilde{\Pi}_A^{LX}(M_{G_c}^2)$ where K_{A_c} is defined in Table IV.

Note that there is another source of explicit symmetry breaking which may *a priori* lead to sizable contributions to the masses. Indeed, when we switch on the SM gauge interactions, new contributions to the masses of the colored states arise. In the following, we will only consider the gauge corrections to the masses of the pNGB states, since the latter are the lightest resonances of the colored sector. Therefore, those corrections are more relevant than e.g. for the other scalar states. The gauge contributions to the pNGB masses are given in general terms in Sec. II E and in Appendix A 2 for the particular case of the $SU(6)$ sector. The pNGB $G_c^{\hat{F}}$ decompose as an octet $O_c \sim 8_0$ and two sextet $(S_c + \bar{S}_c) \sim (6_{4/3} + \bar{6}_{-4/3})$ under $SU(3)_c \times U(1)_D$ [$U(1)_D$ is the hypercharge component in the X sector, and is also defined in Appendix A 2]. Consequently, there are two sources of gauge contributions which lead to a mass splitting between the octet and sextet components: one from the gauging of QCD and one from the gauging of the hypercharge. However, from Eq. (A14) one can see that the QCD corrections are almost the same for the two components as $\Delta M_{O_c}^2/\Delta M_{S_c}^2|_{\rm QCD} = 9/10$. For simplicity we will neglect this small difference. In addition, the contribution coming from the gauging of $U(1)_Y$ is subdominant compared to the one from QCD, and we will safely neglect it. This is due to the small value of the ratio g'/g_s at the energy scale of a few TeVs we are interested in. Then the gauge contributions mainly originate from QCD and to evaluate the latter, we need to compute the integral in Eq. (A14) within the NJL framework. To do that, we simply cut the integral at $Q^2 = \Lambda^2$, where Λ stands for the cutoff of the NJL model, and F_{G_c} is given by the expression

$$F_{G_c}^2 = -2(2N+1)(N-1)M_X^2\tilde{B}_0(M_{G_c}^2, M_X^2)g_{A_c}(M_{G_c}^2), \tag{5.19}$$

which can easily be inferred adapting Eqs. (3.41) and (3.39) to the $SU(6)$ sector. Note that, for simplicity, the mass M_{G_c} in the right-hand side is taken without gauge corrections. The resulting radiative pNGB masses, obtained from Eq. (A14), are illustrated in the left panel of Fig. 13, where by definition $M_{G_c}^2 = \Delta M_{O_c}^2$, as $m_X = 0$. These numerical results will be discussed in more details in Sec. V D. Let us just mention that this gauge-induced mass could be sufficient by itself to comply with the lower collider bounds [91].

C. Masses of colored vector resonances

In order to calculate the masses of the vector and axial-vector resonances present in the colored sector, we start from the following vector-vector four-fermion operators

$$\begin{aligned} \mathcal{L}_{\rm vect}^X = &\frac{\kappa_{C6}}{(2N+1)(N-1)}(\bar{X}T_X^0\bar{\sigma}^\mu X)^2 + \frac{\kappa_{D6}}{(2N+1)(N-1)} \\ &\times [(\bar{X}T^F\bar{\sigma}^\mu X)^2 + (\bar{X}T^{\hat{F}}\bar{\sigma}^\mu X)^2], \end{aligned} \tag{5.20}$$

where as in the electroweak sector, due to the global $SU(6)$ symmetry, the four-fermions coupling κ_{D6} of the vector channel is the same as the axial nonsinglet channel. From the above operators we obtain the vector and axial-vector four-fermions couplings K_{V_c}, K_{A_c} and K_{a_X} (see table IV) and we derive the masses of the vector V_c^F and axial $A_c^{\hat{F}}, a_X$ resonances

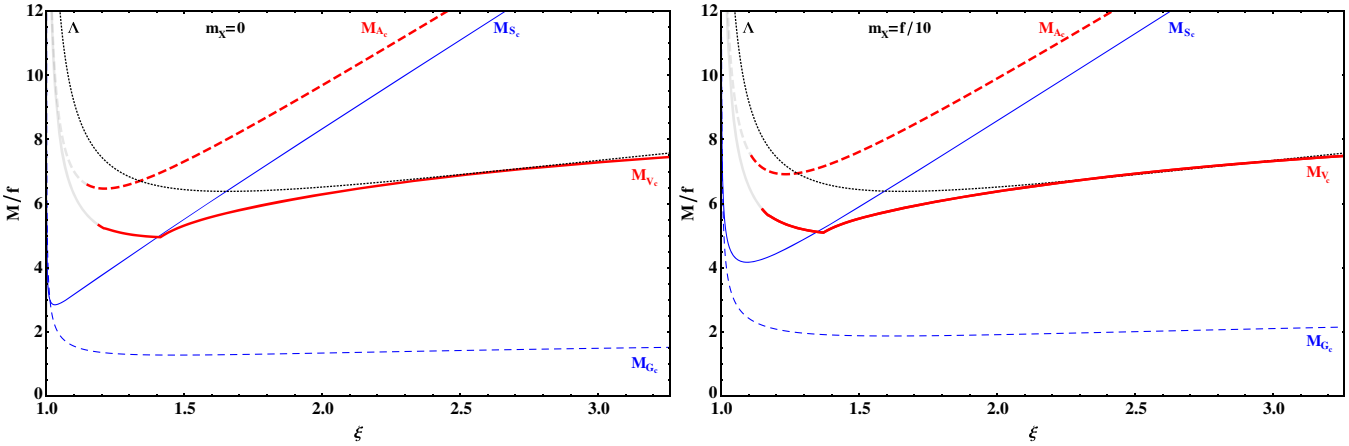

FIG. 13. The masses of the colored resonances in units of the Goldstone decay constant $f \equiv \sqrt{2} f_G$, for $N = 4$ (the masses scale as $1/\sqrt{N}$), as a function of the coupling ξ, for $\kappa_B/\kappa_A = 0.01$, $\kappa_{A6} = \kappa_A$, $m_X = 0$ (left-hand panel) and $m_X = f/10$ (right-hand panel). We displayed the full physical range for ξ, according to Fig. 3. Each curve is shaded when the corresponding pole mass develops a large, unphysical imaginary part, $|\mathrm{Im} g_\phi(M_\phi^2)/\mathrm{Re} g_\phi(M_\phi^2)| > 1$, as defined from Eq. (3.23). The dotted line is the cutoff of the constituent fermion loops. The Goldstone mass M_{G_c} include the radiative corrections as discussed in Sec. V B.

$$M_{V_c}^2 = -\frac{3}{4\kappa_{D6}\tilde{B}_0(M_{V_c}^2, M_X^2)} + 2M_X^2 \frac{\tilde{B}_0(0, M_X^2)}{\tilde{B}_0(M_{V_c}^2, M_X^2)} - 2M_X^2, \tag{5.21}$$

$$M_{A_c}^2 = -\frac{3}{4\kappa_{D6}\tilde{B}_0(M_{A_c}^2, M_X^2)} + 2M_X^2 \frac{\tilde{B}_0(0, M_X^2)}{\tilde{B}_0(M_{A_c}^2, M_X^2)} + 4M_X^2. \tag{5.22}$$

Just like in the electroweak sector, if one neglects the p^2 dependence of the $\tilde{B}_0$ function, one obtains the usual NJL relation between the axial and vector masses, that is $M_{A_c}^2 \simeq M_{V_c}^2 + 6M_X^2$. The mass of the axial singlet a_c^μ is obtained by making the replacements $A_c^\mu \to a_X^\mu$ and $\kappa_{D6} \to \kappa_{C6}$ in Eq. (5.22). Note that we have not considered the following operator

$$\mathcal{L}_{\mathrm{vect}}^{\psi X} = \frac{\kappa_{\psi X}^V}{(2N)} (\bar{\psi} T_\psi^0 \bar{\sigma}^\mu \psi)(\bar{X} T_X^0 \bar{\sigma}_\mu X), \tag{5.23}$$

which induces a mixing between the axial singlets of the two sectors, a_ψ^μ and a_X^μ. This mixing term respects all symmetries of the theory and should be present in general. However, we neglected it as it is not generated by applying a Fierz transformation to the $Sp(2N)$ current-current operators in Eq. (D8).

Note also that, in principle, the spin one masses receive SM gauge contributions as $V_c^\mu \sim 15_{SO(6)} = (1 + 8 + 3 + \bar{3})_{SU(3)_c}$ and $A_c^\mu \sim 20'_{SO(6)} = (8 + 6 + \bar{6})_{SU(3)_c}$. However, following the discussion of Sec. V B for the scalar masses, we will not consider such contributions here.

D. The mass spectrum of the colored resonances

In general the couplings of the four-fermion operators are free parameters. However κ_{A6} and $\kappa_{C6,D6}$ may be related if we assume that the dynamics is induced by $Sp(2N)$ current-current operators. In this case, as in the ψ sector, we find that the scalar and vector four-fermion couplings are equal, see Appendix D 4. However, we also find that the size of these couplings relatively to the ones in the electroweak sector is not fixed by the current-current approximation. The reason is that, contrary to the case of the ψ sector, the X-sector current-current operator cannot be recast in terms of $Sp(2N)$ singlet-singlet operators only; see Appendix D 4. Nonetheless, in this section, for the sake of illustration, we will take equal couplings in the two sectors

$$\kappa_{A6} = \kappa_{C6} = \kappa_{D6} = \kappa_A. \tag{5.24}$$

With this choice, as shown in Fig. 12, the range of validity of the NJL approximation is approximatively the same in the two sectors.

The resonance masses of the colored sector are illustrated in Fig. 13. To ease the comparison with the electroweak sector, the masses are in units of $f = \sqrt{2} F_G \gtrsim 1$ TeV, and are plotted as functions of the coupling ξ defined by Eq. (3.17). Note that in Sec. III F, for the $SU(4)$ sector in isolation, the only constraint from vacuum stability was $\kappa_B/\kappa_A < 1$: here we anticipate a similar but stronger bound, see Eqs. (5.31) and (5.40) below. Consequently the value of κ_B/κ_A is fixed to 0.01 for illustration, which is safely below this upper bound in the case $N = 4$. Then, if one assumes that Eq. (5.24) holds, there is just one additional free parameter compared to the $SU(4)$ sector in isolation, namely the explicit symmetry-breaking mass term m_X. We illustrate two representative cases: one with no explicit breaking,

$m_X = 0$, and another one with explicit symmetry breaking, for which we take as a representative value $m_X = 0.1f$.

In the case with no explicit breaking (left panel of Fig. 13), the behavior of the masses is qualitatively similar to the $SU(4)$ sector, except for the pNGBs G_c. This is due to the relations between the couplings of the four-fermion interactions: $\kappa_A = \kappa_{A6}$ and $\kappa_B \sim \kappa_{B6} \ll \kappa_A$. The pNGB of the colored sector receive a significant contribution to their masses from the gauging of the color group, as discussed in Sec. V B. As it can be seen from Fig. 13, this contribution satisfies $\Delta M_{G_c} \gtrsim 1.3f$, which is enough to comply with the present collider bounds, as long as $f \gtrsim 1$ TeV. Thus, we conclude that it is actually possible to introduce top quark partners without the need of an explicit mass term m_X for the colored fermions. On the other hand, if we want to raise the mass of colored pNGBs, while keeping a low mass scale of the theory, $f = 1$ TeV, one needs to introduce a nonzero m_X, as illustrated in the right panel of Fig. 13 for $m_X = 0.1f$. As all the colored masses receive a contribution from m_X, for sufficiently large values of m_X one could even decouple the colored sector from the electroweak sector.

Finally, we display here the masses of the color resonances for the same parameters as in Eq. (3.54), $N = 4$, $\xi = 1.3$ and $\xi = 2$, fixing $\kappa_B/\kappa_A = 0.01$ and for the two representative values of m_X:

$$\begin{aligned}
&\xi = 1.3, m_X = 0: \quad M_{A_c} \simeq 6.6 \text{ TeV}, \quad M_{V_c} \simeq 5.1 \text{ TeV}, \quad M_{S_c} \simeq 4.3 \text{ TeV}, \quad M_{G_c} \simeq 1.3 \text{ TeV},\\
&\xi = 1.3, m_X = 0.1 \text{ TeV}: \quad M_{A_c} \simeq 7.0 \text{ TeV}, \quad M_{V_c} \simeq 5.2 \text{ TeV}, \quad M_{S_c} \simeq 4.9 \text{ TeV}, \quad M_{G_c} \simeq 2.0 \text{ TeV}.
\end{aligned} \tag{5.25}$$

$$\begin{aligned}
&\xi = 2.0, m_X = 0: \quad M_{A_c} \simeq 9.7 \text{ TeV}, \quad M_{V_c} \simeq 6.3 \text{ TeV}, \quad M_{S_c} \simeq 8.4 \text{ TeV}, \quad M_{G_c} \simeq 1.4 \text{ TeV},\\
&\xi = 2.0, m_X = 0.1 \text{ TeV}: \quad M_{A_c} \simeq 9.9 \text{ TeV}, \quad M_{V_c} \simeq 6.4 \text{ TeV}, \quad M_{S_c} \simeq 8.5 \text{ TeV}, \quad M_{G_c} \simeq 1.8 \text{ TeV}.
\end{aligned} \tag{5.26}$$

E. Flavor-singlet sector

The $\psi - X$ mixing in the (scalar and pseudoscalar) singlet sector, induced by the Lagrangian (4.34), is most conveniently treated in matrix formalism. Furthermore, since our model includes nonvanishing singlet axial-vector couplings both in the $SU(4)$ and $SU(6)$ sectors, we should take into account the additional pseudoscalar-axial mixing, similarly to the case of the $SU(4)$ sector in isolation treated in Sec. III E. Accordingly, we shall consider 2×2 and 4×4 matrix equations for the correlators in the scalar and pseudoscalar sectors, respectively.

1. Scalar-singlet mixing

Let us start with the scalar sector and consider the diagonal one-loop scalar-correlator matrix $\mathbf{\Pi}_{\sigma_\psi \sigma_X}$ and the matrix of scalar couplings $\mathbf{K}_{\sigma_\psi \sigma_X}$,

$$\mathbf{\Pi}_{\sigma_\psi \sigma_X} = \begin{pmatrix} \tilde{\Pi}_S^\psi & 0 \\ 0 & \tilde{\Pi}_S^X \end{pmatrix}, \qquad \mathbf{K}_{\sigma_\psi \sigma_X} = \begin{pmatrix} K_{\sigma_\psi} & K_{\psi X} \\ K_{\psi X} & K_{\sigma_X} \end{pmatrix}, \tag{5.27}$$

where K_{σ_ψ}, K_{σ_X} and $K_{\psi X} \equiv \kappa_{\psi X}/(2N)$ are collected in Tables II and IV. Note that when $K_{\psi X} = 0$ (equivalently $A_{\psi X} = 0$) there is no mixing between the singlets σ_ψ and σ_X. For simplicity, we have introduced the shorthand notations $\tilde{\Pi}_i^\psi \equiv \tilde{\Pi}_i(p^2, M_\psi^2)$ and $\tilde{\Pi}_i^X \equiv \tilde{\Pi}_i(p^2, M_X^2)$ for the one-loop correlators. From the above matrices, one can now define the resummed matrix correlator $\bar{\mathbf{\Pi}}_{\sigma_\psi \sigma_X}$

$$\begin{aligned}
\bar{\mathbf{\Pi}}_{\sigma_\psi \sigma_X} &= \mathbf{\Pi}_{\sigma_\psi \sigma_X} + \mathbf{\Pi}_{\sigma_\psi \sigma_X}(2\mathbf{K}_{\sigma_\psi \sigma_X})\mathbf{\Pi}_{\sigma_\psi \sigma_X} + \cdots \\
&= (\mathbb{1} - 2\mathbf{\Pi}_{\sigma_\psi \sigma_X}\mathbf{K}_{\sigma_\psi \sigma_X})^{-1}\mathbf{\Pi}_{\sigma_\psi \sigma_X},
\end{aligned} \tag{5.28}$$

and the resonance mass eigenvalues are obtained as the roots of the equation $\det(\mathbb{1} - 2\mathbf{\Pi}_{\sigma_\psi \sigma_X}\mathbf{K}_{\sigma_\psi \sigma_X}) = 0$, where

$$\begin{aligned}
&\det(\mathbb{1} - 2\mathbf{\Pi}_{\sigma_\psi \sigma_X}\mathbf{K}_{\sigma_\psi \sigma_X}) \\
&\quad = 1 - 2K_{\sigma_\psi}\tilde{\Pi}_S^\psi - 2K_{\sigma_X}\tilde{\Pi}_S^X + 4(K_{\sigma_\psi}K_{\sigma_X} - K_{\psi X}^2)\tilde{\Pi}_S^\psi \tilde{\Pi}_S^X \\
&\quad = c_0^S(p^2) + c_1^S(p^2)p^2 + c_2^S(p^2)(p^2)^2.
\end{aligned} \tag{5.29}$$

The coefficients $c_i^S(p^2)$ are functions of the couplings K_i, and of the loop functions $\tilde{A}_0(M_\psi^2)$, $\tilde{A}_0(M_X^2)$, $\tilde{B}_0(p^2, M_\psi^2)$, and $\tilde{B}_0(p^2, M_X^2)$. It is convenient to write the determinant as if it were a quadratic form in p^2, because the p^2 dependence of the coefficients $c_i^S(p^2)$, through the loop functions $\tilde{B}_0(p^2, M_{\psi,X}^2)$, does not induce additional pole structure. Then, the scalar-singlet pole masses are obtained as the roots of this quadratic equation, evaluated at a self-consistent value of p^2,

$$\begin{aligned}
&M_{\sigma_0,\sigma'}^2 = \mathrm{Re}[g_{\sigma_0,\sigma'}(M_{\sigma_0,\sigma'}^2)], \\
&g_{\sigma_0,\sigma'}(p^2) \equiv \frac{-c_1^S(p^2) \pm \sqrt{[c_1^S(p^2)]^2 - 4c_2^S(p^2)c_0^S(p^2)}}{2c_2^S(p^2)}.
\end{aligned} \tag{5.30}$$

The explicit expressions of the two scalar singlet masses $M_{\sigma_0}^2, M_{\sigma'}^2$ are straightforwardly derived from the above

equations, but are not very simple or telling, even in the chiral limit $m_X = 0$, so that we refrain from giving them here. In the numerical illustrations below we use these exact expressions.

As we will examine quantitatively below, the lightest scalar mass M_{σ_0} is a *decreasing* function of $r \equiv \kappa_B/\kappa_A$, at least as long as $M_{\psi,X} \ll \Lambda$, and it can even vanish at a critical value r_c, becoming formally tachyonic beyond. This critical value should, therefore, be considered as an intrinsic upper bound, since for $r \geq r_c$ the minimum of the effective scalar potential is destabilized, that is, the solution of the NJL mass-gap equations becomes unreliable. It is clear that M_{σ_0} can only vanish if $c_0^S(0) = 0$ in Eq. (5.29) (irrespective of the additional p^2 dependence from the $\tilde{B}_0$ functions). The latter condition determines r_c as a function of the parameters N, M_X and M_ψ, once one eliminates the coupling κ_{A6} using Eq. (5.3), as well as κ_{B6} and $\kappa_{\psi X}$ using Eqs. (5.6) and (5.15). Then, in the chiral limit $m_X = 0$, the condition $c_0^S(0) = 0$ takes the form

$$1 + 2\left[1 + \frac{f_6}{B_6(0)}\frac{A_4}{M_X^2}\frac{M_\psi^2}{M_X^2}\frac{2N(3N-4)}{2N+1}\right] r + \left[1 - \frac{2f_6}{B_6(0)}\frac{A_4}{M_X^2}\frac{M_\psi^2}{M_X^2}\frac{2N(3N-2)}{2N+1} - \frac{6f_6}{B_6(0)B_4(0)}\frac{A_4^2}{M_X^4}\frac{2N(N-1)}{2N+1}\right] r^2 = 0, \tag{5.31}$$

where $f_6 \equiv 1 + 2B_6(0)M_X^2/A_6$, and we are using the shorthand notations $A_4 \equiv \tilde{A}_0(M_\psi^2)$, $A_6 \equiv \tilde{A}_0(M_X^2)$, and similarly for the functions $B_{4,6}(p^2)$. The mass of σ_0 vanishes as long as Eq. (5.31), that is quadratic in r, has a real and positive root r_c, whose value depends on the dynamical masses $M_{\psi,X}$ and on N. For example, if one fixes $\kappa_{A6} = \kappa_A$, one finds that $\xi \lesssim 1.4$–1.5 implies $\kappa_B/\kappa_A \leq r_c \ll 1$ already for $N = 2$, and the upper bound becomes more stringent proportionally to $\sim 1/N$. For $m_X = 0$ and $\xi = 1.3$, one finds $r_c \simeq 0.103$ for $N = 2$, and $r_c \simeq 0.024$ for $N = 4$. However, for larger values of $\xi \gtrsim 1.7$–1.8, Eq. (5.31) has no longer a real positive root, instead $M_{\sigma_0}(\xi, r)$ has a positive minimum, at increasingly large values of r as ξ increases. As we will see in the next subsection, there is another upper bound on κ_B/κ_A, Eq. (5.40), originating from the pseudoscalar-singlet mixing, also related to vacuum stability. Assuming again $\kappa_{A6} = \kappa_A$, one finds that for $\xi \lesssim 1.4$ the bound from Eq. (5.40) has a numerical value very close to the solution r_c of Eq. (5.31), although its analytic form is different. For larger values of ξ, the bound from Eq. (5.40) is much more stringent and, therefore, supersedes the condition $r < r_c$. As we will examine in concrete illustrations below, these bounds put stringent restrictions on the singlet mass spectrum. As further explained below for the pseudoscalar case, these constraints should be viewed as an appropriate generalization of the constraint $\kappa_B/\kappa_A < 1$, that applies to the $SU(4)$ sector in isolation.

Concerning the scalar decay constants, defined as in Eq. (3.58) with the obvious replacement $S \to S_0^\psi, S_0^X$, they can be derived by generalizing the procedure explained in Sec. III G. They are defined by the residues of the diagonal elements of $\bar{\mathbf{\Pi}}_{\sigma_\psi\sigma_X}$ at the respective pole masses,

$$(G_{\sigma_0}^\psi)^2 \equiv -\lim_{p^2\to M_{\sigma_0}^2}(p^2 - M_{\sigma_0}^2)\bar{\mathbf{\Pi}}^{11}_{\sigma_\psi\sigma_X}(p^2),$$
$$(G_{\sigma_0}^X)^2 \equiv -\lim_{p^2\to M_{\sigma_0}^2}(p^2 - M_{\sigma_0}^2)\bar{\mathbf{\Pi}}^{22}_{\sigma_\psi\sigma_X}(p^2), \tag{5.32}$$

and analogously for $\sigma_0 \to \sigma'$. These decay constants enter in the scalar sum rules in combination with the other (pseudo)scalar decay constants. We refrain here to give their explicit expressions, which are not simple. The results obtained from Eq. (5.32) can be crosschecked with the off-diagonal elements of $\bar{\mathbf{\Pi}}_{\sigma_\psi\sigma_X}$, as $G_{\sigma_0}^\psi G_{\sigma_0}^X = -\lim_{p^2\to M_{\sigma_0}^2}(p^2 - M_{\sigma_0}^2)\bar{\mathbf{\Pi}}^{12}_{\sigma_\psi\sigma_X}(p^2)$, and similarly for σ'.

2. Pseudoscalar singlet mixing

Considering now the more involved pseudoscalar sector, we start from the complete 4×4 matrix coupling and correlator to account both for singlet mixing and pseudoscalar-axial singlet vectors a_ψ^μ, a_X^μ mixing. The latter mixing is treated similarly to the pseudoscalar axial-vector mixing for the Goldstone boson sector as considered in Sec. III E. Accordingly we have

$$\mathbf{K}_{\eta_\psi\eta_X} = \begin{pmatrix} K_{\eta_\psi} & -K_{\psi X} & 0 & 0 \\ -K_{\psi X} & K_{\eta_X} & 0 & 0 \\ 0 & 0 & K_a & 0 \\ 0 & 0 & 0 & K_{a_c} \end{pmatrix},$$
$$\mathbf{\Pi}_{\eta_\psi\eta_X} = \begin{pmatrix} \tilde{\Pi}_P^\psi & 0 & \sqrt{p^2}\tilde{\Pi}_{AP}^\psi & 0 \\ 0 & \tilde{\Pi}_P^X & 0 & \sqrt{p^2}\tilde{\Pi}_{AP}^X \\ \sqrt{p^2}\tilde{\Pi}_{AP}^\psi & 0 & \tilde{\Pi}_A^{L\psi} & 0 \\ 0 & \sqrt{p^2}\tilde{\Pi}_{AP}^X & 0 & \tilde{\Pi}_A^{LX} \end{pmatrix}, \tag{5.33}$$

where all the relevant pseudoscalar and axial-vector correlators and couplings for the $SU(4)$ and $SU(6)$ sectors are given, respectively, in Tables II and IV (and we have used in Eq. (5.33) the same short-hand notation as in Sec. V E 1). From the above matrices, we obtain the resummed two-point correlator defined as

$$\bar{\mathbf{\Pi}}_{\eta_\psi\eta_X} = (\mathbb{1} - 2\mathbf{\Pi}_{\eta_\psi\eta_X}\mathbf{K}_{\eta_\psi\eta_X})^{-1}\mathbf{\Pi}_{\eta_\psi\eta_X}. \tag{5.34}$$

According to the previous equation, the pseudoscalar mass eigenvalues are given by the zeros of the determinant of

$\mathbb{1} - 2\mathbf{K}_{\eta_\psi\eta_X}\mathbf{\Pi}_{\eta_\psi\eta_X}$, which we give explicitly only in the chiral limit $m_X = 0$ for simplicity. Note that the latter determinant keeps the form of a quadratic equation, apart from further p^2 dependence from the $\tilde{B}_0$ function appearing in the coefficients. After using the relevant relations, Eqs. (5.5), (5.6) and (5.15), and the mass gap equations (5.3) in order to express all the effective four-fermion couplings κ_i in terms of κ_B alone, we obtain

$$\det[\mathbb{1} - 2\mathbf{K}_{\eta_\psi\eta_X}\mathbf{\Pi}_{\eta_\psi\eta_X}(p^2)] = p^2[c_1^P(p^2) + p^2 c_2^P(p^2)], \tag{5.35}$$

where in notations similar to the scalar case, we define the relevant coefficients of the quadratic equation as

$$c_1^P(p^2) = 4\frac{\kappa_B A_4}{(2N+1)A_6 M_X^2}[12N(N-1)B_4(p^2)M_\psi^2 g_{a_c}^{-1}(p^2) + (2N+1)B_6(p^2)M_X^2 g_a^{-1}(p^2)], \tag{5.36}$$

$$c_2^P(p^2) = -\frac{B_4(p^2)B_6(p^2)}{(2N+1)A_6^2 M_X^2}[24N(N-1)\kappa_B A_4 M_\psi^2 - (2N+1)(\kappa_A - \kappa_B)A_6 M_X^2]. \tag{5.37}$$

The appearance of the axial singlet form factors g_a, g_{a_c} is a result of the mixing between the singlet pseudoscalar axial-vector

$$g_a^{-1}(p^2) = 1 + \frac{4\kappa_C}{2N}\tilde{\Pi}_A^{L\psi}(p^2),$$
$$g_{a_c}^{-1}(p^2) = 1 + \frac{4\kappa_{C6}}{(2N+1)(N-1)}\tilde{\Pi}_A^{LX}(p^2). \tag{5.38}$$

The pseudoscalar analogue of the term $c_0^S(p^2)$ in the determinant of $\mathbb{1} - 2\mathbf{K}_{\eta_\psi\eta_X}\mathbf{\Pi}_{\eta_\psi\eta_X}$ vanishes in the chiral limit $m_X = 0$, as is explicit from Eq. (5.35), after nontrivial cancellations using the gap equations (5.3), and Eqs. (5.5) and (5.6), thereby exhibiting the remaining singlet Goldstone boson associated with the nonanomalous combination of $U(1)_\psi$ and $U(1)_X$ transformations. Obviously, the other pseudoscalar singlet has a nonvanishing mass even for $m_X = 0$, with a relatively compact expression,

$$M_{\eta'}^2 = \mathrm{Re}[g_{\eta'}(M_{\eta'}^2)] + \mathcal{O}(m_X),$$
$$g_{\eta'}(p^2) \equiv -\frac{c_1^P(p^2)}{c_2^P(p^2)}. \tag{5.39}$$

Note that for sufficiently large N (but keeping in mind $N \leq 18$), $M_{\eta'}^2$ is of order $\mathcal{O}(N^0)$, using that $\kappa_B \simeq 1/N$, while the not-shown $\mathcal{O}(m_X)$ term is of order $1/N$. This is naively compatible with the behavior of the anomaly, which also goes like a constant for sufficiently large values of N, see Eq. (4.2) (considering that $g_{HC}^2 \simeq 1/N$).

An important, interesting feature of the whole model emerges from the examination of Eq. (5.39): for any p^2, the function $g_{\eta'}(p^2)$ has a *pole* at a particular value of κ_B/κ_A, as follows from Eq. (5.37),

$$\frac{\kappa_B/\kappa_A}{1-\kappa_B/\kappa_A} = \frac{1}{24}\frac{2N+1}{N(N-1)}\frac{A_6 M_X^2}{A_4 M_\psi^2}. \tag{5.40}$$

In other words, the η' mass grows rapidly and decouples when approaching from below the critical value of κ_B/κ_A defined by Eq. (5.40). This is not unexpected, as it is simply a generalization of a property already observed in the $SU(4)$ sector in isolation. In the latter case, recall that the mass-gap equation (3.16) has solutions only for $\kappa_B^2 < \kappa_A^2$, as discussed after Eq. (3.17): as also explained in Ref. [8], and apparent in Eqs. (3.12) and (3.13), for $\kappa_B > \kappa_A$ the effective potential is destabilized around the origin, already at tree level and, although one could expect a spontaneous symmetry breaking of some of the symmetries, one cannot perform a proper minimization to determine the vacuum, within the NJL framework. This feature is reflected also directly in the resonance mass spectrum, where the η' mass (for the $SU(4)$ sector in isolation) of Eq. (3.26) clearly has a pole for $\kappa_B = \kappa_A$ and becomes tachyonic for large κ_B. Now the critical value in the full model, determined by Eq. (5.40), should be considered accordingly as an absolute upper bound on κ_B/κ_A. It takes a more involved dynamical form (depending also on the values of the mass gaps M_ψ and M_X) precisely because the mixing, as induced by the effective operators in Eq. (4.34), couples the two sectors, mass gaps and couplings, in a nontrivial way and involves N-dependent combinatorial factors. Note that, upon using the relation (5.6), the critical coupling in (5.40) translates into a simpler upper limit on κ_{B6}, approximately:

$$\frac{\kappa_{B6}}{\kappa_A} < \frac{1}{6(N-1)}\frac{A_4}{A_6}, \tag{5.41}$$

(upon neglecting higher order terms in κ_{B6}^2), in which the combinatoric factor $6(N-1)$ can be understood upon comparing with Eq. (5.14), so that Eq. (5.41) is a more transparent analogue of the limit $\kappa_B < \kappa_A$ in the $SU(4)$ sector in isolation (let aside the presence of the loop functions A_4/A_6, that reflects the nontrivial dynamical connection between the two sectors). The bottom line is that Eq. (5.40) gives a tight upper bound on κ_B/κ_A, due in particular to the small coefficient $1/24$. To get an idea, consider the chiral limit $m_X = 0$ and fix $\kappa_{A6} = \kappa_A$: as discussed in Sec. V A, then M_X lies slightly above M_ψ, with e.g. $M_X/M_\psi \simeq 1.15$ for $N = 2$ and small κ_B/κ_A. Thus, neglecting for simplicity the relatively small differences in the $\tilde{A}_0$ loop functions, Eq. (5.40) gives typically $\kappa_B/\kappa_A < 5/48(M_X^2/M_\psi^2) \simeq 0.12$ for $N = 2$, and the latter ratio decreases quite rapidly for larger N due to the $\sim 1/N$

behavior of Eq. (5.40), for instance $\kappa_B/\kappa_A < 1/32(M_X^2/M_\psi^2) \simeq 0.04$ for $N = 4$.

More precisely, the physical upper bound on κ_B/κ_A is even more stringent. As the "running" mass $g_{\eta'}(p^2)$ grows rapidly when approaching from below the limiting value of κ_B/κ_A defined by Eq. (5.40), the corresponding pole-mass self-consistent equation for $M_{\eta'}^2$, given in Eq. (5.39), ceases to have a solution for a slightly smaller value of κ_B/κ_A. Moreover a large width develops much below this bound, which turns out to rapidly exceed the pole mass. Accordingly, the NJL description of the η' mass looses its validity for even smaller values of κ_B/κ_A. For a not too small $m_X \neq 0$, as discussed above, M_X can be substantially larger than M_ψ; therefore, the bound in Eq. (5.40) is delayed to larger κ_B/κ_A. Still, it remains quite constraining as long as m_X remains moderate with respect to Λ. A hierarchy among the mass gaps, $M_X \gg M_\psi$, can be also realized by taking $\kappa_{A6} > \kappa_A$, again relaxing the upper bound on κ_B/κ_A. In summary, the detailed structure of the mixing sets the maximal allowed value of κ_B/κ_A, with important consequences for the resonance mass spectrum, as we will illustrate below.

For $m_X \neq 0$, the exact expressions of the two pseudoscalar singlet masses $M_{\eta_0}, M_{\eta'}$ (used in our numerical analysis) become rather involved: Eq. (5.35) is modified to a "quadratic" polynomial equation in p^2 (i.e. upon formally neglecting the additional p^2 dependence coming from the loop functions, entering the polynomial coefficients). This is then more similar to the eigenvalue equation of the scalar case above, see Eqs. (5.29) and (5.30), now with coefficients $c_i^P(p^2)$ which depends on m_X, where the coefficient of $(p^2)^0$ takes the form

$$c_0^P = 8A_4\kappa_B \frac{m_X}{M_X} g_a^{-1} g_{a_c}^{-1}. \tag{5.42}$$

Indeed, the pNGB η_0 mass is given to a very good approximation by the first order expansion in c_0^P, namely

$$M_{\eta_0}^2 = -\frac{c_0^P(M_{\eta_0}^2)}{c_1^P(M_{\eta_0}^2)}, \tag{5.43}$$

which essentially captures its correct behavior as long as κ_B/κ_A is moderate and $m_X \ll \Lambda$. For large values of N, $M_{\eta_0}^2$ is of order $1/N$.

Once having determined the η_0 and η' masses, one can proceed to extract all relevant pseudoscalar decay constants from the pole mass residues of the matrix elements $\bar{\mathbf{\Pi}}_{\eta_\psi\eta_X}^{ij}(q^2)$ $(i,j = 1,\ldots,4)$, where the resummed two-point correlator $\bar{\mathbf{\Pi}}_{\eta_\psi\eta_X}(q^2)$ is defined in Eq. (5.34). The procedure is similar to the one explained in Sec. III E for the simpler nonsinglet case. More precisely, from the definitions of the decay constants $F_{\eta_0}^{\psi(X)}$, $G_{\eta_0}^{\psi(X)}$ in Eqs. (4.21) and (4.22), one obtains in general for $m_X \neq 0$

$$\begin{aligned}
&\lim_{q^2\to M_{\eta_0}^2}(q^2 - M_{\eta_0}^2)\bar{\mathbf{\Pi}}_{\eta_\psi\eta_X}^{11(22)}(q^2) \equiv -(G_{\eta_0}^{\psi(X)})^2,\\
&\lim_{q^2\to M_{\eta_0}^2}(q^2 - M_{\eta_0}^2)\bar{\mathbf{\Pi}}_{\eta_\psi\eta_X}^{12,21}(q^2) \equiv -G_{\eta_0}^{\psi}G_{\eta_0}^{\psi},
\end{aligned} \tag{5.44}$$

$$\begin{aligned}
&\lim_{q^2\to M_{\eta_0}^2}\frac{(q^2 - M_{\eta_0}^2)}{\sqrt{p^2}}\bar{\mathbf{\Pi}}_{\eta_\psi\eta_X}^{13,31}(q^2) \equiv -\frac{G_{\eta_0}^{\psi}F_{\eta_0}^{\psi}}{2\sqrt{2}},\\
&\lim_{q^2\to M_{\eta_0}^2}\frac{(q^2 - M_{\eta_0}^2)}{\sqrt{p^2}}\bar{\mathbf{\Pi}}_{\eta_\psi\eta_X}^{14,41}(q^2) \equiv -\frac{G_{\eta_0}^{\psi}F_{\eta_0}^{X}}{2\sqrt{3}},\\
&\lim_{q^2\to M_{\eta_0}^2}\frac{(q^2 - M_{\eta_0}^2)}{\sqrt{p^2}}\bar{\mathbf{\Pi}}_{\eta_\psi\eta_X}^{23,32}(q^2) \equiv -\frac{G_{\eta_0}^{X}F_{\eta_0}^{\psi}}{2\sqrt{2}},\\
&\lim_{q^2\to M_{\eta_0}^2}\frac{(q^2 - M_{\eta_0}^2)}{\sqrt{p^2}}\bar{\mathbf{\Pi}}_{\eta_\psi\eta_X}^{24}(q^2) \equiv -\frac{G_{\eta_0}^{X}F_{\eta_0}^{X}}{2\sqrt{3}},
\end{aligned} \tag{5.45}$$

as well as

$$\begin{aligned}
&\lim_{q^2\to M_{\eta_0}^2}\frac{(q^2 - M_{\eta_0}^2)}{q^2}\bar{\mathbf{\Pi}}_{\eta_\psi\eta_X}^{33}(q^2) \equiv -\frac{(F_{\eta_0}^{\psi})^2}{8},\\
&\lim_{q^2\to M_{\eta_0}^2}\frac{(q^2 - M_{\eta_0}^2)}{q^2}\bar{\mathbf{\Pi}}_{\eta_\psi\eta_X}^{44}(q^2) \equiv -\frac{(F_{\eta_0}^{X})^2}{12},\\
&\lim_{q^2\to M_{\eta_0}^2}\frac{(q^2 - M_{\eta_0}^2)}{q^2}\bar{\mathbf{\Pi}}_{\eta_\psi\eta_X}^{34,43}(q^2) \equiv -\frac{F_{\eta_0}^{\psi}F_{\eta_0}^{X}}{4\sqrt{6}},
\end{aligned} \tag{5.46}$$

where the factors $2\sqrt{2}$ and $2\sqrt{3}$ take into account the normalization of the $U(1)_\psi$ and $U(1)_X$ currents, respectively. Similar expressions hold for the η' with the obvious replacement $\eta_0 \to \eta'$. Notice that the information on both diagonal and nondiagonal terms allow to extract unambiguously the signs of $G_{\eta_0(\eta')}^{\psi(X)}$ and $F_{\eta_0(\eta')}^{\psi(X)}$. In the chiral limit, the pole of the η_0 migrates from the longitudinal to the transverse axial correlator. Consequently, in that case one can not extract the decay constants $F_{\eta_0}^{\psi(X)}$ from Eq. (5.46), but only from Eq. (5.45).

In the following, for reasons of simplicity, we present analytical results only for the chiral limit $m_X = 0$. Let us consider the resummed axial longitudinal correlators, given by $q^2\bar{\Pi}_{a_{\psi(X)}}^L(q^2) = 8(12)\bar{\mathbf{\Pi}}_{\eta_\psi\eta_X}^{33(44)}(q^2)$ and $q^2\bar{\Pi}_{a_\psi a_X}^L(q^2) = 4\sqrt{6}\bar{\mathbf{\Pi}}_{\eta_\psi\eta_X}^{34,43}(q^2)$, see Eq. (5.46). One can check that the linear combination corresponding to the conserved $U(1)$ current, vanishes for any q^2

$$\begin{aligned}
\bar{\Pi}_0^L(q^2) = {}& 9(N-1)^2\bar{\Pi}_{a_\psi}^L(q^2) - 6(N-1)\bar{\Pi}_{a_\psi a_X}^L(q^2)\\
&+ \bar{\Pi}_{a_X}^L(q^2) = 0, \qquad \bar{\Pi}_{a_\psi a_X}^L = \sqrt{\bar{\Pi}_{a_\psi}^L\bar{\Pi}_{a_X}^L}.
\end{aligned} \tag{5.47}$$

This is an important check, since the $U(1)$ current is conserved, despite the nonzero mass gap spoiling the Ward identity at the naive one-loop level. Then, once fully resummed, there is no longitudinal part in the corresponding

axial two-points function, generalizing, for the more involved singlet sector, the results obtained in Sec. III E for the simpler $SU(4)$ sector in isolation with (Goldstone) pseudoscalar-axial mixing. Coming now to the decay constants defined from Eqs. (5.44) and (5.45), using the gap equations (5.3) and the constraints among the effective couplings in Eqs. (5.5), (5.6) and (5.15), and after some algebra, one obtains (in the chiral limit)

$$(G^{\psi}_{\eta_0})^2 = \frac{-12(2N)^2(N-1)A_4^2M_\psi^2 g_a^{-1}(0)g_{a_c}^{-1}(0)}{12N(N-1)B_4(0)M_\psi^2 g_{a_c}^{-1}(0)+(2N+1)B_6(0)M_X^2 g_a^{-1}(0)}, \qquad (G^{X}_{\eta_0})^2 = \frac{(2N+1)^2A_6^2M_X^2}{6(2N)^2A_4^2M_\psi^2}(G^{\psi}_{\eta_0})^2, \qquad (5.48)$$

$$(F^{\psi}_{\eta_0})^2 = \frac{-96(2N)^2(N-1)B_4^2(0)M_\psi^4 g_a(0)g_{a_c}^{-1}(0)}{12N(N-1)B_4(0)M_\psi^2 g_{a_c}^{-1}(0)+(2N+1)B_6(0)M_X^2 g_a^{-1}(0)} = \tilde{\Pi}_A^{L\psi}(0)g_a(0)\left[1-4\kappa_B\frac{A_4B_6(0)g_a^{-1}(0)}{A_6c_1^P(0)}\right], \qquad (5.49)$$

$$(F^{X}_{\eta_0})^2 = \frac{-24(N-1)(2N+1)^2B_6^2(0)M_X^4 g_a(0)^{-1}g_{a_c}(0)}{12N(N-1)B_4(0)M_\psi^2 g_{a_c}^{-1}(0)+(2N+1)B_6(0)M_X^2 g_a^{-1}(0)} = \tilde{\Pi}_A^{LX}(0)g_{a_c}(0)\left[1-24\kappa_B\frac{(2N)(N-1)B_4(0)A_4M_\psi^2 g_{a_c}^{-1}(0)}{(2N+1)A_6M_X^2c_1^P(0)}\right]. \qquad (5.50)$$

Notice from the second expressions of Eqs. (5.49) and (5.50) that the naive expressions of these decay constants, namely when the two sectors are in isolation, are, respectively, recovered for $M_X \to 0$ ($M_\psi \to 0$) as intuitively expected. One can compute in a similar way the decay constants associated with the η'. We do not explicitly give them because the η' is not a pNGB and these expressions are rather involved. The conserved $U(1)$ current $\mathcal{J}_0^\mu$ of Eq. (4.7) implies

$$F_{\eta_0,\eta'} = F^X_{\eta_0,\eta'} - 3(N-1)F^{\psi}_{\eta_0,\eta'}. \qquad (5.51)$$

From Eqs. (5.49) and (5.50), we obtain the decay constant of the η_0 in the chiral limit

$$\begin{aligned} F^2_{\eta_0} &= -24(N-1)[12N(N-1)B_4M_\psi^2 g_a(0) \\ &\quad + (2N+1)B_6M_X^2 g_{a_c}(0)] + \mathcal{O}(m_X), \\ F^2_{\eta'} &= \mathcal{O}(m_X). \end{aligned} \qquad (5.52)$$

As expected on general grounds (see Sec. IV B), F_{η_0} is nonzero in the chiral limit, while $F_{\eta'}$ vanishes. Furthermore, one can also check, after some algebra, that the generally expected relations in Eq. (4.23) are indeed well satisfied (at least up to terms of higher orders in m_X) by our expressions above, which is a very nontrivial crosscheck of the NJL calculations. Likewise the general relations given in Eq. (4.27) are also well satisfied, providing an additional nontrivial crosscheck.

Actually, in the chiral limit the decay constants F_{η_0} for the true Goldstone can be more directly calculated from the resummed transverse axial correlator $\bar{\Pi}_{a_\psi}(q^2)$ and $\bar{\Pi}_{a_X}(q^2)$ evaluated at $q^2 = 0$, in direct analogy with the nonsinglet calculation of F_G. From Eq. (3.39), one obtains

$$\begin{aligned} F^2_{\eta_0} &\equiv \lim_{q^2\to 0}[-q^2\bar{\Pi}_0(q^2)] \\ &= -\lim_{q^2\to 0} q^2[9(N-1)^2\bar{\Pi}_{a_\psi}(q^2) + \bar{\Pi}_{a_X}(q^2)], \end{aligned} \qquad (5.53)$$

where the second equality comes from Eq. (4.7), taking into account that there is no mixing for the transverse contributions, i.e. $\bar{\Pi}_{a_\psi a_X}(q^2) = 0$. The transverse resummed correlators are simply given by expressions similar to the one in Eq. (3.39): $-q^2\bar{\Pi}_{a_\psi}(q^2) = 8\tilde{\Pi}_A^{\psi}(q^2)g_A(q^2)$ and $-q^2\bar{\Pi}_{A_X}(q^2) = 12\tilde{\Pi}_A^{X}(q^2)g_{A_c}(q^2)$. Thus using the expression of the one-loop functions $\tilde{\Pi}_A^{\psi(X)}(0)$ from Table II and Table IV directly gives

$$\begin{aligned} F^2_{\eta_0} &= 9(N-1)^2[-16(2N)M_\psi^2\tilde{B}_0(0,M_\psi^2)g_a(0)] \\ &\quad + [-24(2N+1)(N-1)M_X^2\tilde{B}_0(0,M_X^2)g_{a_c}(0)], \end{aligned} \qquad (5.54)$$

which is consistent with Eq. (5.52).

3. The mass spectrum of the singlet resonances

We now study the mass spectrum of the scalar and pseudoscalar singlet resonances. Before turning to the more involved case including the mixing between the resonances from the electroweak and the colored sectors, let us consider the instructive no-mixing case, where $A_{\psi X} = 0$ and consequently $\kappa_B = \kappa_{B6} = \kappa_{\psi X} = 0$. From Eq. (5.29) we obtain for the scalar singlet masses

$$\begin{aligned} A_{\psi X} = 0\colon\ & M^2_{\sigma_0} = 4M_\psi^2 = M^2_{\sigma_\psi}, \\ & M^2_{\sigma'} = 4M_X^2 - \frac{m_X}{M_X}\frac{1}{2\kappa_{A6}B_6(M^2_{\sigma'})} = M^2_{\sigma_X}, \end{aligned} \qquad (5.55)$$

which of course reproduce the masses in isolation. As discussed above, in our benchmark case where $\kappa_{A6} = \kappa_A$ we

have $M_\psi \leq M_X$, so that in the no-mixing case we have $M^2_{\sigma_0} \leq M^2_{\sigma'}$ where the equality is valid for $m_X = 0$. In the same way, from Eq. (5.35) we obtain for the pseudoscalar masses

$$A_{\psi X} = 0\colon\ M^2_{\eta_0} = 0 = M^2_{\eta_\psi},$$
$$M^2_{\eta'} = -\frac{m_X}{M_X}\frac{g_{a_c}^{-1}}{2\kappa_{A6}B_6} = M^2_{\eta_X}. \tag{5.56}$$

Again, the latter expressions reproduce those in isolation, and $M^2_{\eta_0} \leq M^2_{\eta'}$, where the equality is valid for $m_X = 0$.

Once we switch on the mixing, important new features arise, as discussed above: in particular, the upper bound on κ_B/κ_A from Eq. (5.40), and the corresponding rapid growth of $M_{\eta'}$ when approaching from below the critical value of κ_B/κ_A. This is illustrated in Fig. 14 for $N = 2$ and $N = 4$, as usual assuming $\kappa_{A6} = \kappa_A$. Consequently, the η' mass may be of order f for $\kappa_B/\kappa_A \ll 0.01$, but once κ_B/κ_A grows to larger values, already well below the bound of Eq. (5.40), η' decouples rapidly.

Another interesting feature is implicit in the η_0 mass expression Eq. (5.43): namely, M_{η_0} rapidly reaches an asymptotic limit for moderate κ_B/κ_A values, for fixed N, and this (approximate) maximum decreases as $1/N$ for large N, as also illustrated in Fig. 14. More precisely, in the approximation of neglecting the differences in momenta of the loop functions, one obtains for large N values

$$M^2_{\eta_0} \simeq -\frac{A_6}{B_6}\frac{1}{3N}\frac{m_X}{M_X}\frac{M^2_X}{M^2_\psi} + \mathcal{O}(1/N^2). \tag{5.57}$$

Of course η_0 being a pNGB, $M^2_{\eta_0}$ vanishes linearly in m_X. This shows in addition that M_{η_0} is approximately κ_B/κ_A-independent, once this ratio takes moderately large values, as shown in Fig. 14. Its mass can be well below f, for sufficiently large N and/or small m_X.

The two *scalar* singlet masses are defined implicitly by Eq. (5.30). The heaviest state σ' always lies in the multi-TeV range, as illustrated in Figs. 14 and 15. More interestingly, as explained in Sec. V E 1, for $\xi \lesssim 1.7$–1.8 the lightest scalar mass M_{σ_0} is a decreasing function of κ_B/κ_A and vanishes at a critical value given by the (positive) root of Eq. (5.31). This critical value is different from the one defined by Eq. (5.40), but for $\xi \lesssim 1.4$ it is numerically very close to the latter, more precisely it lies (slightly) below, for any $N \geq 2$. This is illustrated in Fig. 14

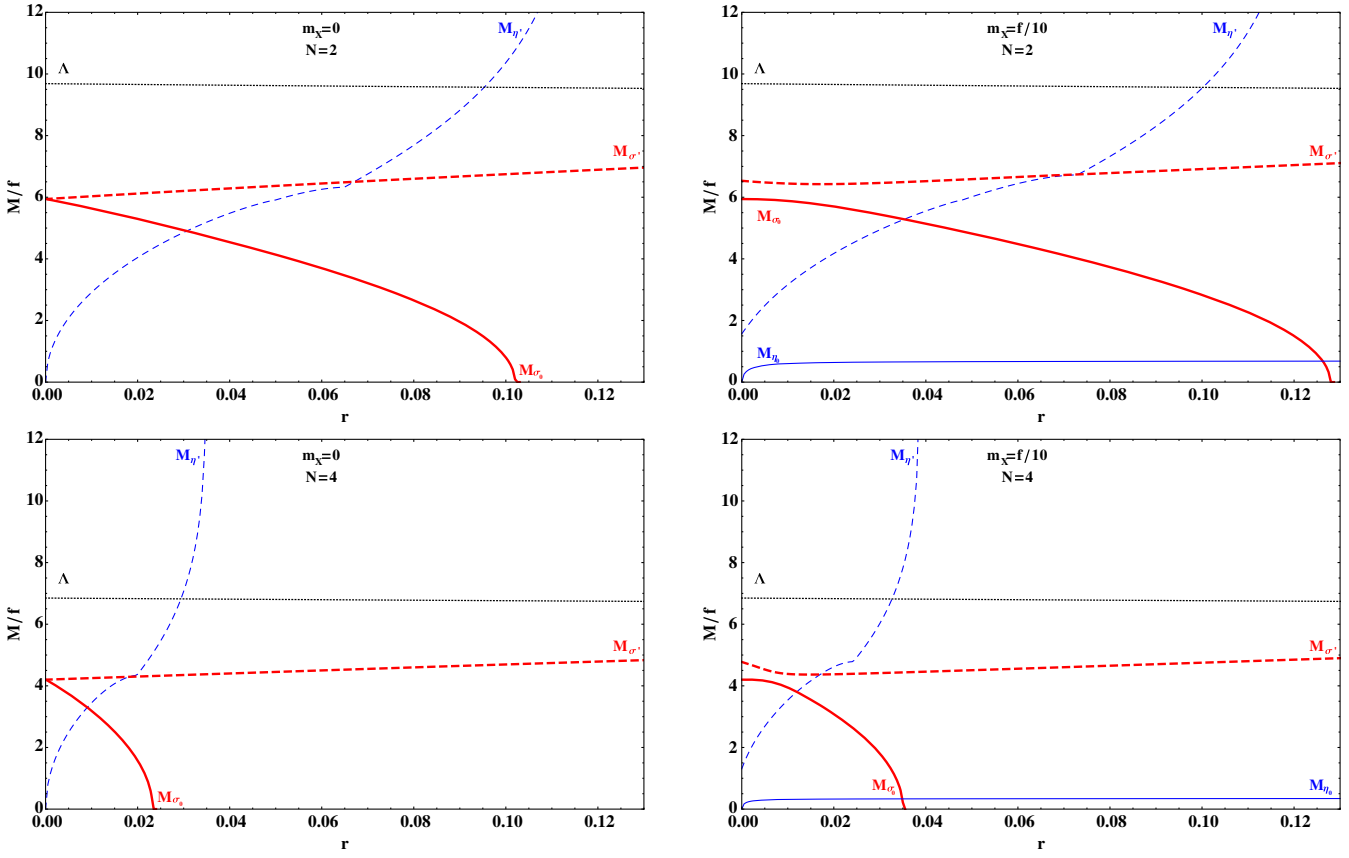

FIG. 14. Singlet scalar and pseudoscalar meson masses in units of f, for a fixed value of the couplings $\xi = 1.3$ and $\kappa_A = \kappa_{A6}$, as a function of $r \equiv \kappa_B/\kappa_A$, for $N = 2$ (top) and $N = 4$ (bottom), and for $m_X = 0$ (left) and $m_X = f/10$ (right). The Goldstone boson η_0 is massless in the chiral limit.

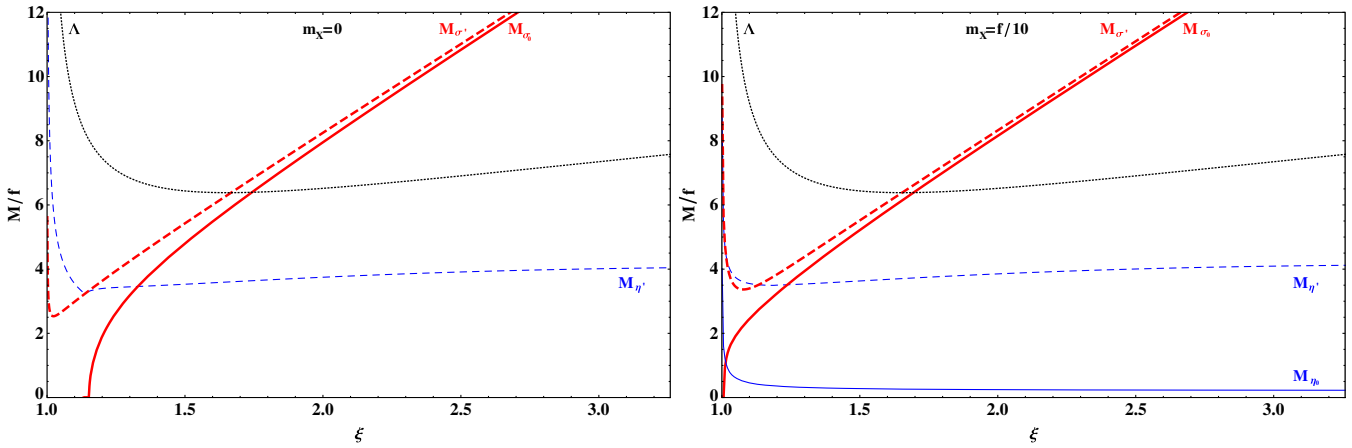

FIG. 15. Singlet scalar and pseudoscalar meson masses in units of f, as a function of ξ for $N=4$, $\kappa_A=\kappa_{A6}$, $\kappa_B/\kappa_A=0.01$, $m_X=0$ (left panel) and $m_X=f/10$ (right panel). The Goldstone boson η_0 is massless in the chiral limit.

for $N=2$ and $N=4$. Beyond the critical value of κ_B/κ_A, σ_0 becomes tachyonic and the effective scalar potential is destabilized; therefore, M_{σ_0} can be very small just before reaching the critical value of κ_B/κ_A. Recall, however, that for $\xi \gtrsim 1.7$, the solution $M_{\sigma_0}=0$ at positive κ_B/κ_A disappears, being replaced by a minimum positive pass, that is reached for an increasing value of κ_B/κ_A as ξ increases. But, in this range for ξ, the bound from Eq. (5.40) is more stringent, restricting κ_B/κ_A to be much smaller and, therefore, rendering nonphysical the behavior of $M_{\sigma_0}(\kappa_B/\kappa_A)$ for larger values of κ_B/κ_A.

Finally, we also illustrate in Fig. 15 the ξ dependence of the scalar and pseudoscalar singlet masses, for representative values of N, and for κ_B/κ_A fixed safely below the upper bound in Eq. (5.40). Notice that M_{σ_0} vanishes for a sufficiently low value of ξ, where one saturates the condition of Eq. (5.31), because the positive root of this equation decreases with ξ. As a consequence, the whole meson mass spectrum should not be trusted for ξ smaller than this critical value, as the vacuum becomes unstable.

To conclude this section, let us briefly discuss the η_0 couplings to the SM gauge bosons. The collider phenomenology of this singlet has already been discussed in general in Ref. [92]. As mentioned at the end of Sec. II E, in the chiral limit the anomalous coupling of a pseudo-Goldstone boson to a pair of gauge bosons is fully determined by the Wess-Zumino-Witten effective action. While the $SU(4)/Sp(4)$ $[SU(6)/SO(6)]$ pseudo-Goldstone bosons may couple only to the electroweak (color) gauge bosons, the η_0 is specially interesting as it couples to both, because it couples to both the ψ and X-fermion number currents $\mathcal{J}^0_{\psi\mu}$ and $\mathcal{J}^0_{X\mu}$. The two currents have a $U(1)_Y$ anomaly, and $\mathcal{J}^0_{\psi\mu}$ $[\mathcal{J}^0_{X\mu}]$ has a $SU(2)_L$ $[SU(3)_c]$ anomaly as well. Then, specializing Eq. (2.37) to our model, the η_0 couplings to the SM gauge bosons take the form

$$\begin{aligned}\mathcal{L}^{WZW}_{\mathrm{eff},\eta_0} &= -\frac{1}{16\pi^2}(2N)[-3(N-1)] \\ &\quad\times\frac{\eta_0}{F_{\eta_0}}(g^2 W_{i\mu\nu}\tilde{W}_i^{\mu\nu}+g'^2 B_{\mu\nu}\tilde{B}^{\mu\nu}) \\ &\quad-\frac{1}{16\pi^2}(2N+1)(N-1) \\ &\quad\times\frac{\eta_0}{F_{\eta_0}}\left(2g_s^2 G_{a\mu\nu}\tilde{G}_a^{\mu\nu}+\frac{16}{3}g'^2 B_{\mu\nu}\tilde{B}^{\mu\nu}\right) \\ &= \eta_0[k^0_{\gamma\gamma}e^2 A_{\mu\nu}\tilde{A}^{\mu\nu}+k^0_{gg}g_s^2 G_{a\mu\nu}\tilde{G}_a^{\mu\nu}+\cdots], \end{aligned} \tag{5.58}$$

where the first (second) line is the contribution of the ψ (X) fermion loops, and the dots stand for couplings involving the Z or W field strengths. Here $\tilde{F}_{\mu\nu}\equiv\epsilon_{\mu\nu\rho\sigma}F^{\rho\sigma}/2$ and the coefficients $k^0_{\gamma\gamma,gg}$ are straightforwardly computed using $B_{\mu\nu}\supset c_w A_{\mu\nu}$, $W_{3\mu\nu}\supset s_w A_{\mu\nu}$, and $e=gs_w=g'c_w$, and similarly for couplings involving the Z or W field strengths. The decay widths into massless gauge bosons are

$$\begin{aligned}\Gamma(\eta_0\to\gamma\gamma) &= 4\pi\alpha^2_{\mathrm{em}}M^3_{\eta_0}(k^0_{\gamma\gamma})^2, \\ \Gamma(\eta_0\to gg) &= 32\pi\alpha_s^2 M^3_{\eta_0}(k^0_{gg})^2. \end{aligned} \tag{5.59}$$

Note that these rates are determined only by group theory factors, up to the decay constant F_{η_0}. The latter can be computed in the NJL approximation, and the result is given in Eq. (5.52). Thus, the golden channel for the discovery of η_0 at the LHC is production via gluon-gluon fusion and decay into two gauge bosons: di-jet, di-photon, γZ, ZZ and WW final states. We recall that the mass of η_0 is induced by the explicit breaking of the anomaly-free $U(1)$ symmetry: this is due either to an explicit mass term for the constituent fermions, $m_X\neq 0$, or to the proto-Yukawa couplings of the SM fermions to the composite sector, that we do not specify in this paper. Our NJL result for M_{η_0} is given in Eqs. (5.43), (5.57). The corrections to Eq. (5.58), that strictly holds in

the chiral limit, are expected to be subleading, as long as η_0 is significantly lighter than the non-Goldstone resonances. Note that the ratio $\Gamma(\eta_0\to gg)/\Gamma(\eta_0\to\gamma\gamma)=18(2N+1)^2/(N-4)^2\cdot\alpha_s^2/\alpha_{\rm em}^2$ is independent from F_{η_0} and M_{η_0}, and is larger than 2×10^4 for any N. Thus a discovery appears more likely in the di-jet channel. Indeed, the alleged di-photon resonance at 750 GeV could not be fitted by η_0, because the gluons-to-photons ratio is too large [93].

F. Comments on spectral sum rules

In this section, we comment on the spectral sum rules when both the electroweak and the colored sectors are included. We will not enter in the details here but rather focus on the main differences as compared to the electroweak sector in isolation. The latter has been extensively discussed in Sec. III G. A few modifications are worth noticing. While in the electroweak sector the sum rule involving $\Pi^{\psi}_{S-P}(q^2)$ is not expected to hold (see footnote 3), in the colored sector $\Pi^{X}_{S-P}(q^2)$ is an order parameter; therefore, the first sum rule in Eq. (2.14) is operative as well. On the other hand, the presence of an explicit symmery-breaking mass term $m_X\neq0$ spoils the convergence of the integrals in Eqs. (2.13) and (2.14), so that one can only write the convergent sum rule of Eq. (2.19). Therefore, the saturation of the colored-sector sum rules is expected to worsen as m_X increases. Recall that the NJL approximation already implies large departures from the sum rules as shown, for the electroweak sector, in Figs. 7 and 8.

Another qualitative difference is induced by the interplay between the two sectors. Indeed, the mixings, defined by Eqs. (5.28) and (5.34), between the (pseudo)scalar singlets of the two sectors modify the two-point (pseudo)scalar singlet correlators as compared to their expressions when considered in isolation. As a consequence, the singlet two-point correlators develop two poles, corresponding to the σ_0 and σ' (η_0 and η') in the (pseudo)scalar case. Let us assume that $m_X=0$ and take the example of the order parameters $\Pi^{\psi(X)}_{S^0-P^0}(q^2)$, which involves only the singlets densities $S^0_{\psi,X}$ and $P^0_{\psi,X}$. The corresponding sum rules are then given by

$$\begin{aligned}\int dt\,{\rm Im}\bar\Pi^{\psi(X)}_{S_0-P_0}(t)&\equiv\int dt[{\rm Im}\bar{\mathbf\Pi}^{11(22)}_{\sigma_\psi\sigma_X}(t)-{\rm Im}\bar{\mathbf\Pi}^{11(22)}_{\eta_\psi\eta_X}(t)]=0\\&=(G^{\psi(X)}_{\sigma_0})^2+(G^{\psi(X)}_{\sigma'})^2\\&\quad-(G^{\psi(X)}_{\eta_0})^2-(G^{\psi(X)}_{\eta'})^2=0,\end{aligned}\tag{5.60}$$

where the second line has been obtained by assuming the saturation, in the narrow-width approximation, of the correlators by the first light resonances. The expressions of the scalar decay constants $G^{\psi(X)}_i$ can be obtained from Secs. V E 1 and V E 2.

When the two sectors are present, an additional $U(1)$ symmetry is also preserved, and leads to two additional sum rules (see Sec. IV B). For simplicity, in the sequel we focus only on the scalar sum rule, in order to avoid the complications coming from the pseudoscalar-axial mixing. The corresponding sum rule takes the following form

$$\int dt\,{\rm Im}\bar\Pi^{\psi X}_{S_0}\equiv\int dt\,{\rm Im}\bar{\mathbf\Pi}^{12}_{\sigma_\psi\sigma_X}(t)=G^{\psi}_{\sigma_0}G^{X}_{\sigma_0}-G^{\psi}_{\sigma'}G^{X}_{\sigma'}=0,\tag{5.61}$$

where in the last equality the saturation of the correlator by the first light resonances has been assumed. Let us focus on this sum rule, as all the new features induced by the interplay between the two sectors are contained in the correlator $\bar\Pi^{\psi X}_{S_0}(q^2)$. First, one clearly sees the two poles associated to σ_0 and σ' in the spectral density, which is displayed in Fig. 16 for different values of ξ and $N=4$. Increasing the value of ξ, the two poles become closer and closer in agreement with Fig. 15. In principle there are two distinct thresholds above which the loops involving the fermions ψ or X develop an imaginary part. However, as the mixing parameter κ_B/κ_A is small, these two thresholds are very close (see Fig. 12) and one can consider in a good approximation only one threshold located around $4M^2_\psi\simeq4M^2_X$. While in the spectral density the second pole associated to the σ' remains always close to this threshold, one sees that the σ_0 pole moves continuously from $p^2\simeq4M^2_\psi$ (for large values of ξ) down to $p^2=0$ (for $\xi\simeq1.15$) when the σ_0 becomes massless (see Fig. 15). From Eq. (5.61), one also sees that the residues of the two poles in the spectral density should have an opposite sign in order to respect the sum rule. This is in agreement with the left panel of Fig. 16. As the scalar singlets are narrow and the continuum part of the spectral density is small, one expects the sum rule of Eq. (5.61) to be well respected by the NJL approximation and the saturation by the first light resonances to be a good approximation.[18]

The saturation of the sum rule (5.61) is illustrated in the right panel of Fig. 16. We plot the absolute value of the ratio of integrals $\int_0^{t_0}dt\,{\rm Im}\Pi^{\psi X}_{S_0}(t)/\int_{t_0}^{\infty}dt\,{\rm Im}\Pi^{\psi X}_{S_0}(t)$, as a function of ξ and for two different values of the number of hypercolors, $N=4$ and $N=2$. In the true theory, this ratio is predicted to be one regardless of the value of the parameter t_0. In our NJL approximation of the strong dynamics, the result of the integration may depend on the value of t_0, that we conventionally choose as the value of t where the spectral density vanishes. In this way, one compares the positive and negative parts of the spectral densities, in the same spirit as for the saturation of the sum

[18]Note that in the electroweak sector in isolation, the continuum of the scalar singlet density is also small and the pole is narrow. However, there is no sum rule involving only scalar singlets, so that the above argument does not apply.

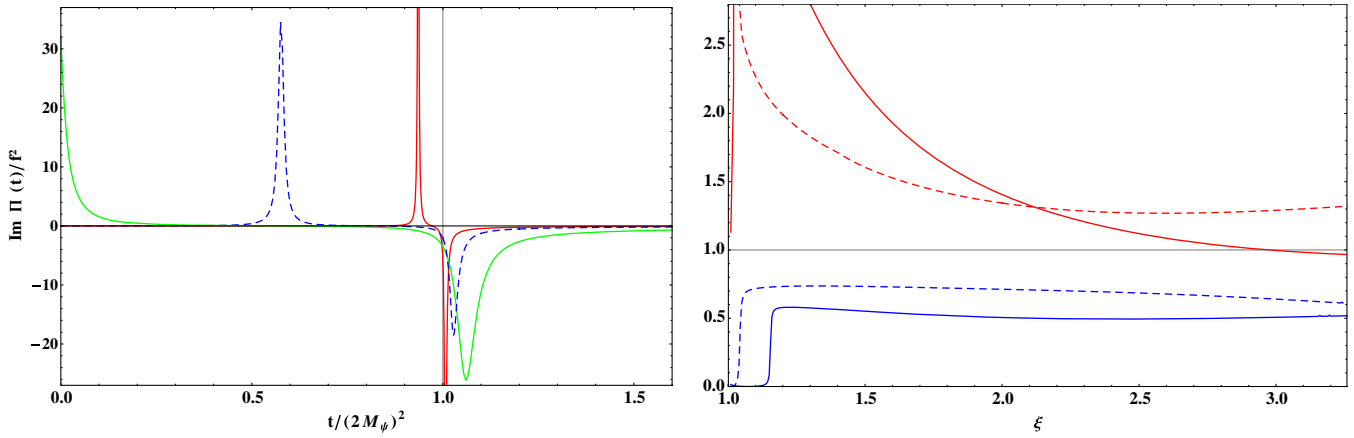

FIG. 16. Left panel: The spectral function $\mathrm{Im}\Pi^{\psi X}_{S_0}(t)$ as a function of $t/(2M_\psi)^2$ for three values $\xi = 1.15$ (solid green line), $\xi = 1.3$ (dashed blue line) and $\xi = 2$ (solid red line). The other parameters are fixed to $N = 4$, $\kappa_{A6}/\kappa_A = 1$, $\kappa_B/\kappa_A = 0.01$ and $m_X = 0$. One clearly sees the two poles, associated with the σ_0 and σ' scalar singlets, which become closer and closer as ξ increases. In the opposite limit where ξ decreases, the σ_0 becomes lighter and lighter up to be massless for $\xi \simeq 1.15$ while the σ' always stays close to the threshold $4M_\psi^2 \simeq 4M_X^2$. The residues of the poles have an opposite sign in agreement with the expectation from the associated sum rule. Right panel: The absolute value of the ratio of the integral $\int_0^{t_0} dt\mathrm{Im}\Pi^{\psi X}_{S_0}(t)/\int_{t_0}^{\infty} dt\mathrm{Im}\Pi^{\psi X}_{S_0}(t)$ (lower blue lines) as a function of ξ for two values of the number of hypercolors $N = 4$ (solid line) and $N = 2$ (dashed line). As explained in the text, t_0 is the value above which the spectral density becomes negative. Also shown is the absolute value of the ratio $(G^{\psi}_{\sigma_0}G^{X}_{\sigma_0})/(G^{\psi}_{\sigma'}G^{X}_{\sigma'})$ (upper red solid and dashed lines). The other parameters are fixed to $\kappa_{A6}/\kappa_A = 1$, $\kappa_B/\kappa_A = 0.01$ and $m_X = 0$.

rule with the two lightest resonances. To illustrate the latter, we plot the absolute value of the ratio $(G^{\psi}_{\sigma_0}G^{X}_{\sigma_0})/(G^{\psi}_{\sigma'}G^{X}_{\sigma'})$, that is obtained in the same way as in Sec. III G, but the explicit expression is more involved due to the mixing and we refrain from giving it here. Below the critical value $\xi \simeq 1.15$ ($\xi \simeq 1.04$) for $N = 4$ ($N = 2$), this ratios becomes meaningless, as the σ_0 pole disappears from the spectral density, such that a large departure from one is observed. In summary, the right panel of Fig. 16 shows that the ratio of integrals (of decay constants) is smaller (larger) than one, but this departure from the sum-rule prediction is reasonably small as long as ξ is well above the instability region (see Sec. III G for a detailed discussion of the limitations of the NJL approximation with regard to the sum rules).

VI. CONCLUSION

The general idea of a composite, Nambu-Goldstone Higgs particle provides a very attractive framework for the EWSB. We considered an asymptotically-free gauge theory confining at the multi-TeV scale and that has the potential to provide a self-consistent, ultraviolet-complete framework to study the composite Higgs phenomenology.

The minimal model features four flavors of constituent fermions ψ^a, which condense as the hypercolor interaction becomes strong. The first, remarkable result is that, unavoidably, the corresponding $SU(4)$ flavor symmetry breaks spontaneously to $Sp(4)$, as required in order to generate a NGB Higgs. This follows from general results on vectorlike gauge theories, reviewed in Secs. II A–II B. Furthermore, such a dynamical symmetry breaking is successfully described by a four-fermion operator, à la NJL: when the four-fermion coupling exceeds a critical value, a nonzero mass gap develops, as shown in Sec. III A. The meson resonances are described by two-point correlators of fermion bilinears. The meson spins (zero or one) and their representations under the flavor group are determined by the quantum numbers of the associated hypercolor-singlet fermion bilinears. Following the standard NJL approach, we computed all the relevant two-point correlators, resummed at leading order in the number of hypercolors N: the meson mass is determined by the correlator pole, while the residue at the pole fixes the meson decay constant. In Sec. III E, we have shown that the NGB decay constant f is almost 10 times smaller than the cutoff of the constituent fermion loops; therefore, our effective theory is well under control up to meson masses of order $\sim 10f$. Recall that electroweak precision measurements require $f \gtrsim 1$ TeV and that fine-tuning in the composite Higgs potential is proportional to the ratio v^2/f^2. In order to correlate the various meson masses, we made the hypothesis that the hypercolor dynamics is dominated by current-current interactions, see Appendix D 1, and we used Fierz transformations to relate the different four-fermion operators. In particular, in Sec. D 4, we derived some $Sp(2N)$ Fierz identities which, to the best of our knowledge, are not available elsewhere in the literature.

In Sec. III F, we illustrated our results for the mass spectrum of electroweak mesons: for a reasonably small number of hypercolors, say $2N \lesssim 10$, the spin-one mesons are always heavier than $5f$, while the spin-zero mesons can

be as light as f, and therefore accessible at the LHC, in the following special cases. The singlet scalar mass M_σ vanishes when the four-fermion coupling approaches its critical value, that is, when the condensate vanishes. The singlet pseudoscalar mass $M_{\eta'}$ is induced by the axial anomaly: the anomalous contribution is expected to scale as $M_{\eta'}^2 \sim 1/N$, but we did not attempt to quantify its absolute size. Therefore, we cannot exclude a very light value for $M_{\eta'}$. Note that these results for σ and η' hold for the electroweak sector in isolation: the effects of the mixing with the singlets of the color sector are summarized below. The nonsinglet scalar S can also be light if both σ and η' are, as $M_S^2 \simeq M_\sigma^2 + M_{\eta'}^2$. In addition, one should keep in mind that the set of NGB is formed by the Higgs doublet plus a SM singlet η; their masses arise only from SM loops, which we did not study here, and are expected to lie at or below the scale f. In Sec. III G, we performed an important test of the accuracy of our methods, by comparing our results with spectral sum rules, that have to be satisfied by the exact two-point correlators. We thus identified the values of the four-fermion coupling that best reproduce the sum rules. Conversely, our results in the effective NJL approximation depart significantly from the sum rules, when the continuum part of the spectral function becomes sizable. We also compared our results with available lattice simulations for $N = 1$, finding a fair agreement within the large error bars, with a preference for certain values of the four-fermion couplings; however our methods are expected to be more accurate when N is large. In Sec. III H, we estimated the contribution of the composite sector to the oblique parameter S, demonstrating that it is under control.

In order to provide composite partners for the top quark, one needs to introduce additional constituent fermions X^f, in a different hypercolor representation, such that fermion-trilinear baryons can be formed, with the quantum numbers of the top quark. A gauge theory with fermions in two different representations presents qualitatively new features, such as one nonanomalous $U(1)$ flavor symmetry, with an associated Nambu-Goldstone meson η_0. In Sec. IV B, we showed that this implies two additional sum rules, as well as a mixing between the singlet scalars and pseudoscalars of the two sectors. In addition, the axial anomaly should only generate operators that respect the nonanomalous $U(1)$ symmetry. As a consequence, we demonstrated in Sec. IV C that the effect of the anomaly is described by an operator of very large dimension, involving $4 + 12(N-1)$ fermions. Our analysis of this operator correctly takes into account all the symmetries of the model, and thus provides fully coherent results, and its large dimension may indicate that the effects of the anomaly are suppressed in such a scenario. On the other hand, we cannot exclude that such suppression is an artifact of our approximation of the true dynamics, in terms of fermionic operators only.

The dynamics of spontaneous flavor symmetry breaking also complicates in the presence of two sectors. Our analysis of anomaly matching in Sec. IV A shows that the condensate $\langle\psi\psi\rangle$ necessarily forms, with the possible exception of the case when N is a multiple of 8. However the condensate $\langle XX\rangle$ may not form in the presence of light, colored baryons. Indeed, in Sec. V A, we showed that the system of two coupled mass-gap equations is very sensitive to the relative size of four-fermion couplings in the two sectors. As the NJL techniques can provide information on the spectrum of colored mesons only in the case of a nonvanishing mass gap, we focused on the region of parameters where a nonzero $\langle XX\rangle$ develops as well. Let us remark that the solution of the gap equations corresponds to a stable minimum of the effective potential only for some range of the four-fermion couplings, and of course meson masses are under control only within this range. In the present case, it turns out that the potential is stable (no tachyons) as long as the operators induced by the axial anomaly are suppressed with respect to the others, by a factor of ten to one hundred, as described in Sec. V E. Therefore, we concentrated on the mass spectrum in this region of parameters.

We computed the masses of colored mesons with the same techniques described for the electroweak sector. The results are illustrated in Sec. V D. Once again, spin-one mesons are extremely heavy, above $\sim 5f$. The situation is much more interesting for the colored NGBs G_c, organized as a real QCD octet and a complex sextet, which are massless in the chiral limit. We computed the contribution to their masses from gluon loops, and we found $M_{G_c} \gtrsim 1.5f$, as long as $2N \lesssim 10$. This may be sufficiently large to comply with present collider searches. Therefore, contrary to common lore, it is not strictly necessary to introduce an explicit mass term $m_X XX$. Nonetheless, we studied also the case $m_X \neq 0$, as some qualitative features of the mass gap and of the meson spectrum are very sensitive to this parameter. In particular, the singlet pseudoscalar η_0 is an exact NGB in the chiral limit; therefore, its mass is controlled by the size of m_X (and by the size of the couplings to external SM fermions), as discussed in Sec. V E. A prominent opportunity for the discovery of composite NGBs at the LHC is offered by their anomalous couplings to two SM gauge bosons, determined by the Wess-Zumino-Witten term. We provided the general formula for these couplings, and we specifically discussed the phenomenological consequences for the η_0 state. The mass of the other singlet pseudoscalar η' is extremely sensitive to the effective anomaly coefficient: one may have $M_{\eta'} \lesssim f$ for $\kappa_B/\kappa_A \ll 0.01$, but as soon as $\kappa_B/\kappa_A \sim 0.1$ this state decouples, $M_{\eta'} \gtrsim 10f$. Finally, the heaviest singlet scalar σ' always lies in the multi-TeV range, while the lightest singlet scalar σ_0 may be as light as f. Indeed, we already remarked that the vacuum provided by the mass-gap equations is stable only within specific ranges of the effective four-fermion couplings. Whenever the latter are close to the boundary of the stability region, M_{σ_0} vanishes. In Sec. V F, we

commented on the spectral sum rules in the presence of two sectors, illustrating in particular the interplay among the singlet spectral functions.

We presented the first thorough analysis of the spectrum of meson resonances, in a confining gauge theory with fermions in two different representations of the gauge group. The main limitation of this study is the absence of interactions with external fermion fields. The interest of such interactions is twofold: to generate Yukawa couplings between the composite Higgs and the SM fermions, and to induce radiatively a Higgs potential that realizes EWSB. As a matter of fact, the colored sector of the model is engineered to contain fermion-trilinear bound states, which may mix linearly with the SM fermions. The mass spectrum of these baryons and their couplings to the mesons can be computed by generalizing the techniques used in this paper. Indeed, in the QCD literature, several analytical predictions for the masses and couplings of baryons are consistent with experiments and with lattice simulations. Thus, one may predict the properties of composite top quark partners that reside in definite representations of the flavor group, and then compute the Higgs effective potential induced by the top sector loops. Such a theory has a lesser number of free parameters than a generic composite Higgs model with no specific ultraviolet completion; therefore, the challenge will be to reproduce the Higgs mass with a minimal amount of fine tuning of the parameters. We aim to study the fermion bound states of the theory in a separate publication [94].

ACKNOWLEGDMENTS

This work has been carried out thanks to the support of the OCEVU Labex (ANR-11-LABX-0060) and the A*MIDEX project (ANR-11-IDEX-0001-02) funded by the "Investissements d'Avenir" French government program managed by the Agence Nationale de la Recherche (ANR). M. F. acknowledges partial support from the European Unions Horizon 2020 research and innovation program, under the Marie Sklodowska-Curie Grant Agreements No. 690575 and No. 674896.

APPENDIX A: GENERATORS OF THE FLAVOR GROUP AND EMBEDDING OF THE SM GROUP

In this appendix, we give explicit representations for the generators of the flavor groups $SU(4)$ and $SU(6)$ and describe how the SM gauge fields are coupled to the elementary fermion fields. There are general procedures to construct a basis of the Gell-Mann type for any $SU(n)$ group, starting from the well-known representations of the generators for the cases $n = 2$ and $n = 3$, see for instance [95]. The relations in Eq. (2.2) allow to distinguish the generators T^A for the unbroken subgroups, $Sp(4)$ and $SO(6)$, from the generators $T^{\hat{A}}$ in the corresponding coset spaces. For $n = 2N_f$ flavors, choosing the $2N_f \times 2N_f$ matrix Σ_ε in the form

$$\Sigma_\varepsilon = \begin{pmatrix} 0 & \mathbb{1} \\ \varepsilon\mathbb{1} & 0 \end{pmatrix}, \tag{A1}$$

the general solution of Eq. (2.2) can be expressed as [31]

$$T^A = \begin{pmatrix} \mathcal{A}^A & \mathcal{B}^A \\ \mathcal{B}^{A\dagger} & -(\mathcal{A}^A)^T \end{pmatrix}, \qquad T^{\hat{A}} = \begin{pmatrix} \mathcal{C}^{\hat{A}} & \mathcal{D}^{\hat{A}} \\ \mathcal{D}^{\hat{A}\dagger} & +(\mathcal{C}^{\hat{A}})^T \end{pmatrix}, \tag{A2}$$

where the $N_f \times N_f$ submatrices $\mathcal{A}^A$ and $\mathcal{C}^{\hat{A}}$ are Hermitian, with $\mathcal{C}^{\hat{A}}$ traceless, whereas $(\mathcal{B}^A)^T = -\varepsilon\mathcal{B}^A$ and $(\mathcal{D}^{\hat{A}})^T = +\varepsilon\mathcal{D}^{\hat{A}}$.

1. The $SU(4)$ sector

According to the preceding discussion, the 15 $SU(4)$ generators can be chosen as follows. The 10 generators of the subgroup $Sp(4)$ read

$$\begin{aligned} T^{1,2,3,4} &= \frac{1}{2\sqrt{2}} \begin{pmatrix} \sigma_{1,2,3,0} & 0 \\ 0 & -\sigma_{1,2,3,0}^T \end{pmatrix}, \\ T^{5,6,7} &= \frac{1}{2\sqrt{2}} \begin{pmatrix} 0 & \sigma_{1,3,0} \\ \sigma_{1,3,0} & 0 \end{pmatrix}, \\ T^{8,9,10} &= \frac{1}{2\sqrt{2}} \begin{pmatrix} 0 & i\sigma_{1,3,0} \\ -i\sigma_{1,3,0} & 0 \end{pmatrix}, \end{aligned} \tag{A3}$$

where σ_i, $i = 1, 2, 3$ denote the Pauli matrices while σ_0 stands for the 2×2 unit matrix. The corresponding coset $SU(4)/Sp(4)$ is then generated by the 5 matrices

$$\begin{aligned} T^{\hat{1},\hat{2},\hat{3}} &= \frac{1}{2\sqrt{2}} \begin{pmatrix} \sigma_{1,2,3} & 0 \\ 0 & \sigma_{1,2,3}^T \end{pmatrix}, \\ T^{\hat{4}} &= \frac{1}{2\sqrt{2}} \begin{pmatrix} 0 & \sigma_2 \\ \sigma_2 & 0 \end{pmatrix}, \\ T^{\hat{5}} &= \frac{1}{2\sqrt{2}} \begin{pmatrix} 0 & i\sigma_2 \\ -i\sigma_2 & 0 \end{pmatrix}. \end{aligned} \tag{A4}$$

The set of generators

$$T_{L,R}^{1,2,3} = \frac{T^7 \mp T^6}{\sqrt{2}}, \qquad -\frac{T^{10} \mp T^9}{\sqrt{2}}, \qquad \frac{T^4 \mp T^3}{\sqrt{2}} \tag{A5}$$

constitute a $SU(2)_L \times SU(2)_R$ subalgebra of $Sp(4)$, and provide the generators for the electroweak interaction and the custodial symmetry. With this convention, a multiplet ψ^a in the fundamental of $SU(4)$ and of $Sp(4)$ decomposes as $(\psi^1\psi^3)^T \sim (1_L, 2_R)$ and $(\psi^2\psi^4)^T \sim (2_L, 1_R)$. The generator $T^{\hat{3}}$ is associated with a NGB singlet under $SU(2)_L \times SU(2)_R$, whereas the remaining four generators of the $SU(4)/Sp(4)$ coset correspond to the Higgs bidoublet H, transforming as $(2_L, 2_R)$. Under the diagonal $SU(2)_V$

subgroup, generated by $T^a_L + T^a_R$, the generators $T^{\hat{2}}$, $T^{\hat{4}}$, $T^{\hat{5}}$ transform as a triplet, and $T^{\hat{1}}$ as a singlet.

The external electroweak gauge fields $W^{1,2,3}_\mu$ and B_μ will then couple to the ψ fermions through the combination

$$-i\mathcal{V}_\mu \equiv -ig(W^1_\mu T^1_L + W^2_\mu T^2_L + W^3_\mu T^3_L) - ig' B_\mu T^3_R. \quad \text{(A6)}$$

According to Eq. (2.28), the masses of the NGBs that are radiatively induced by the gauging are given by

$$\begin{aligned}\Delta M^2_H &= \Delta M^2_{\hat{1},\hat{2},\hat{4},\hat{5}} \\ &= -\frac{3}{4\pi}\times\frac{1}{F_G^2}\int_0^\infty dQ^2 Q^2 \Pi^\psi_{V-A}(-Q^2) \\ &\quad\times\frac{1}{16\pi}(3g^2+g'^2), \\ \Delta M^2_{\hat{3}} &= 0. \end{aligned} \quad \text{(A7)}$$

Of course, this positive contribution to the Higgs doublet mass should be overcome by a negative one from the top quark couplings, in order to trigger EWSB.

One can estimate quantitatively ΔM^2_H from the explicit form of the correlator $\Pi^\psi_{V-A}(-Q^2)$ as computed in the NJL approximation. If one assumes further that the lightest resonances saturate in good approximation the correlator (see Sec. III G), the integrand takes the simplified form

$$-Q^2\bar{\Pi}^\psi_{V-A}(-Q^2) \simeq F_G^2 + f_A^2 M_A^2 \frac{Q^2}{Q^2+M_A^2} - f_V^2 M_V^2 \frac{Q^2}{Q^2+M_V^2}, \quad \text{(A8)}$$

where the expressions of the resonance masses and decay constants are explicitly given Secs. III D, III E and III G. Integrating Eq. (A8) over Q^2 up to the NJL cutoff Λ^2, one obtains

$$\begin{aligned}&-\int_0^{\Lambda^2} dQ^2 Q^2 \bar{\Pi}^\psi_{V-A}(-Q^2) \\ &\simeq (F_G^2 + f_A^2 M_A^2 - f_V^2 M_V^2)\Lambda^2 + f_V^2 M_V^4 \ln\frac{\Lambda^2+M_V^2}{M_V^2} \\ &\quad - f_A^2 M_A^4 \ln\frac{\Lambda^2+M_A^2}{M_A^2}. \end{aligned} \quad \text{(A9)}$$

Assuming that the Weinberg sum rules (3.59) hold, the first term proportional to Λ^2 vanishes while the remaining terms simplify and lead to

$$\Delta M^2_H \simeq \frac{3}{64\pi^2}\frac{1}{F_G^2}(3g^2+g'^2) f_V^2 M_V^4 \ln\frac{M_A^2}{M_V^2}. \quad \text{(A10)}$$

This estimation of ΔM^2_H is of course relevant only if the $V-A$ correlator is well saturated by the lightest resonances and the Weinberg sum rules hold.

2. The $SU(6)$ sector

We decompose the 35 $SU(6)$ generators according to the $SO(6)$ subgroup and the coset $SU(6)/SO(6)$. We denote by λ_a, $a = 1, 2, \ldots 8$, the $SU(3)$ Gell-Mann matrices, and we also define $\lambda_0 = \sqrt{2/3}\,\mathrm{diag}(1,1,1)$. A convenient basis for the 15 unbroken generators is given by

$$\begin{aligned} T^{1,\ldots,8,9} &= \frac{1}{2\sqrt{2}}\begin{pmatrix}\lambda_{1,\ldots,8,0} & 0\\ 0 & -\lambda^T_{1,\ldots,8,0}\end{pmatrix}, \\ T^{10,11,12} &= \frac{1}{2\sqrt{2}}\begin{pmatrix}0 & \lambda_{2,5,7}\\ \lambda_{2,5,7} & 0\end{pmatrix}, \\ T^{13,14,15} &= \frac{1}{2\sqrt{2}}\begin{pmatrix}0 & i\lambda_{2,5,7}\\ -i\lambda_{2,5,7} & 0\end{pmatrix}. \end{aligned} \quad \text{(A11)}$$

The eight generators $T^{1,\ldots,8}$ together with T^9 form a $SU(3)_C \times U(1)_D$ maximal subalgebra, that can accommodate the strong interaction gauge group, as well as a part of the hypercharge gauge group $U(1)_Y$, with $Y = T^3_R + D$, where T^3_R is defined in Eq. (A5) and $D = (4/\sqrt{3})\cdot T_9$. The 20 broken generators read

$$\begin{aligned} T^{\hat{1},\ldots,\hat{8}} &= \frac{1}{2\sqrt{2}}\begin{pmatrix}\lambda_{1,\ldots,8} & 0\\ 0 & \lambda^T_{1,\ldots,8}\end{pmatrix}, \\ T^{\hat{9},\ldots,\hat{14}} &= \frac{1}{2\sqrt{2}}\begin{pmatrix}0 & \lambda_{1,3,4,6,8,0}\\ \lambda_{1,3,4,6,8,0} & 0\end{pmatrix}, \\ T^{\hat{15},\ldots,\hat{20}} &= \frac{1}{2\sqrt{2}}\begin{pmatrix}0 & i\lambda_{1,3,4,6,8,0}\\ -i\lambda_{1,3,4,6,8,0} & 0\end{pmatrix}. \end{aligned} \quad \text{(A12)}$$

The generators $T^{\hat{1},\ldots,\hat{8}}$ are associated to the NGBs multiplet $O_c \sim 8_0$ under $SU(3)_C \times U(1)_D$, while $T^{\hat{9},\ldots,\hat{20}}$ correspond to the NGBs $(S_c + \bar{S}_c) \sim (6_{4/3} + \bar{6}_{-4/3})$.

The constituent fermions X transform as $(3_{2/3} + \bar{3}_{-2/3})$ under $SU(3)_C \times U(1)_D$, where the normalization of the D-charge is chosen to reproduce the correct hypercharge of top quark partners. Therefore, the external color gauge fields $G^{1,\ldots,8}_\mu$ and B_μ couple to the X fermions through the combination

$$-ig_c\sqrt{2}G^a_\mu T^a - ig'\frac{4}{\sqrt{3}}B_\mu T^9. \quad \text{(A13)}$$

According to Eq. (2.28), the masses of the NGBs that are radiatively induced by the gauging are given by

$$\Delta M^2_{O_c} = \Delta M^2_{\hat{1},\ldots,\hat{8}} = -\frac{3}{4\pi}\times\frac{1}{F^2_{G_c}}\int_0^\infty dQ^2 Q^2 \Pi^X_{V-A}(-Q^2)\times\frac{3}{4\pi}g_s^2,$$

$$\Delta M^2_{S_c} = \Delta M^2_{\hat{9},\ldots,\hat{20}} = -\frac{3}{4\pi}\times\frac{1}{F^2_{G_c}}\int_0^\infty dQ^2 Q^2 \Pi^X_{V-A}(-Q^2) \times\frac{1}{4\pi}\left(\frac{10}{3}g_s^2+\frac{16}{9}g'^2\right). \quad \text{(A14)}$$

The quantitative estimate of the integral of the $V-A$ two-point function is discussed in Sec. V B.

APPENDIX B: LOOP FUNCTIONS

The one-loop integrals relevant for our purposes are the one- and two-point functions,

$$\tilde{A}_0(m^2) \equiv i\int\frac{d^4k}{(2\pi)^4}\frac{1}{k^2-m^2+i\epsilon},$$

$$\tilde{B}_0(p^2,m^2) \equiv i\int\frac{d^4k}{(2\pi)^4}\frac{1}{(k^2-m^2)[(p+k)^2-m^2]}. \quad \text{(B1)}$$

[We adopted the notation $\tilde{A}_0$ and $\tilde{B}_0$ in order to avoid confusion with the standard one-loop functions A_0 and B_0 [96], which are defined in Euclidean metric and dimensional regularization, and differ also from the above by an overall factor $i(16\pi^2)$ in $D=4$ dimensions.]

In the context of the NJL model, the one-point function is regularized by introducing a cutoff Λ on the Euclidean four-momentum,

$$\tilde{A}_0(m^2) = \frac{\Lambda^2}{16\pi^2}\left[1-\frac{m^2}{\Lambda^2}\ln\frac{\Lambda^2+m^2}{m^2}\right]. \quad \text{(B2)}$$

The zero-momentum two-point function is given by

$$\tilde{B}_0(0,m^2) = \frac{d\tilde{A}_0(m^2)}{dm^2} = \frac{1}{16\pi^2}\left[\frac{\Lambda^2}{\Lambda^2+m^2}-\ln\frac{\Lambda^2+m^2}{m^2}\right] = \frac{1}{16\pi^2}\left[1-\ln\frac{\Lambda^2}{m^2}+\mathcal{O}\left(\frac{m^2}{\Lambda^2}\right)\right]. \quad \text{(B3)}$$

For the finite, p^2-dependent part of the two-point function, we adopt the simple regularization

$$\tilde{B}_0(p^2,m^2) = \tilde{B}_0(0,m^2)+\frac{1}{32\pi^2}f\left(\frac{p^2}{4m^2}\right), \quad \text{(B4)}$$

where

$$f(r) = \begin{cases} 4\left(\frac{1-r}{r}\right)^{1/2}\arctan\left(\frac{r}{1-r}\right)^{1/2}-4 & (\text{for } 0<r<1)\\ 4\left(\frac{r-1}{r}\right)^{1/2}\left[\ln\left(\sqrt{r}+\sqrt{r-1}\right)-i\frac{\pi}{2}\right]-4 & (\text{for } 1<r)\\ 4\left(\frac{r-1}{r}\right)^{1/2}\left[\ln\left(\sqrt{-r}+\sqrt{1-r}\right)\right]-4 & (\text{for } r<0). \end{cases} \quad \text{(B5)}$$

We remark that the finite terms are regularization dependent; therefore, our expression may differ from analogous ones in the NJL literature at order p^2/Λ^2.

APPENDIX C: TWO-POINT CORRELATORS OF FERMION BILINEARS AT ONE LOOP

In this appendix, we present the detailed computation of the five one-loop two-point functions $\tilde{\Pi}_\phi(q^2,M_f^2) = \tilde{\Pi}^f_\phi(q^2)$ where $\phi = \{S,P,V,A,AP\}$ and M_f is the dynamical mass of the hypercolor fermions $f=\psi, X$. These two-point functions are crucial quantities in the NJL model as they are involved in the estimation of the masses and decay constants of the electroweak and colored composite resonances (see Secs. III and V). For the two-component Weyl spinors, we follow the conventions of Ref. [97] (ψ and $\psi^\dagger$ propagate in the loops). The Feynman rules appearing in the vertices can be extracted from the currents and densities given, respectively, in Eqs. (2.1) and (2.6).

Let us first focus on the electroweak sector. In the scalar and pseudoscalar nonsinglet channels we get

$$i\tilde{\Pi}^\psi_{S(P)}(q^2)\delta^{\hat{A}\,\hat{B}} = (-1)\int^\Lambda\frac{d^4k}{(2\pi)^4}\mathrm{Tr}\left[i\Sigma_0 T^{\hat{A}}\Omega\Gamma_{S(P)}\frac{i\sigma\cdot k}{k^2-M_\psi^2}iT^{\hat{B}}\Sigma_0\Omega\Gamma^\dagger_{S(P)}\frac{i\bar{\sigma}\cdot(k+q)}{(k+q)^2-M_\psi^2}\right] + (-1)\int^\Lambda\frac{d^4k}{(2\pi)^4}\mathrm{Tr}\left[i\Sigma_0 T^{\hat{A}}\Omega\Gamma_{S(P)}\frac{iM_\psi\Sigma_0\Omega}{k^2-M_\psi^2}i\Sigma_0 T^{\hat{B}}\Omega\Gamma_{S(P)}\frac{iM_\psi\Sigma_0\Omega}{(k+q)^2-M_\psi^2}\right], \quad \text{(C1)}$$

where the first (second) integral corresponds to the loop involving the kinetic (massive) part of the propagators. The factors $\Gamma_{S(P)} = 1(i)$, which distinguish the scalar and pseudoscalar channels, are a consequence of Eq. (2.6). These factors are the equivalent of the γ_5 matrix in Dirac notation and they give a relative sign between the two channels in the second term of Eq. (C1), exactly like in QCD. Similarly for the vector and axial-vector two points functions one obtains

$$i\tilde{\Pi}^{\mu\nu,AB(\hat{A}\,\hat{B})}_{V(A)}(q^2,M_\psi^2) = (-1)\int^\Lambda \frac{d^4k}{(2\pi)^4}\mathrm{Tr}\left[iT^{A(\hat{A})}\bar{\sigma}^\mu\frac{i\sigma\cdot k}{k^2-M_\psi^2}iT^{B(\hat{B})}\bar{\sigma}^\nu\frac{i\sigma\cdot(k+q)}{(k+q)^2-M_\psi^2}\right] + (-1)\int^\Lambda \frac{d^4k}{(2\pi)^4}\mathrm{Tr}\left[iT^{A(\hat{A})}\bar{\sigma}^\mu\frac{iM_\psi\Sigma_0\Omega}{k^2-M_\psi^2}(-iT^{B(\hat{B})})^T\sigma^\nu\frac{iM_\psi\Sigma_0\Omega}{(k+q)^2-M_\psi^2}\right], \tag{C2}$$

where the functions $\tilde{\Pi}^{\mu\nu,AB(\hat{A}\,\hat{B})}_{V(A)}(q^2)$ are defined in Eq. (3.34). The vector and axial-vector channels only differ by the flavor trace [see Eqs. (2.2) and (2.3)] which again gives a relative sign between the two channels in the second integral. Finally, for the axial pseudoscalar two-point function one has

$$i\tilde{\Pi}^{\mu,\hat{A}\,\hat{B}}_{AP}(q^2,M_\psi^2) \equiv i\tilde{\Pi}^{\psi}_{AP}(q^2)p^\mu\delta^{\hat{A}\,\hat{B}} = (-1)\int^\Lambda \frac{d^4k}{(2\pi)^4}\mathrm{Tr}\left[iT^{\hat{A}}\bar{\sigma}^\mu\frac{i\sigma\cdot k}{k^2-M_\psi^2}iT^{\hat{B}}\Sigma_0\Omega\Gamma_P\frac{iM_\psi\Sigma_0\Omega}{(k+q)^2-M_\psi^2}\right] + (-1)\int^\Lambda \frac{d^4k}{(2\pi)^4}\mathrm{Tr}\left[iT^{\hat{A}}\cdot\bar{\sigma}^\mu\frac{iM_\psi\Sigma_0\Omega}{k^2-M_\psi^2}i\Sigma_0T^{\hat{B}}\Omega\Gamma_P^\dagger\frac{i\sigma\cdot(k+q)}{(k+q)^2-M_\psi^2}\right], \tag{C3}$$

where this time the integrals contain both the kinetic and the massive parts of the propagators. Evaluating the Lorentz, flavor and hypercolor traces, one can check that the above equations are quite consistent with the ones given in table II. Note that the correlators in the singlet channels are obtained by replacing the generators $T^{\hat{A}}$ by the normalized identity matrix T^0_ψ which only changes the flavor tensor structure of the loops, leading to the same result for the two-point functions $\tilde{\Pi}^f_\phi(q^2)$.

Let us now turn to the correlators of the colored $SU(6)$ sector. The latter can be derived in complete analogy with the ones in the electroweak sector. Besides the obvious replacements $M_\psi \to M_X$, $\Sigma_0 \to \Sigma_0^c$ and $T^0_\psi \to T^0_X$, the major modification originates from the hypercolor traces. Indeed, the fermions X are in the two-index antisymmetric and traceless representation of $Sp(2N)$. Consequently, the hypercolor traces give a factor $(2N+1)(N-1)$ [instead of $(2N)$[19]] which of course corresponds to the dimension of the hypercolor $X-$ representation. Note that this difference with respect to the electroweak sector can easily be inferred by considering the vector form $X^{\hat{I}}$ [$\hat{I} = 1,\ldots,(2N+1)(N-1)$] defined in Eq. (D6). Then, the one-loop two-point functions $\tilde{\Pi}^X_\phi(q^2)$, summarized in table IV, are related to the ones in the electroweak sector as follow

$$\tilde{\Pi}^{\psi}_\phi(q^2) = \tilde{\Pi}_\phi(q^2,M_\psi^2,2N),$$
$$\tilde{\Pi}^{X}_\phi(q^2) = \tilde{\Pi}_\phi[q^2,M_X^2,(2N+1)(N-1)]. \tag{C4}$$

As explained in Sec. III B, the resummation of the above one-loop two-point functions, at leading order in $1/N$, gives the NJL resummed correlators, $\bar{\Pi}_\phi$, from which the masses and decay constants of the composite resonances are extracted. Usually, in the NJL literature, one considers the T-matrix element $\bar{T}_\phi(q^2)$, rather than $\bar{\Pi}_\phi(q^2)$. As illustrated in Fig. 17, the geometrical series that defines $\bar{T}_\phi$ starts with the four-fermion interaction K_ϕ, instead of the one-loop two-point function $\tilde{\Pi}^f_\phi(q^2)$, see Fig. 2. Consequently the T-matrix element is given by

$$\bar{T}_\phi(q^2) = \frac{K_\phi}{1-2K_\phi\tilde{\Pi}^f_\phi(q^2)}. \tag{C5}$$

The poles of $\bar{T}_\phi(q^2)$ and of $\bar{\Pi}_\phi(q^2)$ are of course identical and are given by $1 = 2K_\phi\tilde{\Pi}^f_\phi(M_\phi^2)$. The only difference comparing Eqs. (3.20) and (C5) comes from the numerators of the series, which lead different to residues. The residues of $\bar{\Pi}^f_\phi$ have been extensively studied in Secs. III and V, while the residues of the T matrix are the couplings $g_{\phi ff}$ of the physical resonance ϕ to the fundamental fermions f. In analogy with Eq. (3.63), these couplings are given by

[19]More precisely, due to the antisymmetry of the hypercolor singlet contractions, the corresponding traces of the electroweak sector contribute to the one-loop functions with a factor $\pm(2N)$ where the sign corresponds to a particular (massive or kinetic) loop in a given channel. The minus sign is always compensate by the flavor trace which contains in that case $\Sigma_0^2 = -\mathbb{1}$. On the contrary, the hypercolor and flavor contractions in the colored sectors are symmetric and always positive.

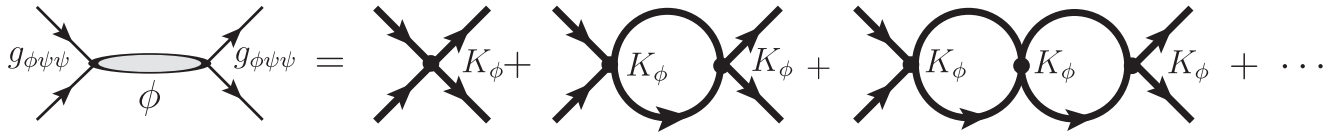

FIG. 17. Resummation of leading $1/N$ graphs for a mesonic T-matrix element, $\bar{T}_\phi$, corresponding to a composite meson exchange.

$$g^2_{\phi ff} = -\lim_{q^2\to M^2_\phi}(q^2 - M^2_\phi)\bar{T}_\phi(q^2) = \left[2\frac{d\tilde{\Pi}^f_\phi(q^2)}{dq^2}\bigg|_{q^2=M^2_\phi}\right]^{-1}. \tag{C6}$$

They behave like $\simeq 1/\sqrt{N}$, as expected from general large-N considerations.

APPENDIX D: RELATING FOUR-FERMION OPERATORS BY FIERZ IDENTITIES

The couplings of the various four-fermions operators may be related under some assumption on the underlying dynamics (see Refs. [66,98] for the case of QCD). In this way one can predict the relative strength of the various physical channels (spin-zero versus spin-one, electroweak sector versus color sector, etc.). We will start from $Sp(2N)$ current-current operators, that encode the ultraviolet dynamics in the "ladder" approximation, that holds when N is (moderately) large, and we will use Fierz transformations to generate the various $Sp(2N)$ singlet-singlet operators. We will also take this opportunity to summarize general results on Fierz transformations associated to the $SU(N)$ and $Sp(2N)$ groups.

1. Hypercolor current-current operators

Let us derive the $Sp(2N)$ current-current operators from the covariant derivatives of the fermions ψ and X. They belong to the fundamental representation, $\psi \sim \square$, and to the two-index, traceless ($X_{ij}\Omega_{ji} = 0$) and antisymmetric ($X_{ij} = -X_{ji}$) representation, $X \sim \begin{smallmatrix}\square\\\square\end{smallmatrix}$. The covariant derivatives read

$$(D^\mu\psi)_i = [\partial^\mu\delta_{ij} - ig_{HC}(T^I)_{ij}\mathcal{G}^\mu_I]\psi_j, \tag{D1}$$

$$\begin{aligned}(D^\mu X)_{ij} &= \partial^\mu X_{ij} - ig_{HC}[(T^I)_{ik}X_{kj} + (T^I)_{jk}X_{ik}]\mathcal{G}^\mu_I \\ &= [\partial^\mu\delta_{ik}\delta_{jl} - ig_{HC}(T^I_X)_{ijkl}\mathcal{G}^\mu_I]X_{kl},\end{aligned} \tag{D2}$$

where $\mathcal{G}^\mu_I$ are the hypergluon fields, and g_{HC} is the hypercolor gauge coupling. The hypercolor generators acting on ψ_j, $(T^I)_{ij}$, and on X_{kl}, $(T^I_X)_{ijkl} \equiv (T^I)_{ik}\delta_{jl} - \delta_{il}(T^I)_{jk}$, are normalized as

$$\begin{aligned}\mathrm{Tr}(T^IT^J) &\equiv \frac{1}{2}\ell\,(\square)\,\delta^{IJ} = \frac{1}{2}\delta^{IJ}, \\ \mathrm{Tr}(T^I_XT^J_X) &\equiv (T^I_X)_{ijkl}(T^J_X)_{klij} \\ &\equiv \frac{1}{2}\ell\left(\begin{smallmatrix}\square\\\square\end{smallmatrix}\right)\delta^{IJ} = (N-1)\delta^{IJ}.\end{aligned} \tag{D3}$$

The nonderivative terms in Eqs. (D1) and (D2) determine the coupling of the technigluons to the $Sp(2N)$-currents $\mathcal{J}^{\mu I}_\psi$ and $\mathcal{J}^{\mu I}_X$, which transform under the adjoint representation $\square\square$,

$$\mathcal{L}_{UV} = g_{HC}(\mathcal{J}^{\mu I}_\psi + \mathcal{J}^{\mu I}_X)\mathcal{G}_{\mu I}, \tag{D4}$$

where

$$\begin{aligned}\mathcal{J}^{\mu I}_\psi &= \psi(\Omega T^I)\sigma^\mu\bar{\psi}, \\ \mathcal{J}^{\mu I}_X &= 2\mathrm{Tr}[X(\Omega T^I)\sigma^\mu\bar{X}\Omega].\end{aligned} \tag{D5}$$

Here Ω_{ij} is the $Sp(2N)$ invariant tensor, the trace is taken over $Sp(2N)$ indexes, and the expression of $\mathcal{J}^{\mu I}_X$ has been simplified using $\mathrm{Tr}[X\Omega\sigma^\mu\bar{X}(\Omega T^I)] = -\mathrm{Tr}[X(\Omega T^I)\sigma^\mu\bar{X}\Omega]$. It is understood that each fermion flavor ψ^a (X^f) behaves equally with respect to the $Sp(2N)$ dynamics, that is, the $Sp(2N)$ currents are flavor singlets. It will be useful to rearrange the fermion components X_{ij} as a vector $X^{\hat{I}}$, with one index $\hat{I}$ of the representation $\begin{smallmatrix}\square\\\square\end{smallmatrix}$,

$$X_{ij} = \sqrt{2}(T^{\hat{I}}\Omega)_{ij}X^{\hat{I}}, \qquad X^{\hat{I}} = -\sqrt{2}(\Omega T^{\hat{I}})_{ij}X_{ji}, \tag{D6}$$

so that the second current in Eq. (D5) can be written in terms of the generators in the representation $\begin{smallmatrix}\square\\\square\end{smallmatrix}$, that are given by $SU(2N)$ structure constants,

$$\begin{aligned}\mathcal{J}^{\mu I}_X &= X^{\hat{I}}(T^I_{\begin{smallmatrix}\square\\\square\end{smallmatrix}})^{\hat{I}\hat{J}}\sigma^\mu\overline{X}^{\hat{J}}, \\ (T^I_{\begin{smallmatrix}\square\\\square\end{smallmatrix}})^{\hat{I}\hat{J}} &\equiv if^{\hat{I}I\hat{J}} = 2\mathrm{Tr}\left([T^{\hat{I}}, T^I]T^{\hat{J}}\right).\end{aligned} \tag{D7}$$

We assume that the confining strong dynamics can be described, in first approximation, by the exchange of one hypergluon which acquired a dynamical mass, which is the usual NJL assumption in QCD [24]. Then, the strong dynamics is supposed to generate, in the "ladder" approximation, $Sp(2N)$ current-current operators only,

$$\mathcal{L}_{\rm eff} = \frac{\kappa_{UV}}{2N}[\mathcal{J}^{\mu I}_{\psi}\mathcal{J}^{I}_{\psi\mu} + \mathcal{J}^{\mu I}_{X}\mathcal{J}^{I}_{X\mu} + 2\mathcal{J}^{\mu I}_{\psi}\mathcal{J}^{I}_{X\mu}], \quad \text{(D8)}$$

where $\kappa_{UV}/(2N) \sim g^2_{HC}/\Lambda^2$ stands for the exchange of one "massive" hypergluon. The large-N scaling of the gauge coupling is $g_{HC} \sim 1/\sqrt{2N}$, while κ_{UV} and Λ are N independent. The operators in Eq. (D8) are the product of fermion bilinears in the adjoint representation of $Sp(2N)$. In order to study physical resonances, which correspond to $Sp(2N)$-singlet fermion bilinears, we need to rewrite these operators by using Fierz transformations in the Lorentz, flavor and hypercolor spaces. Note that the last operator in Eq. (D8) does not contribute to any meson resonance, because by a Fierz transformation one obtains only 'diquark-diquark' operators, such as $(\psi X)(\bar{\psi}\bar{X})$, which are not hypercolor singlets, and therefore are not relevant for our analysis.

The Fierz transformations of Weyl indices are determined by the well-known identities

$$(\sigma^{\mu})_{\alpha\dot{\alpha}}(\sigma_{\mu})_{\beta\dot{\beta}} = -(\sigma^{\mu})_{\alpha\dot{\beta}}(\sigma_{\mu})_{\beta\dot{\alpha}} = 2\varepsilon_{\alpha\beta}\varepsilon_{\dot{\alpha}\dot{\beta}}. \quad \text{(D9)}$$

The $SU(N)$ and $Sp(2N)$ Fierz transformations, relevant for flavor and hypercolor indexes, respectively, are presented in Secs. D 3 and D 4 below.

2. General properties of Fierz transformations

In this section, we derive general properties of the coefficients in Fierz transformations. For a given irreducible representation R of the symmetry group under consideration, let us construct the tensor products $\mathcal{R}\otimes\bar{\mathcal{R}} = \sum_A \mathcal{R}_{\mathcal{A}}$ and $\mathcal{R}\otimes\mathcal{R} = \tilde{\sum}_{\mathcal{A}}\mathcal{R}_{\mathcal{A}}$, where the index $\mathcal{A}$ runs over the irreducible representations contained in the product. One can choose [99] a set of matrices $\{\Gamma^{\mathcal{A}}_a\}$ ($\{\tilde{\Gamma}^{\mathcal{A}}_a\}$), with $a = 1,\ldots,\dim\mathcal{R}_{\mathcal{A}}$, which form a basis of the vector space $\mathcal{R}\otimes\bar{\mathcal{R}}$ ($\mathcal{R}\otimes\mathcal{R}$). In the following, we will add a tilde wherever there is no conjugate in the tensor product. Such matrices have size $\dim\mathcal{R}\times\dim\mathcal{R}$ and satisfy the orthogonality relations

$$\begin{aligned}\mathrm{Tr}(\Gamma^{\mathcal{A}}_a\Gamma^{\mathcal{B}}_b) &= \alpha\delta^{\mathcal{A}\mathcal{B}}g^{\mathcal{A}}_{ab},\\ \mathrm{Tr}(\tilde{\Gamma}^{\mathcal{A}}_a\tilde{\Gamma}^{\mathcal{B}\dagger}_b) &= \alpha\delta^{\mathcal{A}\mathcal{B}}g^{\mathcal{A}}_{ab},\end{aligned} \quad \text{(D10)}$$

where α is a normalization constant and $g^{\mathcal{A}}_{ab}$ is a generic metric (in particular, $g^{\mathcal{A}}_{ab}g^{\mathcal{A}bc} = \delta^c_a$ and $\Gamma^{a\mathcal{A}} \equiv g^{\mathcal{A}ab}\Gamma^{\mathcal{A}}_b$). Any $\dim\mathcal{R}\times\dim\mathcal{R}$ matrix M can be decomposed on the basis $\{\Gamma^{\mathcal{A}}_a\}$ as

$$\begin{aligned}M &= \sum_{\mathcal{A}}\sum_a c^{a\mathcal{A}}\Gamma^{\mathcal{A}}_a = \tilde{\sum_{\mathcal{A}}}\sum_a d^{a\mathcal{A}}\tilde{\Gamma}^{\mathcal{A}}_a,\\ c^{a\mathcal{A}} &= \frac{1}{\alpha}\mathrm{Tr}(\Gamma^{a\mathcal{A}}M), \qquad d^{a\mathcal{A}} = \frac{1}{\alpha}\mathrm{Tr}(\tilde{\Gamma}^{a\mathcal{A}\dagger}M).\end{aligned} \quad \text{(D11)}$$

Replacing the explicit form of $c^{a\mathcal{A}}$ and $d^{a\mathcal{A}}$ in M we obtain the completeness relations

$$\sum_{\mathcal{A}}\sum_a(\Gamma^{a\mathcal{A}})_{ij}(\Gamma^{\mathcal{A}}_a)_{kl} = \tilde{\sum_{\mathcal{A}}}\sum_a(\tilde{\Gamma}^{a\mathcal{A}})_{ij}(\tilde{\Gamma}^{\mathcal{A}\dagger}_a)_{kl} = \alpha\delta_{il}\delta_{kj}. \quad \text{(D12)}$$

which are relevant to derive the Fierz coefficients.

Let us consider an interaction among four objects transforming as $(\mathcal{R}\otimes\bar{\mathcal{R}})_{\mathcal{A}}(\mathcal{R}\otimes\bar{\mathcal{R}})_{\mathcal{A}}$, where the subscripts indicate that each pair is contracted in the component $\mathcal{R}_{\mathcal{A}}$. Then, the Fierz transformations can be written as

$$\begin{aligned}\sum_a(\Gamma^{a\mathcal{A}})_{ij}(\Gamma^{\mathcal{A}}_a)_{kl} &= \sum_{\mathcal{B}}C_{\mathcal{A}\mathcal{B}}\sum_b(\Gamma^{b\mathcal{B}})_{il}(\Gamma^{\mathcal{B}}_b)_{kj}\\ &= \tilde{\sum_{\mathcal{B}}}D_{\mathcal{A}\mathcal{B}}\sum_b(\tilde{\Gamma}^{b\mathcal{B}})_{ik}(\tilde{\Gamma}^{\mathcal{B}\dagger}_b)_{jl},\end{aligned} \quad \text{(D13)}$$

where $C_{\mathcal{A}\mathcal{B}}$ and $D_{\mathcal{A}\mathcal{B}}$ are the Fierz coefficients for the channels $j\leftrightarrow l$ and $j\leftrightarrow k$, respectively. In terms of "quarks" $\sim\mathcal{R}$ and "antiquarks" $\sim\bar{\mathcal{R}}$, one can dub them the "quark-antiquark" and the "quark-quark" channels, respectively. Analogously, for the interaction $(\mathcal{R}\otimes\mathcal{R})_{\mathcal{A}}\times(\bar{\mathcal{R}}\otimes\bar{\mathcal{R}})_{\bar{\mathcal{A}}}$, the Fierz transformations read

$$\begin{aligned}\sum_a(\tilde{\Gamma}^{a\mathcal{A}})_{ij}(\tilde{\Gamma}^{\mathcal{A}\dagger}_a)_{kl} &= \sum_{\mathcal{B}}\tilde{C}_{\mathcal{A}\mathcal{B}}\sum_b(\Gamma^{b\mathcal{B}})_{il}(\Gamma^{\mathcal{B}T}_b)_{kj}\\ &= \sum_{\mathcal{B}}\tilde{D}_{\mathcal{A}\mathcal{B}}\sum_b(\Gamma^{b\mathcal{B}})_{ik}(\Gamma^{\mathcal{B}}_b)_{jl}.\end{aligned} \quad \text{(D14)}$$

One can derive several, general constraints on the Fierz-coefficient matrices $C, D, \tilde{C}, \tilde{D}$. Applying twice a Fierz transformation on the same indexes, the original contraction is recovered; therefore, one obtains

$$\begin{aligned}&\sum_{\mathcal{B}}C_{\mathcal{A}\mathcal{B}}C_{\mathcal{B}\mathcal{C}} = \delta_{\mathcal{A}\mathcal{C}}, \qquad \tilde{\sum_{\mathcal{B}}}D_{\mathcal{A}\mathcal{B}}\tilde{D}_{\mathcal{B}\mathcal{C}} = \delta_{\mathcal{A}\mathcal{C}},\\ &\sum_{\mathcal{B}}\tilde{C}_{\mathcal{A}\mathcal{B}}D_{\mathcal{B}\mathcal{C}} = s_{\mathcal{A}}\delta_{\mathcal{A}\mathcal{C}}, \qquad \sum_{\mathcal{B}}\tilde{D}_{\mathcal{A}\mathcal{B}}D_{\mathcal{B}\mathcal{C}} = \delta_{\mathcal{A}\mathcal{C}},\end{aligned} \quad \text{(D15)}$$

where $s_{\mathcal{A}} = +1$ (-1) when the representation $\mathcal{R}_{\mathcal{A}}$ belongs to the (anti)symmetric part of the tensor product $\mathcal{R}\otimes\mathcal{R}$, and correspondingly the matrices $\tilde{\Gamma}^{\mathcal{A}}_a$ are (anti)symmetric. Therefore, one has $C = C^{-1}$, while both $\tilde{C}$ and $\tilde{D}$ can be fully determined in terms of the matrix D. The contraction associated to the singlet representation, $\mathcal{R}_{\bullet}\subset\mathcal{R}\otimes\bar{\mathcal{R}}$, can be chosen as $\Gamma^{\bullet}_{ij} = \delta_{ij}\sqrt{\alpha/\dim\mathcal{R}}$. Therefore, Eq. (D12) determines the first row of C and D,

$$C_{\bullet\mathcal{A}} = \frac{1}{\dim\mathcal{R}}, \quad \forall\ \mathcal{R}_\mathcal{A} \subset \mathcal{R}\otimes\bar{\mathcal{R}},$$
$$D_{\bullet\mathcal{A}} = \frac{s_\mathcal{A}}{\dim\mathcal{R}}, \quad \forall\ \mathcal{R}_\mathcal{A} \subset \mathcal{R}\otimes\mathcal{R}. \tag{D16}$$

Indeed, from Eq. (D13) one can obtain explicit expressions of the Fierz coefficients,

$$C_{\mathcal{A}\mathcal{B}} = \frac{1}{\alpha^2}\sum_a \mathrm{Tr}[\Gamma^{a\mathcal{A}}\Gamma_b^\mathcal{B}\Gamma_a^\mathcal{A}\Gamma^{b\mathcal{B}}],$$
$$D_{\mathcal{A}\mathcal{B}} = \frac{1}{\alpha^2}\sum_a \mathrm{Tr}[\Gamma^{a\mathcal{A}}(\tilde{\Gamma}_b^\mathcal{B})^T(\Gamma_a^\mathcal{A})^T\tilde{\Gamma}^{b\mathcal{B}\dagger}], \tag{D17}$$

which are valid for every b. The direct computation of such expressions, however, may be very complicated in practice. By summing over b the two identities in Eq. (D17), one obtains quantities invariant under the exchanges $\mathcal{A}\leftrightarrow\mathcal{B}$ and $C\leftrightarrow C^{-1}$ ($D\leftrightarrow D^{-1}$); therefore, one concludes that

$$C_{\mathcal{A}\mathcal{B}}\dim\mathcal{R}_\mathcal{B} = C_{\mathcal{B}\mathcal{A}}\dim\mathcal{R}_\mathcal{A},$$
$$D_{\mathcal{A}\mathcal{B}}\dim\mathcal{R}_\mathcal{B} = (D^{-1})_{\mathcal{B}\mathcal{A}}\dim\mathcal{R}_\mathcal{A}. \tag{D18}$$

In particular, Eq. (D16) implies $C_{\mathcal{A}\bullet} = C_{\bullet\mathcal{A}}\dim\mathcal{R}_\mathcal{A} = \dim\mathcal{R}_\mathcal{A}/\dim\mathcal{R}$.

In the special case of a (pseudo)real representation $\mathcal{R}$, taking $\psi\sim\mathcal{R}$ and $\psi^\dagger\sim\bar{\mathcal{R}}$, one has $\bar{\psi}_i \equiv \psi_j^\dagger(\Omega_\epsilon)_{ji}\sim\mathcal{R}$, where Ω_ϵ is the invariant tensor establishing the equivalence of $\mathcal{R}$ and $\bar{\mathcal{R}}$, which is symmetric ($\epsilon=+1$) or antisymmetric ($\epsilon=-1$) in the case of real or pseudoreal representations, respectively. Therefore, the set of matrices $\{\Gamma_a^\mathcal{A}\}$ and $\{\tilde{\Gamma}_a^\mathcal{A}\}$ can be identified, according to $\tilde{\Gamma}_a^\mathcal{A} = \Gamma_a^\mathcal{A}\Omega_\epsilon$. In addition, the equality $\Omega_\epsilon\tilde{\Gamma}_a^{\mathcal{A}\dagger} = \epsilon\tilde{\Gamma}_a^\mathcal{A}\Omega_\epsilon$ holds, which implies in particular $(\psi\tilde{\Gamma}_a^\mathcal{A}\psi)^\dagger = \epsilon\bar{\psi}\tilde{\Gamma}_a^\mathcal{A}\bar{\psi}$. Then, it is convenient to rewrite the Fierz transformations in Eq. (D13) [or, equivalently, Eq. (D14)] in terms of the interaction $(\mathcal{R}\otimes\mathcal{R})_\mathcal{A}(\mathcal{R}\otimes\mathcal{R})_\mathcal{A}$,

$$\sum_a(\tilde{\Gamma}^{a\mathcal{A}})_{ij}(\tilde{\Gamma}_a^\mathcal{A})_{kl} = \sum_\mathcal{B}^{\sim} C_{\mathcal{A}\mathcal{B}}\sum_b(\tilde{\Gamma}^{b\mathcal{B}})_{il}(\tilde{\Gamma}_b^\mathcal{B})_{kj}$$
$$= \epsilon\sum_\mathcal{B}^{\sim} D_{\mathcal{A}\mathcal{B}}\sum_b(\tilde{\Gamma}^{b\mathcal{B}})_{ik}(\tilde{\Gamma}_b^\mathcal{B})_{jl}. \tag{D19}$$

It follows immediately that the two sets of Fierz coefficients are related as

$$\epsilon D_{\mathcal{A}\mathcal{B}} = s_\mathcal{A}C_{\mathcal{A}\mathcal{B}}s_\mathcal{B}, \tag{D20}$$

where $s_{\mathcal{A},\mathcal{B}}=\pm1$ denotes, once again, the (anti)symmetry of $\mathcal{R}_{\mathcal{A},\mathcal{B}}$ within $\mathcal{R}\otimes\mathcal{R}$. In this (pseudo)real case the singlet contraction corresponds to $\tilde{\Gamma}^\bullet_{ij} = (\Omega_\epsilon)_{ij}\sqrt{\alpha/\dim\mathcal{R}}$; therefore, $s_\bullet=\epsilon$, and one recovers Eq. (D16).

3. $SU(N)$ Fierz transformations

Let us derive the Fierz transformations associated to the fundamental representation of $SU(N)$ (see e.g. [100]). In our model, they are relevant for the flavor indexes, as the fermions ψ^a and X^f transform in the fundamental of $SU(4)$ and $SU(6)$, respectively.

In the "quark-antiquark" channel, $(\bar{N}_aN^b)(\bar{N}_cN^d)\to(\bar{N}_aN^d)(\bar{N}_cN^b)$, one can employ the completeness relation of Eq. (D12) for $\bar{N}\otimes N$,

$$\sum_{I=1}^{N^2-1}(T^I)^a{}_b(T^I)^c{}_d + (T^0)^a{}_b(T_0)^c{}_d = \frac{1}{2}\delta^a{}_d\delta^c{}_b, \tag{D21}$$

where T^I are the (N^2-1) generators of $SU(N)$, $T^0\equiv\mathbb{1}/\sqrt{2N}$, and $\alpha=\ell(N)/2=\ell(\bar{N})/2=1/2$ as we adopted the normalization $\mathrm{Tr}(T^IT^J)=\delta^{IJ}/2$. The first row of the Fierz-coefficient matrix $C_{\mathcal{A}\mathcal{B}}$ is simply obtained by reshuffling the indexes in Eq. (D21),

$$(T^0)^a{}_b(T^0)^c{}_d = \frac{1}{N}(T^0)^a{}_b(T^0)^c{}_d + \frac{1}{N}\sum_I(T^I)^a{}_d(T^I)^c{}_b, \tag{D22}$$

The second row can be determined by imposing $C^2\equiv\mathbb{1}$, as follows from Eq. (D15). Thus, one concludes that

$$\begin{pmatrix}(T^0)^a{}_b(T^0)^c{}_d\\ \sum_I(T^I)^a{}_b(T^I)^c{}_d\end{pmatrix} = C\begin{pmatrix}(T^0)^a{}_d(T^0)^c{}_b\\ \sum_I(T^I)^a{}_d(T^I)^c{}_b\end{pmatrix}$$
$$= \begin{pmatrix}\frac{1}{N} & \frac{1}{N}\\ \frac{N^2-1}{N} & -\frac{1}{N}\end{pmatrix}\begin{pmatrix}(T^0)^a{}_d(T^0)^c{}_b\\ \sum_I(T^I)^a{}_d(T^I)^c{}_b\end{pmatrix}. \tag{D23}$$

In the 'quark-quark' channel, $(\bar{N}_aN^b)(\bar{N}_cN^d)\to(\bar{N}_a\bar{N}_c)(N^bN^d)$, one needs also the completeness relation for $N\otimes N$, that involves $N(N+1)/2$ symmetric matrices Γ_S^I, and $N(N-1)/2$ antisymmetric matrices Γ_A^I,

$$\sum_{I=1}^{N(N+1)/2}(\Gamma_S^{I\dagger})^{ab}(\Gamma_S^I)_{cd} + \sum_{I=1}^{N(N-1)/2}(\Gamma_A^{I\dagger})^{ab}(\Gamma_A^I)_{cd} = \frac{1}{2}\delta^a{}_d\delta^b{}_c. \tag{D24}$$

A convenient basis of (anti)symmetric matrices is provided by $\Gamma^0\equiv\Sigma_\epsilon T^0$, $\Gamma^I\equiv\Sigma_\epsilon T^I$, and $\Gamma^{\hat{I}}\equiv\Sigma_\epsilon T^{\hat{I}}$, where $(\Sigma_\epsilon)_{ab}$ is the invariant tensor of a maximal $SU(N)$ subgroup, which is $SO(N)$ in the case $\epsilon=+1$, and $Sp(N)$ in the case $\epsilon=-1$ (present only for N even). Here the index I runs over the subgroup generators only, and the index $\hat{I}$ spans the coset. When $\epsilon=+1(-1)$, Σ_ϵ is a symmetric (antisymmetric) matrix and, according to Eq. (2.2), Γ^0 and $\Gamma^{\hat{I}}$ are

symmetric (antisymmetric), while Γ^I are antisymmetric (symmetric). Using this basis for the matrices $\Gamma^I_{S,A}$, one can construct explicitly the Fierz-coefficient matrix $D_{\mathcal{AB}}$,

$$\begin{pmatrix} (T^0)^a{}_b (T^0)^c{}_d \\ \sum_I (T^I)^a{}_b (T^I)^c{}_d \end{pmatrix} = D \begin{pmatrix} \sum_I (\Gamma^{I\dagger}_S)^{ac} (\Gamma^I_S)_{bd} \\ \sum_I (\Gamma^{I\dagger}_A)^{ac} (\Gamma^I_A)_{bd} \end{pmatrix} = \begin{pmatrix} \frac{1}{N} & -\frac{1}{N} \\ \frac{N-1}{N} & \frac{N+1}{N} \end{pmatrix} \begin{pmatrix} \sum_I (\Gamma^{I\dagger}_S)^{ac} (\Gamma^I_S)_{bd} \\ \sum_I (\Gamma^{I\dagger}_A)^{ac} (\Gamma^I_A)_{bd} \end{pmatrix}. \tag{D25}$$

For example, the first row of $D_{\mathcal{AB}}$ can be obtained from Eq. (D22) by contracting with $(\Sigma_\epsilon)^{dd'}(\Sigma_\epsilon)_{c'c}$, and inverting appropriate pairs of (anti)symmetrized indexes: the result agrees with Eq. (D16). The second row is determined e.g. by Eq. (D18), up to an overall sign, that can be fixed once again by (anti)symmetrizing over appropriate indexes.

4. $Sp(2N)$ Fierz transformations

Let us derive the Fierz transformations associated to the hypercolor representations of the fermions ψ_i and X_{ij}, that is, $\square$ and $\begin{smallmatrix}\square\\\square\end{smallmatrix}$, respectively. The group $Sp(2N)$ is a subgroup of $SU(2N)$, corresponding to the vacuum direction $\Sigma_- \equiv \Omega$, defined in Eq. (3.3). Taking advantage of Eq. (2.2), one can decompose the $U(2N)$ completeness relation (D21) into two parts, corresponding to the $Sp(2N)$ subalgebra and its coset,

$$\sum_{I=1}^{N(2N+1)} (T^I)_{ij}(T^I)_{kl} = \frac{1}{4}(\delta_{il}\delta_{kj} - \Omega_{ik}\Omega_{jl}) : \; Sp(2N), \tag{D26}$$

$$\sum_{\hat{I}=1}^{(2N+1)(N-1)} (T^{\hat{I}})_{ij}(T^{\hat{I}})_{kl} + (T^0)_{ij}(T^0)_{kl} = \frac{1}{4}(\delta_{il}\delta_{kj} + \Omega_{ik}\Omega_{jl}) : \; U(2N)/Sp(2N). \tag{D27}$$

The product of two fundamental representations of $Sp(2N)$ reads

$$\square \times \square = \bullet_a \; + \; \square\square_s \; + \; \begin{smallmatrix}\square\square\\\square\end{smallmatrix}_a \, , \tag{D28}$$

where the bullet stands for the singlet and the subscripts indicate whether the contraction is symmetric or antisymmetric under the exchange of the two factors. These representations have dimensions

$$d(\square) = 2N\,, \qquad d(\bullet) = 1\,, \qquad d(\square\square) = N(2N+1)\,,$$
$$d\left(\begin{smallmatrix}\square\square\\\square\end{smallmatrix}\right) = N(2N-1) - 1 = (2N+1)(N-1)\,. \tag{D29}$$

Note that, for $N = 1$, the two-index antisymmetric representation is absent. The two indexes in $\square_i\square_j$ are contracted by an appropriate set of (anti)symmetric matrices $\tilde{\Gamma}^a_{\mathcal{A}}$, that can be conveniently chosen as

$$\tilde{\Gamma}_\bullet \equiv \Omega T^0 = \frac{\Omega}{\sqrt{4N}}\,, \qquad \tilde{\Gamma}^I_{\square\square} \equiv \Omega T^I\,, \qquad \tilde{\Gamma}^{\hat{I}}_{\begin{smallmatrix}\square\square\\\square\end{smallmatrix}} \equiv \Omega T^{\hat{I}}\,, \tag{D30}$$

in one-to-one correspondence with the generators of $U(2N)$. Multiplying (D26) and (D27) by $\Omega_{mi}\Omega_{nk}$, one obtains useful equalities to determine the Fierz transformations of $(\square_i\square_j)(\square_k\square_l)$. Thus, the matrix of Fierz coefficients for the channel $(il)(kj)$, $C_{\mathcal{AB}}$, can be fully determined in agreement with the general results of Sec. D 2:

$$\begin{pmatrix} (\Omega T^0)_{ij}(\Omega T^0)_{kl} \\ \sum_I (\Omega T^I)_{ij}(\Omega T^I)_{kl} \\ \sum_{\hat{I}} (\Omega T^{\hat{I}})_{ij}(\Omega T^{\hat{I}})_{kl} \end{pmatrix} = \begin{pmatrix} \frac{1}{2N} & \frac{1}{2N} & \frac{1}{2N} \\ \frac{2N+1}{2} & -\frac{1}{2} & \frac{1}{2} \\ \frac{(2N+1)(N-1)}{2N} & \frac{N-1}{2N} & -\frac{N+1}{2N} \end{pmatrix} \times \begin{pmatrix} (\Omega T^0)_{il}(\Omega T^0)_{kj} \\ \sum_I (\Omega T^I)_{il}(\Omega T^I)_{kj} \\ \sum_{\hat{I}} (\Omega T^{\hat{I}})_{il}(\Omega T^{\hat{I}})_{kj} \end{pmatrix}, \tag{D31}$$

According to Eq. (D20), the Fierz coefficients in the channel $(ik)(jl)$ are given by $D_{\mathcal{AB}} = -C_{\mathcal{AB}}$ when both $\mathcal{A}$ and $\mathcal{B}$ are (anti)symmetric contractions, and $D_{\mathcal{AB}} = C_{\mathcal{AB}}$ otherwise.

We can now determine the coefficients $\kappa_{A,C,D}$ of the four-fermion operators in the ψ sector, which are defined by Eqs. (3.14) and (3.30), assuming that the dynamics is well approximated by the ψ-sector current-current operator of Eq. (D8), with coefficient κ_{UV}. Note that the 't Hooft operator with coefficient κ_B, defined by the second line of Eq. (3.14), is not generated by the current-current interaction, as the latter preserves the anomalous $U(1)_\psi$ symmetry; therefore, the size of κ_B is unrelated to κ_{UV}. On the contrary, the sizes of $\kappa_{A,B,C}$ can be related to κ_{UV} by performing the pertinent set of Fierz transformations over Lorentz, $SU(4)$ flavor, and $Sp(2N)$ hypercolor indexes. Naively, with this procedure the current-current operator is recast into a sum over several operators: those with two

hypercolor-singlet fermion bilinears, which correspond to physical meson states, plus those with two hypercolor-nonsinglet fermion bilinears. The former operators receive a coefficient

$$\kappa_A = \kappa_C = \kappa_D = \frac{2N+1}{4N}\kappa_{UV}. \tag{D32}$$

However, the latter operators could also contribute to these couplings, by further Fierz transformations. Therefore, the above equalities cannot be firmly established on this basis. Fortunately, there exists a unique way to express the current-current operator in terms of hypercolor-singlet fermion bilinears only, by using the identity

$$\sum_I (\Omega T^I)_{ij}(\Omega T^I)_{kl} = \frac{1}{4}(\Omega_{il}\Omega_{kj} - \Omega_{ik}\Omega_{jl}), \tag{D33}$$

which is obtained e.g. by considering the first row of Eq. (D31) and symmetrizing over the indexes (il), or equivalently by multiplying the $Sp(2N)$ completeness relation (D26) by $\Omega_{i'i}\Omega_{k'k}$. Employing this relation we obtain

$$\kappa_A = \kappa_C = \kappa_D = \frac{1}{2}\kappa_{UV}. \tag{D34}$$

Therefore, in the current-current approximation, the scalar coupling κ_A and the vector couplings $\kappa_{C,D}$ are equal and N independent when N becomes large, as κ_{UV} is. Notice that the naive relations in Eq. (D32) were correct al leading order in $1/N$. The equality between vector and scalar couplings also holds in the standard NJL model for QCD [8].

Let us now analyze the product of two $Sp(2N)$ two-index traceless antisymmetric representations $\square\!\square$, that exist only for $N > 1$, and are relevant for the color sector of our model. The tensor product,

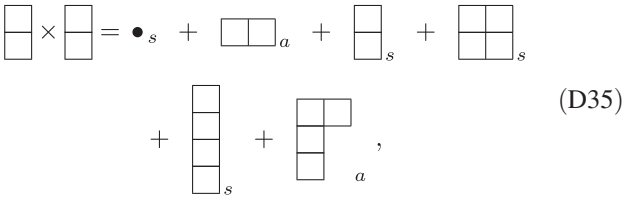

(D35)

contains three four-index representations, of dimensions

$$\begin{aligned} d\left(\square\!\square\,\square\!\square\right) &= \frac{N}{3}\left(4N^3 - 7N + 3\right), \\ d\left(\begin{smallmatrix}\square\!\square\\ \square\!\square\end{smallmatrix}\right) &= \frac{N}{6}\left(4N^3 - 12N^2 - N + 3\right), \\ d\left(\begin{smallmatrix}\square\!\square\,\square\!\square\\ \square\!\square\end{smallmatrix}\right) &= \frac{1}{2}\left(4N^4 - 4N^3 - 9N^2 + N + 2\right). \end{aligned} \tag{D36}$$

These numbers can be derived taking into account the symmetry properties of each representation in Eq. (D35), and subtracting the dimensions of the smaller representations, obtained by taking traces, as given in Eq. (D29). Note that, for $N = 2$, the third, fifth and sixth representation on the right-hand side of Eq. (D35) are absent: $5 \times 5 = 1_s + 10_a + 14_s$. For $N = 3$, the fifth representation only is absent: $14 \times 14 = 1_s + 21_a + 14_s + 90_s + 70_a$. Finally, for $N > 3$ all the components of the tensor product exist.

The indexes in $\square\!\square_{ij}\square\!\square_{kl}$ are contracted into the representation $\mathcal{R}$ by a set of tensors $(\tilde{\Gamma}^a_{\mathcal{R}})_{ijkl}$, with $a = 1, \ldots, \dim \mathcal{R}$. Equivalently, one can use a single index running over the $(2N+1)(N-1)$ components of $\square\!\square$,

$$X_{li}(\tilde{\Gamma}^a_{\mathcal{R}})_{ijkl}X_{jk} = X_{\hat{\imath}}(\tilde{\Gamma}^a_{\mathcal{R}})_{\hat{\imath}\hat{\jmath}}X_{\hat{\jmath}}. \tag{D37}$$

where X_{ij} and $X_{\hat{\imath}}$ are related by Eq. (D6). In this notation, the completeness relation reads

$$\begin{aligned} \sum_{\mathcal{R}}\sum_a (\tilde{\Gamma}^a_{\mathcal{R}})_{\hat{\imath}\hat{\jmath}}(\tilde{\Gamma}^a_{\mathcal{R}})_{\hat{K}\hat{L}} &= \frac{1}{2}\ell(\square\!\square)\delta_{\hat{\imath}\hat{L}}\delta_{\hat{K}\hat{\jmath}} \\ &= (N-1)\delta_{\hat{\imath}\hat{L}}\delta_{\hat{K}\hat{\jmath}}\,, \\ \mathcal{R} &= \bullet, \square\!\square, \square\!\square, \square\!\square\,\square\!\square, \begin{smallmatrix}\square\!\square\,\square\!\square\\ \square\!\square\end{smallmatrix}, \begin{smallmatrix}\square\!\square\,\square\!\square\\ \square\!\square\end{smallmatrix}\,. \end{aligned} \tag{D38}$$

In fact, the set of matrices $\{\tilde{\Gamma}^a_{\mathcal{R}}\}$ corresponds to the generators of the group $U[(2N+1)(N-1)]$, normalized as $\square\!\square$. Let us provide the explicit form of these matrices for the smallest representations. The singlet contraction is given by

$$\begin{aligned} (\tilde{\Gamma}_{\bullet})_{ijkl} &= \frac{1}{\sqrt{2N+1}}\Omega_{ij}\Omega_{kl}, \\ (\tilde{\Gamma}_{\bullet})_{\hat{\imath}\hat{\jmath}} &= \frac{1}{\sqrt{2N+1}}\delta_{\hat{\imath}\hat{\jmath}}. \end{aligned} \tag{D39}$$

The adjoint contraction, already employed in Sec. D 1, is given by

$$\begin{aligned} (\tilde{\Gamma}^K_{\square\!\square})_{ijkl} &= (\Omega T^K)_{ij}\Omega_{kl} - \Omega_{ij}(\Omega T^K)_{kl}\,, \\ (\tilde{\Gamma}^K_{\square\!\square})_{\hat{\imath}\hat{\jmath}} &= -if^{\hat{\imath}\hat{\jmath}K} = -2\mathrm{Tr}([T^{\hat{\imath}}, T^{\hat{\jmath}}]T^K)\,. \end{aligned} \tag{D40}$$

The two-index antisymmetric contraction has a similar structure, with the unbroken generators T^I replaced by the broken ones $T^{\hat{I}}$,

$$\begin{aligned} (\tilde{\Gamma}^{\hat{K}}_{\square})_{ijkl} &= (\Omega T^{\hat{K}})_{ij}\Omega_{kl} + \Omega_{ij}(\Omega T^{\hat{K}})_{kl}\,, \\ (\tilde{\Gamma}^{\hat{K}}_{\square})_{\hat{\imath}\hat{\jmath}} &= d^{\hat{\imath}\hat{\jmath}\hat{K}} = 2\mathrm{Tr}(\{T^{\hat{\imath}}, T^{\hat{\jmath}}\}T^{\hat{K}})\,. \end{aligned} \tag{D41}$$

One can easily check that the symmetry properties of the contractions in Eqs. (D39), (D40) and (D41) agree with those indicated in Eq. (D35).

The singlet Fierz coefficients in the channel $(\hat{I}\,\hat{L})(\hat{K}\,\hat{J})$, $C_{\bullet\mathcal{R}}$, are easily determined from the completeness relation (D38), in agreement with Eq. (D16). The coefficients $C_{\mathcal{R}\bullet}$ are determined in turn by Eq. (D18). Thus, we can write

$$\begin{pmatrix} (\tilde{\Gamma}_\bullet)_{\hat{I}\hat{J}}(\tilde{\Gamma}_\bullet)_{\hat{K}\hat{L}} \\ \sum_a (\tilde{\Gamma}^a_{\square\square})_{\hat{I}\hat{J}}(\tilde{\Gamma}^a_{\square\square})_{\hat{K}\hat{L}} \\ \sum_a (\tilde{\Gamma}^a_{\square})_{\hat{I}\hat{J}}(\tilde{\Gamma}^a_{\square})_{\hat{K}\hat{L}} \\ \sum_a (\tilde{\Gamma}^a_{\square\square})_{\hat{I}\hat{J}}(\tilde{\Gamma}^a_{\square\square})_{\hat{K}\hat{L}} \\ \sum_a (\tilde{\Gamma}^a_{\begin{smallmatrix}\square\\\square\end{smallmatrix}})_{\hat{I}\hat{J}}(\tilde{\Gamma}^a_{\begin{smallmatrix}\square\\\square\end{smallmatrix}})_{\hat{K}\hat{L}} \\ \sum_a (\tilde{\Gamma}^a_{\begin{smallmatrix}\square\square\\\square\end{smallmatrix}})_{\hat{I}\hat{J}}(\tilde{\Gamma}^a_{\begin{smallmatrix}\square\square\\\square\end{smallmatrix}})_{\hat{K}\hat{L}} \end{pmatrix} = \begin{pmatrix} \frac{1}{d(\square)} & \frac{1}{d(\square)} & \frac{1}{d(\square)} & \frac{1}{d(\square)} & \frac{1}{d(\square)} & \frac{1}{d(\square)} \\ \frac{d(\square\square)}{d(\square)} & \cdots & \cdots & \cdots & \cdots & \cdots \\ 1 & \cdots & \cdots & \cdots & \cdots & \cdots \\ \frac{d(\square\square)}{d(\square)} & \cdots & \cdots & \cdots & \cdots & \cdots \\ \frac{d(\begin{smallmatrix}\square\\\square\end{smallmatrix})}{d(\square)} & \cdots & \cdots & \cdots & \cdots & \cdots \\ \frac{d(\begin{smallmatrix}\square\square\\\square\end{smallmatrix})}{d(\square)} & \cdots & \cdots & \cdots & \cdots & \cdots \end{pmatrix} \begin{pmatrix} (\tilde{\Gamma}_\bullet)_{\hat{I}\hat{L}}(\tilde{\Gamma}_\bullet)_{\hat{K}\hat{J}} \\ \sum_a (\tilde{\Gamma}^a_{\square\square})_{\hat{I}\hat{L}}(\tilde{\Gamma}^a_{\square\square})_{\hat{K}\hat{J}} \\ \sum_a (\tilde{\Gamma}^a_{\square})_{\hat{I}\hat{L}}(\tilde{\Gamma}^a_{\square})_{\hat{K}\hat{J}} \\ \sum_a (\tilde{\Gamma}^a_{\square\square})_{\hat{I}\hat{L}}(\tilde{\Gamma}^a_{\square\square})_{\hat{K}\hat{J}} \\ \sum_a (\tilde{\Gamma}^a_{\begin{smallmatrix}\square\\\square\end{smallmatrix}})_{\hat{I}\hat{L}}(\tilde{\Gamma}^a_{\begin{smallmatrix}\square\\\square\end{smallmatrix}})_{\hat{K}\hat{J}} \\ \sum_a (\tilde{\Gamma}^a_{\begin{smallmatrix}\square\square\\\square\end{smallmatrix}})_{\hat{I}\hat{L}}(\tilde{\Gamma}^a_{\begin{smallmatrix}\square\square\\\square\end{smallmatrix}})_{\hat{K}\hat{J}} \end{pmatrix} . \tag{D42}$$

One needs further algebraic manipulations to determine the nonsinglet Fierz coefficients $C_{\mathcal{R}\mathcal{R}'}$, which anyhow will not be needed for our purposes. For concreteness, let us display the explicit result in the case $N = 2$, where there are only three representations in the tensor product $\square \times \square$. Using repeatedly the completeness relation and the (anti)symmetrization over appropriate pairs of indexes, we conclude that the matrix C in the case $N = 2$ takes the form

$$\begin{pmatrix} (\tilde{\Gamma}_\bullet)_{\hat{I}\hat{J}}(\tilde{\Gamma}_\bullet)_{\hat{K}\hat{L}} \\ \sum_a (\tilde{\Gamma}^a_{\square\square})_{\hat{I}\hat{J}}(\tilde{\Gamma}^a_{\square\square})_{\hat{K}\hat{L}} \\ \sum_a (\tilde{\Gamma}^a_{\begin{smallmatrix}\square\square\\\square\end{smallmatrix}})_{\hat{I}\hat{J}}(\tilde{\Gamma}^a_{\begin{smallmatrix}\square\square\\\square\end{smallmatrix}})_{\hat{K}\hat{L}} \end{pmatrix} = \begin{pmatrix} \frac{1}{5} & \frac{1}{5} & \frac{1}{5} \\ 2 & \frac{1}{2} & -\frac{1}{2} \\ \frac{14}{5} & -\frac{7}{10} & \frac{3}{10} \end{pmatrix} \begin{pmatrix} (\tilde{\Gamma}_\bullet)_{\hat{I}\hat{L}}(\tilde{\Gamma}_\bullet)_{\hat{K}\hat{J}} \\ \sum_a (\tilde{\Gamma}^a_{\square\square})_{\hat{I}\hat{L}}(\tilde{\Gamma}^a_{\square\square})_{\hat{K}\hat{J}} \\ \sum_a (\tilde{\Gamma}^a_{\begin{smallmatrix}\square\square\\\square\end{smallmatrix}})_{\hat{I}\hat{L}}(\tilde{\Gamma}^a_{\begin{smallmatrix}\square\square\\\square\end{smallmatrix}})_{\hat{K}\hat{J}} \end{pmatrix} . \tag{D43}$$

The Fierz coefficients $D_{\mathcal{R}\mathcal{R}'}$ in the channel $(\hat{I}\,\hat{K})(\hat{J}\,\hat{L})$ are determined by Eq. (D20), with $\epsilon = +1$ as $\square$ is a real representation. Since we aim to rewrite the X-sector current-current operator of Eq. (D8) in terms of hypercolur-singlet fermion bilinears, the relevant Fierz coefficients are

$$C_{\square\bullet} = -D_{\square\bullet} = \frac{N}{N-1} . \tag{D44}$$

In analogy with the above procedure in the ψ sector, one can try to determine the coefficients $\kappa_{A6,C6,D6}$ of the four-fermion operators in the X sector, which are defined by Eqs. (5.1) and (5.20). If one applies a pertinent Fierz transformation, over Lorentz, $SU(6)$ and $Sp(2N)$ indexes, to the X-sector current-current operator in Eq. (D8), one obtains

$$\kappa_{A6} = \kappa_{C6} = \kappa_{D6} = \kappa_{UV} . \tag{D45}$$

This indicates that the scalar and vector operators of the colored sector receive the same coefficient, that is twice as large as for the corresponding operators of the electroweak sector; see Eq. (D34). However, at the same time κ_{UV} also contributes to other operators that involve hypercolor-nonsinglet fermion bilinears; therefore, the above relations are ambiguous, as they rely on a specific recasting of the current-current operator, that is not unique. Another possible recasting is obtained by antisymmetrizing Eq. (D38), with respect to the pair of indexes $(\hat{K}\,\hat{L})$, to remove the symmetric components of Eq. (D35),

$$\sum_a (\tilde{\Gamma}^a_{\square\square})_{\hat{I}\hat{J}}(\tilde{\Gamma}^a_{\square\square})_{\hat{K}\hat{L}} + \sum_a (\tilde{\Gamma}^a_{\begin{smallmatrix}\square\square\\\square\end{smallmatrix}})_{\hat{I}\hat{J}}(\tilde{\Gamma}^a_{\begin{smallmatrix}\square\square\\\square\end{smallmatrix}})_{\hat{K}\hat{L}} = \frac{(2N+1)(N-1)}{2}\left[(\tilde{\Gamma}_\bullet)_{\hat{I}\hat{L}}(\tilde{\Gamma}_\bullet)_{\hat{K}\hat{J}} - (\tilde{\Gamma}_\bullet)_{\hat{I}\hat{K}}(\tilde{\Gamma}_\bullet)_{\hat{J}\hat{L}}\right] . \tag{D46}$$

This relation is the analog of Eq. (D33), associated to the tensor product $\square \times \square$. In general, this procedure does not allow to express the current-current contraction in terms of singlet-singlet contractions only, because the product $\begin{smallmatrix}\square\\\square\end{smallmatrix} \times \begin{smallmatrix}\square\\\square\end{smallmatrix}$ contains another antisymmetric representation, besides the adjoint. The exception is the case $N = 2$, where the second term on the left-hand side of Eq. (D46) is absent. If one neglects this second term even for $N > 2$, the relation between the current-current operator and the singlet-singlet operators becomes

$$\kappa_{A6} = \kappa_{C6} = \kappa_{D6} = \frac{(2N+1)(N-1)^2}{2N}\kappa_{UV}. \qquad \text{(D47)}$$

Note that these couplings can be much larger than those in Eq. (D45), when N is large. The problem is that the current-current operator contains terms leading in $1/N$, that cannot be written as singlet-singlet contractions only, except for $N = 2$. In the latter case, Eq. (D47) is exact and its right-hand side reads $5\kappa_{UV}/4$, to be compared with Eq. (D34) in the electroweak sector.

We conclude that, for $N > 2$, the strength of the colored-sector couplings cannot be fixed in terms of κ_{UV}, and we treat it as a free parameter. In particular, κ_{A6} is independent from the strength of the electroweak-sector coupling κ_A: in our phenomenological analysis we take $\kappa_{A6} \sim \kappa_A$, such that the domain of validity of the NJL calculations is similar in the two sectors, and the NJL predictions can be compared. On the other hand, the equality between the scalar and vector couplings in each sector is a solid prediction of the current-current approximation, that holds independently from their absolute sizes. Finally, we remind that all predictions discussed in this appendix depend on the validity of the effective Lagrangian of Eq. (D8), that relies on the "ladder" approximation for the hypercolor dynamics. Therefore, significant departures from these predictions cannot be excluded.

[1] D. B. Kaplan and H. Georgi, SU(2) × U(1) breaking by vacuum misalignment, Phys. Lett. B **136**, 183 (1984).
[2] D. B. Kaplan, H. Georgi, and S. Dimopoulos, Composite Higgs scalars, Phys. Lett. B **136**, 187 (1984).
[3] M. J. Dugan, H. Georgi, and D. B. Kaplan, Anatomy of a composite Higgs model, Nucl. Phys. **B254**, 299 (1985).
[4] K. Agashe, R. Contino, and A. Pomarol, The minimal composite Higgs model, Nucl. Phys. **B719**, 165 (2005).
[5] S. Weinberg, Implications of dynamical symmetry breaking, Phys. Rev. D **13**, 974 (1976).
[6] L. Susskind, Dynamics of spontaneous symmetry breaking in the Weinberg-Salam theory, Phys. Rev. D **20**, 2619 (1979).
[7] J. Galloway, J. A. Evans, M. A. Luty, and R. A. Tacchi, Minimal conformal technicolor and precision electroweak tests, J. High Energy Phys. 10 (2010) 086.
[8] J. Barnard, T. Gherghetta, and T. S. Ray, UV descriptions of composite Higgs models without elementary scalars, J. High Energy Phys. 02 (2014) 002.
[9] G. Cacciapaglia and F. Sannino, Fundamental composite (Goldstone) Higgs dynamics, J. High Energy Phys. 04 (2014) 111.
[10] G. Ferretti, UV completions of partial compositeness: The case for a SU(4) gauge group, J. High Energy Phys. 06 (2014) 142.
[11] L. Vecchi, A "dangerous irrelevant" UV-completion of the composite Higgs, J. High Energy Phys. 02 (2017) 094.
[12] T. Ma and G. Cacciapaglia, Fundamental composite 2HDM: SU(N) with 4 flavours, J. High Energy Phys. 03 (2016) 211.
[13] G. Ferretti and D. Karateev, Fermionic UV completions of composite Higgs models, J. High Energy Phys. 03 (2014) 077.
[14] F. Caracciolo, A. Parolini, and M. Serone, UV completions of composite Higgs models with partial compositeness, J. High Energy Phys. 02 (2013) 066.
[15] G. von Gersdorff, E. Ponton, and R. Rosenfeld, The dynamical composite Higgs, J. High Energy Phys. 06 (2015) 119.
[16] S. Fichet, G. von Gersdorff, E. Ponton, and R. Rosenfeld, The excitation of the global symmetry-breaking vacuum in composite Higgs models, J. High Energy Phys. 09 (2016) 158.
[17] J. Galloway, A. L. Kagan, and A. Martin, A UV complete partially composite-pNGB Higgs, Phys. Rev. D **95**, 035038 (2017).
[18] G. 't Hooft, Naturalness, chiral symmetry, and spontaneous chiral symmetry breaking, NATO Sci. Ser. B **59**, 135 (1980).
[19] S. Weinberg, Precise Relations between the Spectra of Vector and Axial Vector Mesons, Phys. Rev. Lett. **18**, 507 (1967).
[20] G. 't Hooft, A planar diagram theory for strong interactions, Nucl. Phys. **B72**, 461 (1974).
[21] E. Witten, Baryons in the 1/n expansion, Nucl. Phys. **B160**, 57 (1979).
[22] Y. Nambu and G. Jona-Lasinio, Dynamical Model of Elementary Particles Based on an Analogy with Superconductivity. 1., Ann. N.Y. Acad. Sci. **122**, 345 (1961).
[23] Y. Nambu and G. Jona-Lasinio, Dynamical model of elementary particles based on an analogy with superconductivity. II, Ann. N.Y. Acad. Sci. **124**, 246 (1961).
[24] S. P. Klevansky, The Nambu-Jona-Lasinio model of quantum chromodynamics, Rev. Mod. Phys. **64**, 649 (1992).

[25] T. Hatsuda and T. Kunihiro, QCD phenomenology based on a chiral effective Lagrangian, Phys. Rep. **247**, 221 (1994).
[26] D. B. Kaplan, Flavor at SSC energies: A New mechanism for dynamically generated fermion masses, Nucl. Phys. **B365**, 259 (1991).
[27] R. Contino, The Higgs as a composite Nambu-Goldstone boson, in *Proceedings of Physics of the large and the small, TASI 09, proceedings of the Theoretical Advanced Study Institute in Elementary Particle Physics, Boulder, Colorado, USA, 2009*, p. 235, http://dx.doi.org/10.1142/9789814327183_0005.
[28] G. Panico and A. Wulzer, The composite Nambu-Goldstone Higgs, Lect. Notes Phys. **913**, 1 (2016).
[29] C. Vafa and E. Witten, Restrictions on symmetry breaking in vector-like gauge theories, Nucl. Phys. **B234**, 173 (1984).
[30] D. A. Kosower, Symmetry breaking patterns in pseudoreal and real gauge theories, Phys. Lett. B **144**, 215 (1984).
[31] M. E. Peskin, The alignment of the vacuum in theories of technicolor, Nucl. Phys. **B175**, 197 (1980).
[32] Ya. I. Kogan, M. A. Shifman, and M. I. Vysotsky, Spontaneous breaking of chiral symmetry for real fermions and N = 2 SUSY Yang-Mills theory, Yad. Fiz. **42**, 504 (1985) [Sov. J. Nucl. Phys. **42**, 318 (1985)].
[33] J. S. Bell and R. Jackiw, A PCAC puzzle: $\pi^0 \to \gamma\gamma$ in the sigma model, Nuovo Cimento A **60**, 47 (1969).
[34] S. L. Adler, Axial vector vertex in spinor electrodynamics, Phys. Rev. **177**, 2426 (1969).
[35] S. L. Adler and W. A. Bardeen, Absence of higher order corrections in the anomalous axial vector divergence equation, Phys. Rev. **182**, 1517 (1969).
[36] Y. Frishman, A. Schwimmer, T. Banks, and S. Yankielowicz, The axial anomaly and the bound state spectrum in confining theories, Nucl. Phys. **B177**, 157 (1981).
[37] S. R. Coleman and B. Grossman, 't Hooft's consistency condition as a consequence of analyticity and unitarity, Nucl. Phys. **B203**, 205 (1982).
[38] D. Weingarten, Mass Inequalities for QCD, Phys. Rev. Lett. **51**, 1830 (1983).
[39] E. Witten, Some Inequalities Among Hadron Masses, Phys. Rev. Lett. **51**, 2351 (1983).
[40] S. Nussinov, Baryon meson mass inequality, Phys. Rev. Lett. **51**, 2081 (1983).
[41] D. Espriu, M. Gross, and J. F. Wheater, Rigorous inequalities in vector-like gauge theories, Phys. Lett. B **146**, 67 (1984).
[42] S. Nussinov and B. Sathiapalan, Mass and scattering length inequalities in QCD and QCD like theories, Nucl. Phys. **B256**, 285 (1985).
[43] S. Nussinov and M. A. Lampert, QCD inequalities, Phys. Rep. **362**, 193 (2002).
[44] C. W. Bernard, A. Duncan, J. LoSecco, and S. Weinberg, Exact spectral function sum rules, Phys. Rev. *D* **12**, 792 (1975).
[45] K. G. Wilson, Nonlagrangian models of current algebra, Phys. Rev. **179**, 1499 (1969).
[46] M. A. Shifman, A. I. Vainshtein, and V. I. Zakharov, QCD and resonance physics: Applications, Nucl. Phys. **B147**, 448 (1979).
[47] E. G. Floratos, S. Narison, and E. de Rafael, Spectral function sum rules in quantum chromodynamics. 1. Charged currents sector, Nucl. Phys. **B155**, 115 (1979).
[48] J. Preskill, Subgroup alignment in hypercolor theories, Nucl. Phys. **B177**, 21 (1981).
[49] T. Das, G. S. Guralnik, V. S. Mathur, F. E. Low, and J. E. Young, Electromagnetic Mass Difference of Pions, Phys. Rev. Lett. **18**, 759 (1967).
[50] M. Knecht and E. de Rafael, Patterns of spontaneous chiral symmetry breaking in the large N(c) limit of QCD—like theories, Phys. Lett. B **424**, 335 (1998).
[51] H. Georgi, $SU(2) \times U(1)$ breaking, compositeness and flavor, Conference Proceedings **C850701**, 339 (1985).
[52] J. Wess and B. Zumino, Consequences of anomalous Ward identities, Phys. Lett. B **37**, 95 (1971).
[53] E. Witten, Global aspects of current algebra, Nucl. Phys. **B223**, 422 (1983).
[54] C.-S. Chu, P.-M. Ho, and B. Zumino, NonAbelian anomalies and effective actions for a homogeneous space G/H, Nucl. Phys. **B475**, 484 (1996).
[55] E. Katz, A. E. Nelson, and D. G. E. Walker, The Intermediate Higgs, J. High Energy Phys. 08 (2005) 074.
[56] B. Gripaios, A. Pomarol, F. Riva, and J. Serra, Beyond the minimal composite Higgs model, J. High Energy Phys. 04 (2009) 070.
[57] M. Frigerio, A. Pomarol, F. Riva, and A. Urbano, Composite scalar dark matter, J. High Energy Phys. 07 (2012) 015.
[58] T. A. Ryttov and F. Sannino, Ultra minimal technicolor and its dark matter TIMP, Phys. Rev. D **78**, 115010 (2008).
[59] G. 't Hooft, Symmetry Breaking Through Bell-Jackiw Anomalies, Phys. Rev. Lett. **37**, 8 (1976).
[60] G. 't Hooft, Computation of the Quantum Effects Due to a Four-Dimensional Pseudoparticle, Phys. Rev. D **14**, 3432 (1976); Erratum, Phys. Rev. D **18**, 2199(E) (1978).
[61] G. 't Hooft, How instantons solve the U(1) problem, Phys. Rep. **142**, 357 (1986).
[62] D. Diakonov, Chiral quark-soliton model, arXiv:hep-ph/9802298.
[63] M. Kobayashi, H. Kondo, and T. Maskawa, Symmetry breaking of the chiral $u(3) \times u(3)$ and the quark model, Prog. Theor. Phys. **45**, 1955 (1971).
[64] V. Bernard, R. L. Jaffe, and U. G. Meissner, Flavor mixing via dynamical chiral symmetry breaking, Phys. Lett. B *B* **198**, 92 (1987).
[65] V. Bernard, R. L. Jaffe, and U. G. Meissner, Strangeness mixing and quenching in the Nambu-Jona-Lasinio model, Nucl. Phys. **B308**, 753 (1988).
[66] S. Klimt, M. F. M. Lutz, U. Vogl, and W. Weise, Generalized SU(3) Nambu-Jona-Lasinio model. Part. 1. Mesonic modes, Nucl. Phys. **A516**, 429 (1990).
[67] S. R. Coleman and E. J. Weinberg, Radiative corrections as the origin of spontaneous symmetry breaking, Phys. Rev. D **7**, 1888 (1973).
[68] J. Bijnens, E. de Rafael, and H.-q. Zheng, Low-energy behavior of two point functions of quark currents, Z. Phys. C **62**, 437 (1994).

[69] M. Takizawa, K. Kubodera, and F. Myhrer, Novel feature of the vector meson solution in the Nambu-Jona-Lasinio model, Phys. Lett. B **261**, 221 (1991).
[70] S. P. Klevansky and R. H. Lemmer, Spectral density functions and their sum rules in an effective chiral field theory, arXiv:hep-ph/9707206.
[71] E. Witten, Current algebra theorems for the U(1) goldstone boson, Nucl. Phys. **B156**, 269 (1979).
[72] J. Bijnens, C. Bruno, and E. de Rafael, Nambu-Jona-Lasinio like models and the low-energy effective action of QCD, Nucl. Phys. **B390**, 501 (1993).
[73] R. Arthur, V. Drach, M. Hansen, A. Hietanen, C. Pica, and F. Sannino, SU(2) gauge theory with two fundamental flavours: A minimal template for model building, Phys. Rev. D **94**, 094507 (2016).
[74] R. Arthur, V. Drach, A. Hietanen, C. Pica, and F. Sannino, $SU(2)$ Gauge theory with two fundamental flavours: Scalar and pseudoscalar spectrum, arXiv:1607.06654.
[75] T. DeGrand, Y. Liu, E. T. Neil, Y. Shamir, and B. Svetitsky, Spectroscopy of SU(4) gauge theory with two flavors of sextet fermions, Phys. Rev. D **91**, 114502 (2015).
[76] T. DeGrand and Y. Liu, Lattice study of large N_c QCD, Phys. Rev. D **94**, 034506 (2016).
[77] V. Dmitrasinovic, S. P. Klevansky, and R. H. Lemmer, Weinberg sum rules in an effective chiral field theory, Phys. Lett. B **386**, 45 (1996).
[78] S. Peris, M. Perrottet, and E. de Rafael, Matching long and short distances in large N(c) QCD, J. High Energy Phys. 05 (1998) 011.
[79] M. E. Peskin and T. Takeuchi, Estimation of oblique electroweak corrections, Phys. Rev. D **46**, 381 (1992).
[80] M. Baak, J. Cúth, J. Haller, A. Hoecker, R. Kogler, K. Mönig, M. Schott, and J. Stelzer (Gfitter Group Collaboration), The global electroweak fit at NNLO and prospects for the LHC and ILC, Eur. Phys. J. C **74**, 3046 (2014).
[81] R. Barbieri, B. Bellazzini, V. S. Rychkov, and A. Varagnolo, The Higgs boson from an extended symmetry, Phys. Rev. D **76**, 115008 (2007).
[82] R. Contino and A. Pomarol, Holography for fermions, J. High Energy Phys. 11 (2004) 058.
[83] N. Yamatsu, Finite-dimensional Lie algebras and their representations for unified model building, arXiv:1511.08771.
[84] R. F. Dashen, Chiral $SU(3) \times SU(3)$ as a symmetry of the strong interactions, Phys. Rev. **183**, 1245 (1969).
[85] I. I. Kogan, A. Kovner, and M. A. Shifman, Chiral symmetry breaking without bilinear condensates, unbroken axial Z(N) symmetry, and exact QCD inequalities, Phys. Rev. D **59**, 016001 (1998).
[86] G. Cacciapaglia and A. Parolini, Light 't Hooft top partners, Phys. Rev. D **93**, 071701 (2016).
[87] S. R. Coleman, The uses of instantons, Subnuclear series **15**, 805 (1979); Reprinted in S. Coleman, *Aspects of Symmetries* (Cambridge University Press, Cambridge, England, 1985).
[88] D. I. Olive, S. Sciuto, and R. J. Crewther, Instantons in field theory, Riv. Nuovo Cimento **2**, 1 (1979).
[89] S. Vandoren and P. van Nieuwenhuizen, Lectures on instantons, arXiv:0802.1862.
[90] A. I. Vainshtein and V. I. Zakharov, Calculation of the fermion determinant in chiral and supersymmetrical theories, Pis'ma Zh. Eksp. Teor. Fiz. **35**, 258 (1982) [JETP Lett. **35**, 323 (1982)].
[91] G. Cacciapaglia, H. Cai, A. Deandrea, T. Flacke, S. J. Lee, and A. Parolini, Composite scalars at the LHC: the Higgs, the Sextet and the Octet, J. High Energy Phys. 11 (2015) 201.
[92] A. Belyaev, G. Cacciapaglia, H. Cai, G. Ferretti, T. Flacke, A. Parolini, and H. Serodio, Di-boson signatures as standard candles for partial compositeness, J. High Energy Phys. 01 (2017) 094.
[93] A. Belyaev, G. Cacciapaglia, H. Cai, T. Flacke, A. Parolini, and H. Serodio, Singlets in composite Higgs models in light of the LHC di-photon searches, Phys. Rev. D **94**, 015004 (2016).
[94] N. Bizot, M. Frigerio, M. Knecht, and J.-L. Kneur (to be published).
[95] A. O. Bouzas, Mixing renormalization for scalar fields, Int. J. Mod. Phys. A **18**, 3695 (2003) Erratum, Int. J. Mod. Phys. A **21**, 1157 (2006).
[96] G. Passarino and M. J. G. Veltman, One loop corrections for e + e− annihilation into mu + mu− in the Weinberg model, Nucl. Phys. **B160**, 151 (1979).
[97] H. K. Dreiner, H. E. Haber, and S. P. Martin, Two-component spinor techniques and Feynman rules for quantum field theory and supersymmetry, Phys. Rep. **494**, 1 (2010).
[98] A. Buck, R. Alkofer, and H. Reinhardt, Baryons as bound states of diquarks and quarks in the Nambu-Jona-Lasinio model, Phys. Lett. B **286**, 29 (1992).
[99] T. Brauner, Fierz transformations, https://sites.google.com/site/braunercz/notes.
[100] M. Buballa, NJL model analysis of quark matter at large density, Phys. Rep. **407**, 205 (2005).